Low-dimensional modeling of hillslope subsurface flow processes

Developing and testing the hillslope-storage Boussinesq model

A.G.J. Hilberts

Low-dimensional modeling of hillslope subsurface flow processes

Developing and testing the hillslope-storage Boussinesq model

promotor:	Prof.dr.ir P.A. Troch Hoogleraar Hydrologie en Kwantitatief Waterbeheer (1999-2005), Wageningen Universiteit. Professor of Hydrology and Water Resources, Professor of Civil Engineering and Engineering Mechanics, University of Arizona, USA.
co-promotor:	Prof.dr. C. Paniconi Institut National de la Recherche Scientifique - Centre Eau, Terre et Environnement, Université du Québec, Canada

Samenstelling promotiecommissie:
Prof.dr.ir. A. Leijnse, Wageningen Universiteit
Prof.dr. A. Bronstert, Potsdam University, Germany
Prof.dr.ir. M.F.P. Bierkens, Universiteit Utrecht
Prof.dr.ir. M.S. Hassanizadeh, Universiteit Utrecht

Dit onderzoek is uitgevoerd binnen de onderzoeksschool SENSE.

Low-dimensional modeling of hillslope subsurface flow processes

Developing and testing the hillslope-storage Boussinesq model

Arno Gerardus Jeanne Hilberts

Proefschrift

ter verkrijging van de graad van doctor
op gezag van de rector magnificus
van Wageningen Universiteit,
Prof.dr. M.J. Kropff,
in het openbaar te verdedigen
op dinsdag 31 oktober 2006
des namiddags te half twee in de Aula.

Hilberts, A.G.J.
Low-dimensional modeling of hillslope subsurface flow processes
Developing and testing the hillslope-storage Boussinesq model
Dissertation Wageningen Universiteit, Wageningen, 2006
ISBN 90-8504-516-9

Copyright © A.G.J. Hilberts, 2006.

Abstract

Hilberts, A.G.J. *Low-dimensional modeling of hillslope subsurface flow processes - Developing and testing the hillslope-storage Boussinesq model.* Ph.D. thesis, Wageningen University, The Netherlands.

In this thesis the focus is on investigating the hillslope hydrological behavior, as a crucial part in understanding the catchment hydrological response. To overcome difficulties associated with most of the existing models, i.e., high computational costs and difficulties in model parameterization and calibration, the focus is on low-dimensional physically based models. The central question is whether it is possible to formulate low-dimensional physically based models such that the essential physical behavior of the natural system is preserved.

Several models are compared to each other and to measurements from a laboratory and from a field site. The comparisons are carried out for a diversity of bedrock slopes, hillslope shapes, and profile curvatures. The low-dimensional models that are formulated are essentially based on the hillslope-storage Boussinesq (HSB) model. Several modifications to the model are conducted in order to investigate the model response under different conditions: a) a generalized HSB formulation is derived that allows model evaluation on curved bedrock profiles, b) a new HSB model is derived in which the effects of capillarity are partly accounted for based on the assumption of hydraulic equilibrium in the unsaturated zone, and c) a coupled saturated-unsaturated HSB model is derived in which the unsaturated zone dynamics are described with a one-dimensional Richards model. Evaluation of the developed low-dimensional models generally shows that: a) the HSB model saturated zone dynamics alone can describe the outflow rates and water table dynamics accurately when the influence of capillarity is small; b) for very shallow soils or water tables in the proximity of the soil surface, the effects of capillarity are more clearly noticeable and it is possible to improve the simulated water table dynamics during drainage experiments significantly by regarding the parameter drainable porosity as a state-dependent parameter of which the value depends on the unsaturated depth; c) for drainage and recharge scenario's, a low-dimensional coupled saturated-unsaturated model that is developed to dynamically account for the unsaturated zone processes is very well capable of describing outflow rates and water table dynamics; d) the comparison of the results of the coupled model run in an uncalibrated mode to field data yields a reasonable match in terms of hydrographs and water table dynamics. However, the water table response is highly sensitive due to limited free pore space caused by capillarity effects.

Key words: hillslope hydrology, low-dimensional modeling, Boussinesq equation, Richards equation, water table dynamics.

Contents

1 Introduction 1

1.1 Background . . . 1

1.2 Research objectives . . . 2

1.3 Hydraulic groundwater models . . . 3

1.3.1 The Boussinesq equation . . . 3

1.3.2 The hillslope-storage Boussinesq model . . . 3

1.3.3 The hillslope-storage kinematic wave model . . . 4

1.4 Outline of dissertation . . . 5

2 The hillslope-storage Boussinesq model for non-constant bedrock slope 7

2.1 Introduction . . . 8

2.2 Development of the generalized hillslope-storage Boussinesq model 10

2.3 The hillslope-storage kinematic wave model and the Richards equation based model . . . 13

2.4 Experiment setup . . . 14

2.4.1 Nine characteristic hillslopes . . . 14

2.4.2 Discretization . . . 14

2.4.3 Initial and boundary conditions . . . 14

2.4.4 Parameterization . . . 15

2.4.5 Dimensional analysis . . . 16

2.5 Drainage response . . . 17

2.5.1 Introduction . . . 17

2.5.2 Interpretation of the KW storage profiles for 5% and 30% bedrock slope . . . 18

2.5.3 Interpretation of storage profiles for 5% bedrock slope . . 18

2.5.4 Interpretation of storage profiles for 30% bedrock slope . 19

2.5.5 Comparison of storage profiles for 5% and 30% bedrock slope 19

2.5.6 Comparison of hydrographs for 5% and 30% bedrock slope 20

2.6 Discussion and conclusions . . . 21

3 Storage-dependent drainable porosity for complex hillslopes 25

3.1 Introduction . . . 27

3.2 Drainable porosity and groundwater storage . . . 29

3.2.1 Storage in the saturated and unsaturated zone for a horizontal bedrock . . . 29

3.2.2 Integration of soil moisture curves for a horizontal bedrock 30

3.2.3 Drainable porosity for a horizontal bedrock 31
3.2.4 Drainable porosity for a sloping bedrock 31
3.2.5 Interpretation 33
3.3 Implementation of storage-dependent drainable porosity into the HSB model 34
3.4 Experimental setup 36
3.4.1 The laboratory hillslopes and the drainage experiment . 36
3.4.2 Boundary conditions 37
3.4.3 Parameterization of the revised HSB model 38
3.4.4 Parameterization of the original HSB model 38
3.4.5 Parameter interpretation 39
3.5 Results 40
3.5.1 Uncalibrated models 40
3.5.2 Calibrated models 40
3.6 Discussion and conclusions 43

4 An attempt to explain the high and low frequency behavior of the complex drainable porosity in a tidal aquifer 49
4.1 The frequency response and the influence of capillarity 50
4.1.1 Low frequency response 50
4.1.2 High frequency response 52
4.1.3 An attempt to explain the modeled and measured high frequency decay of $|n_\omega$— 54
4.2 Criteria to determine the influence of capillarity 56

5 Low-dimensional modeling of hillslope subsurface flow: the relationship between rainfall, recharge, and unsaturated storage dynamics 59
5.1 Introduction 60
5.2 Governing equations 62
5.2.1 Unsaturated and saturated zone of the coupled model . . 62
5.2.2 Interactions between the saturated and the unsaturated zone 64
5.2.3 Governing equations with inclusion of the capillary fringe 67
5.2.4 An alternate derivation involving singularity 68
5.2.5 The three-dimensional Richards equation-based model . 69
5.3 Interpretation 69
5.3.1 Interpretation of the equations for the coupled model . . 69
5.3.2 The relationship between rainfall, recharge, and unsaturated storage 71
5.4 Model comparison setup 71
5.4.1 The models and hillslopes 71
5.4.2 Boundary and initial conditions 72
5.4.3 Hillslope and soil parameters 73
5.4.4 Parameterization of the capillary fringe 74
5.5 Model comparison results 75
5.5.1 Hydrographs and water tables 75

5.5.2 Recharge rates 77
5.6 Discussion 78
5.7 Conclusions 80

6 Evaluation of a low-dimensional coupled hillslope-hydrological model using data from a plot-scale experimental site in Troy (ID), USA. 83
6.1 Introduction 84
6.2 Model description 84
6.3 Site description 86
6.4 Modeling procedure 86
6.4.1 Assumptions underlying the modeling procedure 86
6.4.2 Soil parameters 87
6.4.3 Boundary and initial conditions 88
6.4.4 Model inputs 89
6.5 Hydrograph response and perched groundwater dynamics 90
6.5.1 Fixed-head lower boundary condition 90
6.5.2 Seepage face lower boundary condition 91
6.6 Discussion 91
6.7 Conclusions 93

7 Summary and conclusions 95
7.1 Principal conclusions 95
7.2 Perspectives 97

References 101

Samenvatting 107

Dankbetuiging/Acknowledgement 113

Curriculum vitae 115

List of publications 116

Chapter 1

Introduction

1.1 Background

Catchment hydrological processes determine the transportation of water, sediments and pollutants, as well as the height, timing and duration of flood peaks. Since landscape form and catchment hydrological processes show many interactions and feedbacks, it is of crucial importance for catchment scale water and land management to understand the mechanisms behind these interactions and feedbacks.

Hillslopes can be regarded as the basic elements of many landscapes. In an attempt to advance our understanding of the functioning of catchment hydrological processes, there has been a strong emphasis on investigating hillslope hydrological processes since the 1960's. Among the first to acknowledge the importance of hillslope processes in the generation of stream flood peaks in temperate regions, were *Betson* [1964] and *Ragan* [1968]. These papers demonstrated that during rainfall events, the bulk of stream runoff originates from a relatively small part of the catchment area that gradually becomes saturated. The areas were termed “partial areas” or “variable sources areas”, and they were found to be mostly located at the foot of hillslopes and around the channel network ([*Kirkby*, 1988]). In *Dunne and Black* [1970], a field experiment was conducted in which the importance of the variable source areas was confirmed. In papers by *Whipkey* [1965], *Hewlett and Hibbert* [1967], and *Freeze* [1972a], the important contribution of subsurface flow to the stream hydrographs, and its importance in generating variable source areas was shown. The conclusions from these papers, that understanding variable source areas and subsurface flow on hillslopes are crucial in understanding the catchment response was a breakthrough, since for a long time infiltration-excess (a concept stemming from the work of *Horton* [1933]) had been commonly accepted as the driving mechanism behind production of overland flow. These benchmark papers have therefore brought about a new view on catchment and hillslope hydrology, and triggered many new studies that investigate hillslope processes either experimentally or numerically.

In books edited by *Kirkby* [1978] and *Anderson and Brooks* [1996], an overview is given of the hillslope modeling studies that were developed over the past decades. All of the models intended for catchment and hillslope research that are presented in these books are essentially either based on complex numerical integrations of the three-dimensional flow equations, or simplified hydraulic groundwater equations. With regard to the complex numerical models, the conclusion can be drawn that they generally show little forecasting advantage over simpler approaches [*Kirkby*, 1988]. However, the simplified hydraulic groundwater models are typically one-dimensional, and do not account for the three-dimensional hillslope shape in which the groundwater flow and storage processes take place. Thus, simple but physically realistic models that represent hydrological processes at the hillslope and catchment scales, and that account for catchment and hillslope geometry are needed for reliable simulation of overland flow and subsurface flow [*Beven*, 2001; *Hornberger and Boyer*, 1995].

1.2 Research objectives

In an attempt to accurately model the three-dimensional hillslope hydrological processes, three-dimensional numerical Richards equation models are often used. The Richards equation was derived by *Richards* [1931] and, within its range of validity, it provides the most accurate description of flow processes through variably saturated porous media. However, these types of models typically require fine spatio-temporal grids to avoid numerical convergence problems, which places large demands on the computational costs and memory usage, even for modeling studies on the hillslope scale. Moreover, the parameterization and calibration of these models is often cumbersome due to the small amount and low accuracy of the available data. Therefore, in order to improve our understanding of the hydrological response hillslopes, and ultimately catchments, to atmospheric forcings, simplified yet physically-based models are required. The central research question in this thesis is:

Can low-dimensional dynamic models of hillslope-scale flow and storage processes be formulated, such that the essential physical behavior of the natural system is preserved?

Towards the end of the 1990's several breakthroughs were realized in the field of low-dimensional catchment and hillslope modeling. *Duffy* [1996] presented a two-state integral-balance model for soil moisture and groundwater dynamics in complex terrain. Later *Reggiani et al.* [1998] extended this approach by including other subregions of the hydrological cycle (e.g., overland flow, saturated areas and the channel network). Parallel to these developments, models were formulated by *Fan and Bras* [1998], and *Troch et al.* [2002, 2003] that are based on hydraulic groundwater theory ([*Boussinesq*, 1877]). In *Fan and Bras* [1998] the concept of mapping the three-dimensional soil mantle onto a one-dimensional pore or storage space is introduced. The governing equations in *Fan and Bras* [1998] and *Troch et al.* [2002, 2003] are one-dimensional partial differential equations of saturated moisture storage on complex hillslopes, which can be solved numerically, or analytically under certain restrictive conditions. The major advantage of this kind of formulation is that the interaction between hillslope shape and hydrological response can easily be quantified.

The main objectives of this thesis is to thoroughly test the theory underlying the work of *Troch et al.* [2003], to further develop the hillslope hydrological model that was developed by *Troch et al.* [2003], and to advance our understanding of the interactions between hillslope shape and hydrological response.

In the following an introduction will be given to the models that are used and analyzed in this thesis, and an overview of the numerical and analytical solutions that were already derived will be presented.

1.3 Hydraulic groundwater models

1.3.1 The Boussinesq equation

Subsurface flow along a unit-width hillslope with sloping bedrock can be described with the Boussinesq equation [*Boussinesq*, 1877], which is obtained when the flow equation

$$q = -kh\left(\frac{\partial h}{\partial x}\cos(i) + \sin(i)\right) \tag{1.1}$$

is substituted in the mass-balance equation

$$f\frac{\partial h}{\partial t} = -\frac{\partial q}{\partial x} + N \tag{1.2}$$

yielding:

$$\frac{\partial h}{\partial t} = \frac{k}{f}\left[\cos i\frac{\partial}{\partial x}\left(h\frac{\partial h}{\partial x}\right) + \sin i\frac{\partial h}{\partial x}\right] + \frac{N}{f} \tag{1.3}$$

where $h(x,t)$ is the elevation of the groundwater table measured perpendicular to an underlying impermeable layer which has a slope angle i, k is the hydraulic conductivity, f is the drainable porosity, x is the distance from the outlet measured parallel to the impermeable layer, t is time, and N represents the recharge to the groundwater table.

The application of Equation 1.3 is limited because it does not account for the three-dimensional soil mantle in which flow processes take place, whereas literature shows that the three-dimensional shape of a hillslope (i.e., geometry and topography) forms a dominant control on the hydrological response (e.g, *McDonnell* [1990]; *Woods et al.* [1997])

1.3.2 The hillslope-storage Boussinesq model

In *Troch et al.* [2003] a reformulation of the Boussinesq equation is given, that allows us to account for complex hillslope geometries (e.g., convergent and divergent plan shapes), through the introduction of a hillslope width function $w(x)$, where it is assumed that no flow occurs in the lateral direction perpendicular to x. The derived model's behavior for free drainage and under recharge is investigated on a set of seven characteristic hillslopes. The governing equation in [*Troch et al.*, 2003] was termed the hillslope-storage Boussinesq (HSB) equation,

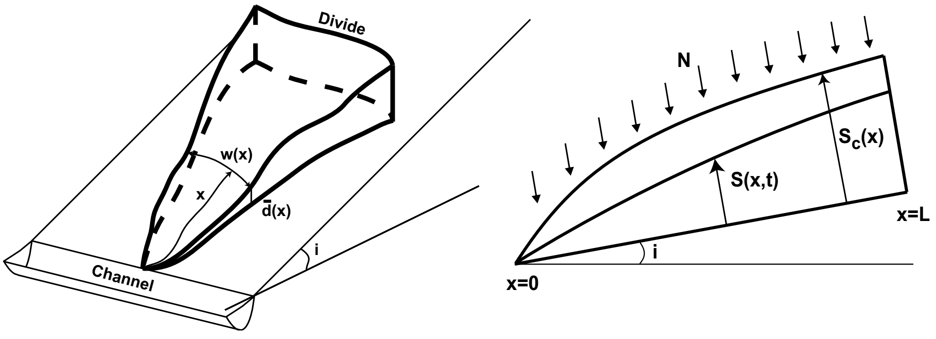

Figure 1.1: A three dimensional view of a convergent hillslope overlying a straight bedrock profile (left), and a definition sketch of the cross section of a one-dimensional hillslope aquifer overlying a bedrock with a constant bedrock slope angle (right).

and reads:

$$f\frac{\partial S}{\partial t} = \frac{k\cos i}{f}\frac{\partial}{\partial x}\left[\frac{S}{w}(\frac{\partial S}{\partial x} - \frac{S}{w}\frac{\partial w}{\partial x})\right] + k\sin i\frac{\partial S}{\partial x} + fNw \tag{1.4}$$

where $S = S(x,t) = wf\overline{h}$ is the subsurface water storage, $\overline{h} = \overline{h}(x,t)$ is the water table height averaged over the width of the hillslope, and $w(x)$ is the hillslope width function. The total storage capacity along the hillslope can be expressed as $S_c(x) = fw(x)\overline{d}(x)$, where $\overline{d}$ is the soil depth averaged over the width of the hillslope. The hillslope properties and coordinates are illustrated in Figure 1.1.

Several simplified and linearized versions of Equation 1.4 are investigated and compared in *Troch et al.* [2003] on a set of seven hillslopes and two bedrock slope angles. In *Paniconi et al.* [2003], the HSB model is compared to a three-dimensional Richards based model on the same set of hillslopes and for the same bedrock slopes.

In *Troch et al.* [2004] analytical solutions to a linearized HSB equation are determined using Laplace transformation, under the assumption that the hillslope width function $w(x)$ can be described with an exponential function, and an expression for a hillslope Péclet number is derived.

1.3.3 The hillslope-storage kinematic wave model

In *Fan and Bras* [1998] a simplified version of Equation 1.4 is investigated. It is assumed that the subsurface flow rates can be described with a kinematic wave (KW) approximation of Darcy's law:

$$Q = -k\frac{S'}{f}\frac{\mathrm{d}z}{\mathrm{d}x'} \tag{1.5}$$

where $S' = S'(x',t)$ is the saturated storage as in Equation 1.4, but measured vertically, and z and x' are respectively the vertical and horizontal coordinate. The hillslope topography is described using a quadratic polynomial. The derived equations are solved analytically using the method of characteristics, and applied to three differently shaped hillslopes.

In *Troch et al.* [2002], the approach of *Fan and Bras* [1998] is generalized by describing the bedrock shape and curvature with a n-th order polynomial, that allows for a more flexible fit of the function to the available topographic data. Analytical solutions are determined, and the results of model runs on nine characteristic hillslopes, ranging from convergent to divergent plan shape and from concave to convex profile shape, are presented in dimensionless variables.

1.4 Outline of dissertation

The HSB model as described in *Troch et al.* [2003] is developed for and analyzed on hillslopes with various plan shapes (i.e., convergent, divergent), but the application is limited to non-curved (i.e., straight) bedrock shapes. In **Chapter 2**, the HSB model of *Troch et al.* [2003] is cast in a generalized formulation enabling the model to handle non-constant bedrock slope. The generalized HSB model response is investigated on the nine hillslopes described in *Troch et al.* [2002], with varying curvature of bedrock shape. The model is compared to the KW model of *Troch et al.* [2002], and the three-dimensional Richards model of *Paniconi and Wood* [1993] for a free drainage scenario for 5% and 30% bedrock slope.

Chapter 3 deals with the effects of unsaturated storage on groundwater dynamics. A physically-based analytical expression for the drainable porosity is derived to account, in part, for the unsaturated zone effects in shallow aquifers during drainage experiments. The derived equations are implemented in the HSB model. The model is compared to the original HSB model, and to measurements from a 6.0x2.5x0.5m laboratory setup for a divergent and convergent slope shape and for bedrock slope angles of 5%, 10%, and 15%.

Chapter 4 describes an application of the theory described in Chapter 3 to a tidal aquifer study described in *Cartwright et al.* [2005]. In *Cartwright et al.* [2005] the effects of oscillating water tables in a tidal aquifer on the drainable porosity are investigated, and a curious phenomenon for high frequency oscillations is noted. This chapter comments on the work by *Cartwright et al.* [2005] and suggests a possible explanation for the particular behavior mentioned in that paper.

In **Chapter 5**, a coupling is presented between a one-dimensional Richards equation model to describe the unsaturated zone processes, and the HSB model describing the saturated zone processes. The coupled formulation allows for quantitative investigation of the role of unsaturated storage on the relationship between rainfall and recharge. The model results are compared to the HSB model and the three-dimensional Richards model of *Paniconi and Wood* [1993] on the seven characteristic hillslopes described in *Troch et al.* [2003] and for a bedrock slope angle of 5%.

In **Chapter 6**, the coupled model described in Chapter 5 is slightly adapted to enable handling of saturated hydraulic conductivity to vary with depth, and to allow for a seepage face type downslope boundary condition. The model is applied to a well-instrumented 36x18x0.67m hillslope plot near Troy (ID), USA. The effects of using a seepage face instead of a fixed-head type boundary condition are investigated. The model results are compared on an hourly basis to measurements obtained from the plot over a period of approximately 130 days.

In **Chapter 7** the most important conclusions are summarized and suggestions for future research are given.

Chapter 2

The hillslope-storage Boussinesq model for non-constant bedrock slope

Abstract

In this study the recently introduced hillslope-storage Boussinesq (HSB) model is cast in a generalized formulation enabling the model to handle non-constant bedrock slopes (i.e. bedrock profile curvature). This generalization extends the analysis of hydrological behavior to hillslopes of arbitrary geometrical shape, including hillslopes having curved profile shapes. The generalized HSB model performance for a free drainage scenario is evaluated by comparison to a full three-dimensional Richards equation (RE) based model. The model results are presented in the form of dimensionless storage profiles and dimensionless outflow hydrographs. In addition, comparison of both models to a storage based kinematic wave (KW) model enables us to assess the relative importance of diffusion processes for different hillslope shapes, and to analyze the influence of profile curvature on storage and flow patterns specifically. The comparison setup consists of a set of nine gentle (5% bedrock slope) and nine steep (30% bedrock slope) hillslopes of varying plan shape and profile curvature. Interpretation of the results shows that for highly conductive soils the simulated storage profiles and outflow hydrographs of the generalized HSB model and RE model match remarkably for 5% bedrock slope and for all plan and profile curvatures. The match is slightly poorer on average for 30% bedrock slope, in particular on divergently shaped hillslopes. In the assessment of the influence of hydraulic diffusion, we find good agreement in simulation results for the KW model compared to results from the generalized HSB model and the RE model for steep divergent and uniform hillslopes, due to a relatively low ratio between water table gradient and bedrock slope compared to convergent or gentle hillslopes. Overall, we demonstrate that, in addition to bedrock slope, hillslope shape as represented by plan and profile curvature is an important control on subsurface flow response.

This chapter is based on the paper “Hilberts, A.G.J., E.E. van Loon, P.A. Troch and C. Paniconi, The hillslope-storage Boussinesq model for non-constant bedrock slope, *Journal of Hydrology, 291*, 160–173, 2004.”

2.1 Introduction

Landscape geometry influences hydrological response, thus clear insight into the effects of the shape and characteristics of landscape elements is required to further our understanding of and our ability to model hydrological processes. For some time research has focused on identifying and quantifying hillslope processes as a first step towards assessment of (sub)catchment response. In catchment hydrology the importance of subsurface flow processes in generating variable source areas was first addressed by *Dunne and Black* [1970] and *Freeze* [1972a,b]. Later *Kirkby* [1988] reported that almost all of the water in streamflow has passed over or through a hillside and its soils before reaching the channel, thereby emphasizing the role of hillslope hydrological processes. These references indicate a need for quantifying the hydrological processes on hillslopes, and for the development of appropriate models to describe these processes. Many models have been developed over the past 30 years. *Pikul et al.* [1974] formulated a coupled model based on the Richards and Boussinesq equations and evaluated it by comparison to a two-dimensional Richards based model. *Sloan and Moore* [1984] compared Richards equation based models of *Nieber and Walter* [1981] and *Nieber* [1982], a kinematic wave model of *Beven* [1981] and a storage discharge model to measurements on a hillslope with a uniform width function. Other examples include *Fipps and Skaggs* [1989], who applied a two-dimensional Richards based model to a unit-width hillslope with a constant slope inclination; *Verhoest and Troch* [2000], who determined the analytical solution to the Boussinesq equation applied to a non-curved unit-width aquifer; and *Ogden and Watts* [2000], who analyzed the behavior of a numerically solved two-dimensional model for steady and unsteady flow types on a unit-width non-curved hillslope. None of these studies present models that account for the effect of the three-dimensional hillslope shape on storage and flow patterns, although other recent research has begun to address these issues. For example *Paniconi and Wood* [1993] presented a three-dimensional Richards based model for subsurface flow on complex hillslopes; *Duffy* [1996] formulated a volume-weighted integral-balance model for complex terrain types and applied it to steep slightly curved hillslope to analyze subsurface flow, overland flow and variable source areas; and *Woods et al.* [1997] modeled subsurface flow processes using a topographic index and compared results to extensive field measurements on thirty steep inclined shallow troughs of various shape (convergent, planar and divergent).

To overcome difficulties associated with three-dimensional models, a series of new low-dimensional hillslope models have been developed [*Troch et al.*, 2002, 2003]. These models are able to treat geometric complexity in a simple way based on a concept presented by *Fan and Bras* [1998], resulting in a significant reduction in model complexity, and they can cope with varying hillslope width functions and bedrock slope. In *Troch et al.* [2002] the analytical solutions to a kinematic wave equation that is expressed in terms of storage using the mapping method of *Fan and Bras* [1998] are evaluated by applying them to nine hillslopes with different plan and profile curvature. The resulting hillslope-storage kinematic wave (KW) model shows quite different dynamic behavior during a free drainage and a recharge experiment. The authors conclude that the kinematic wave assumption is limited to moderate to steep slopes, and that for more gentle slopes a new model formulation based on the Boussinesq equation would be necessary. In *Troch et al.* [2003] the hillslope-storage Boussinesq (HSB) model together with several simplified versions (e.g., linearized) are derived and evaluated under free drainage and recharge scenarios. The evaluation is conducted on a subset of the nine hillslopes presented in *Troch et al.* [2002]. Results are compared to those of the KW model and the authors find that dynamic response of the hillslopes is strongly dependent on plan shape and bedrock slope, and that convergent hillslopes tend to drain much more slowly than divergent ones due to a reduced flow domain near the outlet. Concerning the several simplified versions of the HSB model it is concluded that for gentle slopes (5% bedrock slope) none of these simpler models is able to fully capture the dynamics of the full HSB model, while for steep slopes (30% bedrock slope) the performance is better. In *Paniconi et al.* [2003] the HSB model is compared to a three-dimensional Richards equation (RE) based model on the same subset of hillslopes, in order to identify the circumstances under which the different models generate comparable responses. In this work the RE model is regarded as the benchmark. The overall conclusion is that the HSB model is able to capture the general features of storage and outflow response. Overall a closer match between the HSB and RE models was observed for convergent hillslopes than divergent, and the match was quite independent of slope steepness. A poorer match was observed in case of the recharge simulations compared to the free drainage scenario, most likely due to absence of a description of the unsaturated zone in the HSB model, important in the transmission of water through a hillslope soil during a rainfall or recharge event. The absence of an unsaturated zone component in the HSB model also causes the water table heights for the HSB model to be slightly higher and the flow values to be slightly lower than the RE model in almost all cases.

These previous papers on the HSB model suggested several extensions of the model to make it more representative of complex hillslopes, including the capability to handle non-constant bedrock slope in order to more accurately account for hillslope profile curvature, which is the focus of the present paper. An illustration of the importance of profile curvature in hillslope response is shown in Figure 2.1 where simulated water table profiles and outflow hydrographs for a shallow sand loam soil overlying a bedrock with an average slope of 5% are depicted for a concave, straight, and convex profile shape. The outflow hydrographs clearly differ: after approximately 5 days, we see a rising hydrograph for the concave hillslope, whereas the straight and convex hillslopes show a falling and a relatively constant hydrograph respectively. After 10 days we also see differently shaped water tables: “compacted” for the concave hillslope, “stretched” for the convex hillslope (with high water table values, due to low outflow), and intermediate for the straight hillslope.

The objectives of this paper are thus to 1) derive a more general formulation of the HSB model for non-constant bedrock slope; 2) assess the effects of topography and plan and profile curvature of hillslopes on the dynamical hydrological response; 3) intercompare free drainage simulation of the HSB, KW and RE models for hillslopes with varying plan and profile curvature. The generalized HSB model allows a quantitative analysis of water tables and hydrographs, and

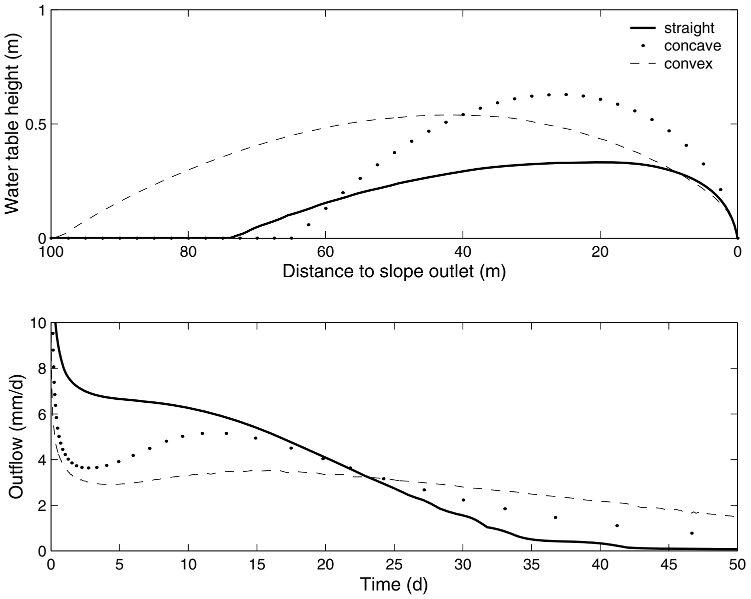

Figure 2.1: Simulated water table heights and outflow hydrographs for a free drainage experiment on a concave, a straight, and a convex hillslope profile, using a three-dimensional Richards equation based model. The hillslopes have an average bedrock slope of 5%, a constant width of 50 m, a length of 100 m, and a depth of 2 m. The soil is a sandy loam with a saturated conductivity of 1 m/h, and a porosity of 0.30. The water table outputs are at $t = 10$ days.

thereby enables us to conduct a very accurate analysis of the effects of topography and geometry on hydrological processes on these hillslopes, since it allows simulations for virtually any hillslope shape and bedrock slope. The generalized HSB model will be compared to the full three-dimensional RE model that was also applied in *Paniconi et al.* [2003]. The behavior of the models will be analyzed for the nine hillslopes of varying plan and profile curvature that are described in *Troch et al.* [2002], and model results will be presented in dimensionless variables. In addition the relative influence of diffusion processes in both models will be evaluated by comparison to the hillslope-storage kinematic wave model of *Troch et al.* [2002].

2.2 Development of the generalized hillslope-storage Boussinesq model

The mass balance equation for describing subsurface flow along a unit-width hillslope reads:

$$\frac{\partial}{\partial t}(fh) = -\frac{\partial q}{\partial x} + N \tag{2.1}$$

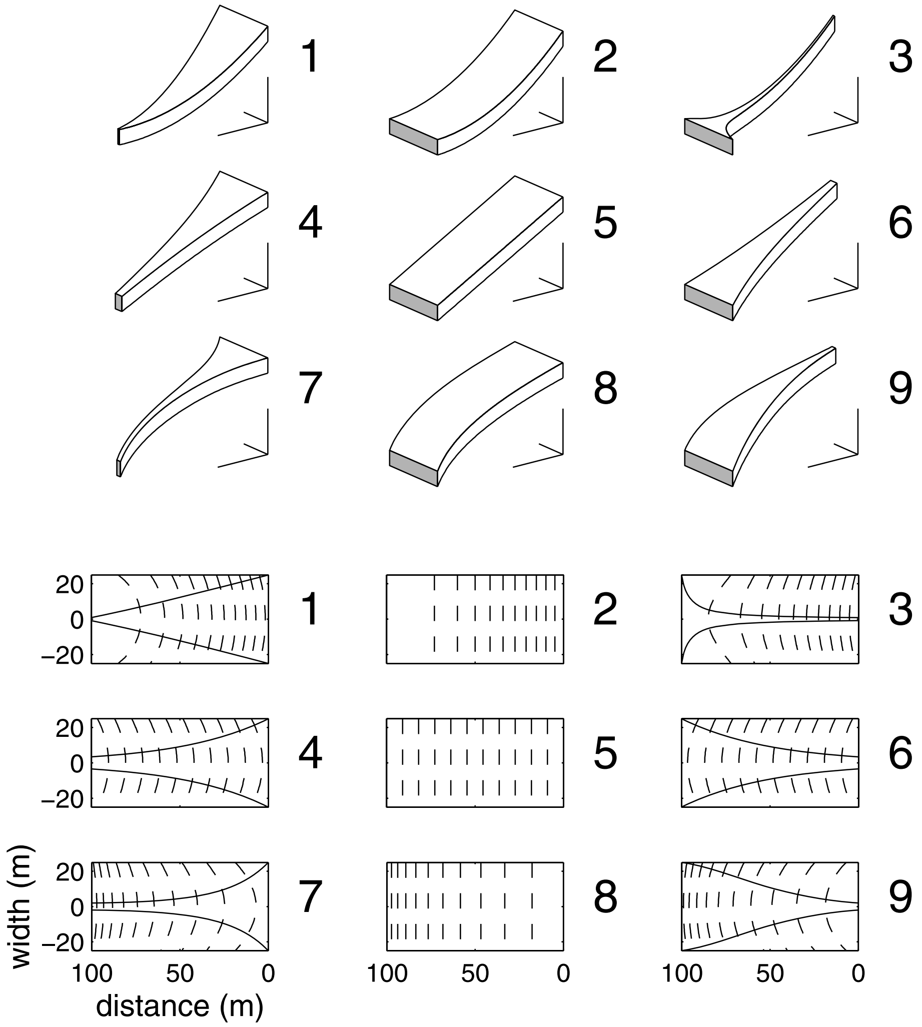

Figure 2.2: Three-dimensional view (top), and a two-dimensional plot of the contour lines and slope divides (bottom) of the nine hillslopes considered in this study.

where $h = h(x,t)$ is the elevation of the groundwater table measured perpendicular to the underlying impermeable layer, f is drainable porosity, x is distance to the outlet measured parallel to the impermeable layer, $q = q(x,t)$ is subsurface flux along the hillslope bedrock, t is time, and N is a source term, representing rainfall recharge to the groundwater table. Equation 2.1 is derived for a unit-width hillslope and therefore does not account for the three-dimensional shape of a hillslope. Investigating the effect of geometry on hydrological response thus requires a more general form of Equation 2.1. This is obtained by first expressing the equation in terms of storage by using the relationship of *Fan and Bras* [1998] to map the three-dimensional soil mantle onto a one-dimensional soil pore space:

$S = f \cdot w \cdot \overline{h}$, where $S = S(x,t)$ is actual storage, $w = w(x)$ is hillslope width at position x, and $\overline{h} = \overline{h}(x,t)$ is the width averaged water table height:

$$\overline{h}(x,t) = \frac{1}{w(x)} \int_w h(x,y,t)\mathrm{d}y \tag{2.2}$$

where y is the perpendicular direction to x. Including hillslope width as an integral part of Equation 2.1 allows description of subsurface flow within a hillslope of arbitrary plan geometry:

$$\frac{\partial}{\partial t}\left(fw\overline{h}\right) = -\frac{\partial}{\partial x}(wq) + Nw \tag{2.3}$$

Subsurface flux $q = q(x,t)$ is formulated by *Boussinesq* [1877] as:

$$q = -k\overline{h}\left(\frac{\partial \overline{h}}{\partial x}\cos i + \sin i\right) \tag{2.4}$$

where k is hydraulic conductivity, and i is bedrock slope. Combining Equations 2.3 and 2.4 yields the HSB equation as formulated by *Troch et al.* [2003],

$$f\frac{\partial S}{\partial t} = \frac{k\cos i}{f}\frac{\partial}{\partial x}\left[\frac{S}{w}\left(\frac{\partial S}{\partial x} - \frac{S}{w}\frac{\partial w}{\partial x}\right)\right] + k\sin i\frac{\partial S}{\partial x} + fNw \tag{2.5}$$

Equation 2.5 allows us to investigate the hydrological behavior of the original Boussinesq equation on hillslopes of variable plan geometry. In order to analyze the effect of non-constant profile curvature, we need to define the bedrock slope as being non-constant (i.e. $i = i(x)$). Treating the bedrock slope parameter as such, upon combining Equations 2.3 and 2.4 we obtain the generalized HSB equation:

$$f\frac{\partial S}{\partial t} = \frac{\partial}{\partial x}\left(\frac{kS}{f}\cos i(x)\frac{\partial (S/w)}{\partial x}\right) + \frac{\partial}{\partial x}\left(kS\sin i(x)\right) + fNw \tag{2.6}$$

which when expanded yields the governing equation of the HSB model for non-constant bedrock slope:

$$\begin{aligned} f\frac{\partial S}{\partial t} &= \frac{k}{f}\cos i(x)\left[B\frac{\partial S}{\partial x} + S\frac{\partial B}{\partial x} + fS\frac{\partial i(x)}{\partial x}\right] \\ &\quad + \frac{k}{f}\sin i(x)\left[f\frac{\partial S}{\partial x} - SB\frac{\partial i(x)}{\partial x}\right] + fNw \end{aligned} \tag{2.7}$$

where

$$B = \frac{\partial}{\partial x}\left(\frac{S}{w}\right)$$

Note that the flow lines for Equations 2.5 and 2.7 are assumed to be parallel to the bedrock. For the original HSB Equation 2.5 this implies uncurved flow lines; the flow lines for the generalized HSB model of Equation 2.7 allow a curved flow path. For constant bedrock slope $i(x) = i$, Equation 2.7 reduces to the HSB equation (Equation 2.5). For convenience we will henceforth refer to the extended model described by Equation 2.7 as the HSB model.

2.3 The hillslope-storage kinematic wave model and the Richards equation based model

In *Troch et al.* [2002] a kinematic wave model is presented that is also based on the principle of *Fan and Bras* [1998] for collapsing a three-dimensional soil mantle into a one-dimensional pore space. The governing equation for the KW model reads:

$$f\frac{\partial S}{\partial t} = k\frac{\partial S}{\partial x'}\frac{\partial z}{\partial x'} + kS\frac{\partial^2 z}{\partial x'^2} + fNw(x') \tag{2.8}$$

in which z is elevation of the impervious layer above a given datum and x' is the horizontal distance to the hillslope crest. The third model to be evaluated is fully three-dimensional, and is based on Richards' equation:

$$\eta(\psi)\frac{\partial \psi}{\partial t} = \nabla \cdot (K_s K_r(\psi)(\nabla\psi + \mathbf{e}_z)) \tag{2.9}$$

where $\eta = S_w S_s + \theta_s(dS_w/d\psi)$ is the general storage term, S_w is the water saturation defined as θ/θ_s ,θ is the volumetric moisture content, θ_s is the saturated moisture content, S_s is the aquifer specific storage coefficient, ψ is pressure head, $\mathbf{e}_z$ is the vector $(0,0,1)^T$ (positive upward), and the hydraulic conductivity tensor is expressed as a product of the saturated conductivity K_s and the relative conductivity $K_r(\psi)$. K_s corresponds to hydraulic conductivity k of the HSB and KW models. The nonlinear unsaturated zone characteristics are described using the Brooks-Corey relationships [*Brooks and Corey*, 1964]:

$$\begin{aligned} S_e(\psi) &= (\psi_c/\psi)^{\beta}, & \psi < \psi_c \\ S_e(\psi) &= 1, & \psi \geq \psi_c \end{aligned} \tag{2.10}$$

and

$$\begin{aligned} K_r(\psi) &= (\psi_c/\psi)^{2+3\beta}, & \psi < \psi_c \\ K_r(\psi) &= 1, & \psi \geq \psi_c \end{aligned} \tag{2.11}$$

where S_e is the effective saturation, defined as $(\theta-\theta_r)/(\theta_s-\theta_r)$, θ_r is the residual moisture content, β is a constant representing the pore size distribution index, and ψ_c represents the capillary fringe height. The RE model used in this work is the subsurface module of a coupled surface-subsurface numerical model [*Bixio et al.*, 2000] using a tetrahedral finite element discretization in space, a weighted finite difference scheme in time, and Newton or Picard iteration to resolve the nonlinearity [*Paniconi and Putti*, 1994]. It can be applied to hillslopes and subcatchments of arbitrary geometry, and handles heterogeneous parameters and boundary conditions, including atmospheric forcing and seepage faces.

2.4 Experiment setup

2.4.1 Nine characteristic hillslopes

To evaluate hillslope hydrologic response as a function of profile and plan curvature we apply the HSB, KW, and RE models to a set of nine characteristic hillslopes. The nine characteristic hillslopes consist of three divergent, three straight and three convergent hillslopes with profile curvature varying from convex to straight to concave. The same hillslope parameterization as in *Troch et al.* [2002] is used, with the exception that slope length is measured parallel to the bedrock and is set at $L = 100$ m for all slopes.

It has been reported in the literature that for high slope inclination the kinematic wave assumption becomes valid [*Beven*, 1981; *Henderson and Wooding*, 1964; *Woolhiser and Liggett*, 1967] and that the Boussinesq equation is applicable for settings in which there are relatively shallow highly conductive soils [*Childs*, 1971; *Freeze*, 1972a; *Sloan and Moore*, 1984]. To thoroughly test the different approaches and to assess the limits within which they are valid, simulations on the nine hillslopes are carried out for gentle (5% bedrock slope) and steep slope types (30% bedrock slope). A three-dimensional view of the nine hillslopes and the two-dimensional plot of contour lines and slope divides is given in Figure 2.2. The hillslopes have a flow path of length $L = 100$ m and soil depth is set at $d = 2$ m, corresponding to a relatively shallow unconfined aquifer. Hillslope response can be studied by performing either free drainage experiments after initial (partial) saturation, or constant recharge experiments to equilibrium. In *Troch et al.* [2002] it is noted that for a kinematic wave model, drainage response and recharge experiments contain the same information of the hydrological model, since outflow and storage changes in both cases can be converted to overlapping functions in space and time by means of dimensional analysis. In this work we have therefore selected drainage response experiments for a first assessment of the characteristic response of the three different hydrological models.

2.4.2 Discretization

In this study for the RE simulations the hillslopes were discretized using $\triangle x = L/200 = 0.5$ m and $\triangle y = w(x)/6$ m, giving a surface mesh of 2400 triangles. The vertical coordinate was discretized with $\triangle z = d/40 = 0.05$ m yielding a total of 288000 tetrahedra. For the HSB simulations Equation 2.7 is discretized in the spatial coordinate ($\triangle x = 0.5$ m) and then solved using a variable-order ordinary differential equation solver based on the numerical differentiation formulas. For the KW model analytical solutions obtained by *Troch et al.* [2002] were used.

2.4.3 Initial and boundary conditions

For all models we impose as an initial condition a uniformly distributed water table height along the hillslopes. Water table height is set to $\overline{h} = 0.40$ m (20% of the storage capacity), for all models. We selected these initial conditions in order to avoid occurrence of saturation on the hillslopes, enabling us to investigate subsurface processes alone in almost all cases. For the RE model an initial condition of vertical hydrostatic pressure distribution was used, with a water table height at 0.40 m vertically above bedrock level, giving a pressure head value of -1.6 m at the hillslope surface and 0.40 m at the bedrock. Note that for the RE model the water table is at 0.40 m above the bedrock whereas the boundary of the saturated zone is at a higher level, due to the water bound in the capillary fringe zone.

For all models the bedrock, hillslope crest and lateral hillslope divides are treated as zero-flux boundaries. At the outlet free drainage conditions apply for all models: storage and consequently also water table height is assigned a fixed value of zero (Dirichlet-type boundary condition) for the HSB and the KW models. For the RE model the bottom layer of nodes at the outlet have a constant head boundary of zero pressure head. To keep the boundary conditions as close to those of the HSB and KW model, the nodes in the layers above are assigned a zero-flux condition. Consequently, only the most downslope node(s) form an outlet for soil moisture for all three models.

2.4.4 Parameterization

In the simulations presented in this paper parameters are used that correspond to those of a highly conductive sandy loam soil [*Bras*, 1990]: $k = K_s = 1$ m/h, $\theta_s = 0.30$, $\theta_r = 0$, $\beta = 3.3$, $\psi_c = -0.12$ m, and $S_s = 0.01$ m^{-1}. The drainable porosity parameter f in the HSB and KW models is an ambiguously defined parameter that in most cases serves the purpose of representing some of the effects of the unsaturated zone. This parameter may be interpreted as the fraction of the total soil volume (matrix and pore space) that is available for transport of soil moisture. Typically, drainable porosity is estimated as the volume of water that an unconfined aquifer releases from or takes into storage per unit aquifer area per unit change in water table depth [*Bear*, 1972]. In this study the drainable porosity is fitted as [*Paniconi et al.*, 2003],

$$f = \theta_s \cdot V_{tfinal}/V_i \tag{2.12}$$

where θ_s is saturated moisture content (which is treated as being equal to porosity), V_{tfinal} is the cumulative volume of water drained from the hillslope in a steady state situation at the end of simulation and V_i is the initial volume of water present in the soil calculated on the basis of the results of the RE model. The drainable porosity is a dynamical parameter that is dependent on hillslope shape, initial conditions and other factors, and therefore values for f are different for all hillslopes and simulation settings. In Table 2.1 the values for f that were used to run the HSB and KW models are listed for the nine hillslopes, and we note that all porosity values are in the range $[0.25, 0.30]$ except for the 30% hillslope number 1, for which a lower value is likely due to the extremely slow subsurface drainage of the hillslope.

2.4.5 Dimensional analysis

Differences exist in hydrological system behavior (i.e. hydrographs, storage profiles) on gently sloping hillslopes compared to steep slopes. The same holds for hillslopes with differences in conductivity, soil depth, hillslope length and for simulations with different initial conditions. In order to generalize the results a dimensional analysis is conducted. A dimensionless representation will lead to model results that are "scaled" for the parameters mentioned above. The work of *Troch et al.* [2002] shows that for the kinematic wave case, simulation results under different conditions (i.e. varying slope angle, recharge rate, soil properties etc.) all collapse into a single characteristic response function, when the appropriate dimensionless variables are selected. We define the following dimensionless variables:

$$
\begin{aligned}
\tau &= \frac{tk\bar{i}}{fL} \\
\chi &= 1 - \frac{x}{L} \\
\chi &= \frac{x'}{L} \\
\phi &= \frac{Qcum(t)}{V_i} \\
\sigma = \frac{S(x,t)}{S_c(x)} &= \frac{\bar{h}(x,t)}{d}
\end{aligned}
$$

where $\bar{i}$ is the average bedrock slope (in this work 5% or 30%), defined as

$$\bar{i} = \frac{1}{L}\int_0^L i(x)\mathrm{d}x$$

$Qcum(t)$ is cumulative flow volume up to time t:

$$Qcum(t) = \int_0^t Q(t)\mathrm{d}t$$

where $Q(t)$ is the outflow at the outlet, and $S_c(x) = f \cdot w(x) \cdot d$ is the storage capacity at a given position on the hillslope. The variable τ defines kinematic time [*Ogden and Watts*, 2000] generalized for varying values for f as in [*Beven*, 1981], χ defines flow distance as a fraction of the total length of the flow path L,

Table 2.1: Drainable porosity values (in %) for the nine characteristic hillslopes used in this study. The superscript indicates hillslope number. The left number within a cell corresponds to results obtained on the 5% slopes, and right number corresponds to the 30% results.

$^{\mathbf{1}}$ 26 , 22	$^{\mathbf{2}}$ 27 , 26	$^{\mathbf{3}}$ 25 , 26
$^{\mathbf{4}}$ 28 , 26	$^{\mathbf{5}}$ 28 , 27	$^{\mathbf{6}}$ 28 , 29
$^{\mathbf{7}}$ 28 , 27	$^{\mathbf{8}}$ 28 , 28	$^{\mathbf{9}}$ 28 , 30

and ϕ and σ are the new dimensionless flow and storage variables respectively. Note that the variable χ is defined differently for the KW model, when compared to the HSB and RE models, since the x'-axis of the KW model differs from the x-axis of the HSB and RE models: the x'-axis is horizontal, originates from the hillslope crest, and is positive in the direction of the outlet, whereas the HSB and RE x-axes originate from the outlet and are positive slope upward. To intercompare the results the HSB and RE χ-axes have been reversed by using the relationships above.

As the values of saturated conductivity k and average bedrock slope $\bar{i}$ increase, and the values of drainable porosity f and hillslope length along the flow path L decrease, the hydrological system will drain more rapidly. Mapping the variables onto a dimensionless time space using time variable τ causes a scaling ("compression" or "stretching") of the time axis, which facilitates comparison of the results obtained, since results are scaled for convective processes and consequently also scaled for the kinematic component in the flow process. If no overland flow occurs, differences between dimensionless outflow hydrographs $\phi(\tau)$ and dimensionless storage plots $\sigma(\chi, \tau)$ can thus be ascribed to diffusion processes. The flow variable ϕ can be regarded as the fraction of the total initial soil water storage that has drained from the hillslope up to kinematic time τ, and the storage variable σ is the saturation fraction for a given time and point on the hillslope. Note that for the HSB and KW models initial volume of stored water is defined as $V_i = A \cdot f \cdot \overline{h}(x, 0)$, where A is the slope surface area, whereas for the RE model it is defined as $V_i = V_{tfinal}$. The rationale behind using total cumulative flow volume instead of V_i as a basis for calculating the dimensionless flow value for the RE model is that for the RE model, a fraction of the initial storage will be retained in the hillslope as residual unsaturated storage. Values for V_{tfinal} are slope and simulation dependent and are directly related to drainable porosity values through Equation 2.12.

2.5 Drainage response

2.5.1 Introduction

We will analyze the spatio-temporal behavior of the three models using pseudocolor plots of (dimensionless) storage patterns $\sigma(\chi, \tau)$ and dimensionless hydrographs $\phi(\tau)$. In these figures the value of $\sigma(\chi, \tau)$ is indicated by color: low values tend towards the blue end of the spectrum whereas the higher values tend towards the red end. A scaling bar is depicted next to all plots. Note that for maximum detail three different types of scaling are applied: for the convergent slopes (i.e. slope numbers 1, 4, and 7) the values for σ range up to 0.6, for the straight slopes (i.e. 2, 5, and 8) up to 0.4 and for the divergent slopes (i.e. 3, 6, and 9) up to 0.2. Looking at an individual figure, a horizontal transect for a given kinematic time τ will show a saturation fraction σ over the hillslope length fraction χ. A vertical transect of the figures for a given χ shows a dimensionless stage hydrograph: the variation of saturation fraction in kinematic time τ at a given location χ on the hillslope. In all the plots the outlet of the hillslopes is at

$\chi = 1$, and the top at $\chi = 0$.

An important note on the different coordinate systems for the models was made in *Paniconi et al.* [2003], where it was shown that despite some differences in hillslope configuration for the HSB and RE models, the models are fully comparable. This also holds for the comparison of the HSB and RE models with the KW model. The KW model has no diffusion dynamics, making the outflow hydrograph and storage patterns solely dependent on hillslope geometry once the appropriate dimensionless variables have been selected.

2.5.2 Interpretation of the KW storage profiles for 5% and 30% bedrock slope

In Figure 2.3a the dimensionless storage patterns of the KW models are depicted for all nine hillslopes for a bedrock slope of both 5% and 30% and different drainable porosity values. Due to the selection of appropriate (kinematic) dimensionless variables, storage patterns for the 5% and 30% bedrock slopes and for different drainable porosity values all can be collapsed into one σ profile. On all nine slopes we see a clear propagation of a discontinuity in σ in the χ, τ-domain without any diffusion characteristics. After initiation of the simulation we can trace the tail of the wave by looking at the line that divides the blue area (zero storage) from the rest (non-zero values). Note that the inverse of the tangent to this divide in the χ, τ-domain is a measure of dimensionless wave velocity (celerity). Also note that for equal profile curvature the propagation of the tail of the wave is identical. For slope numbers 1, 2 and 3 we see that the tail velocity decreases as τ and χ increase, since the slope steepness decreases near the outlet (i.e. concave slope profile). For the straight profile shapes (i.e 4, 5 and 6) we see a constant tail velocity and for the convex profiles (i.e. 7, 8 and 9) we get an increase in tail velocity as χ and τ increase. Note that for the convex profile shapes, the wave shape tends to disperse and the σ profiles tend to flatten out, as can be seen for slopes 8 and 9. For slope 7 however we see an accumulation, especially in the middle segment of the hillslope, due to a convergent slope shape. Whereas the velocity of the wave is determined by bedrock slope, the storage values are determined by both plan curvature (through the width function) and profile curvature.

2.5.3 Interpretation of storage profiles for 5% bedrock slope

In Figure 2.3b the dimensionless storage profiles for the HSB model when applied to a 5% bedrock slope are depicted . Foremost we notice that the wave front is less pronounced than for the KW model. Due to diffusion, strong gradients in storage values (and consequently in σ values) tend to smoothen out. This effect is clearest for hillslopes 1, 2, 3, 4 and 7 where σ values are significantly lower than for the KW model. For slopes 1 to 3 concavity of profile shape causes strong gradients in storage value (and consequently large effect of diffusion) and for slopes 1, 4 and 7 the effect is caused by convergence of plan shape. Consequently, the diffusive effect of profile curvature on σ profiles is amplified on slope number 1. Slopes 5, 6, 8 and 9 show a relatively good resemblance to the KW results due to low gradients and consequently a marginal effect of diffusion. This is best illustrated looking at hillslope 5, where results are very similar to the KW results except for the front and rear end of the wave where strong gradients cause diffusion in the HSB results, whereas the KW model shows the expected ramp function during drainage. Note that for the front end (at the outlet), gradients are a result of the imposed boundary condition $\sigma(1, \tau) = 0$.

It is interesting to compare the results of these relatively simple one-dimensional models (Figures 2.3a and 2.3b) to the results of the more complex three-dimensional RE model when applied to 5% hillslopes (Figure 2.3c). The RE results show a remarkable match with the results obtained with the HSB model for all hillslope shapes. On the convergent slopes (1, 4 and 7) we notice slightly higher σ values and a small delay in drainage for the RE model compared to the HSB results. On the divergent slopes (3, 6 and 9) the HSB model produces slightly higher σ values and a somewhat faster drainage. Some irregularities for low σ values are visible in Figure 2.3c on slopes 2 and 3 in particular. They are caused by numerical difficulties in solving the strong nonlinearity in the Brooks-Corey relations for small pressure head values. This implies that a finer spatio-temporal discretization is required for the RE simulations, especially for the steeper slopes discussed next.

2.5.4 Interpretation of storage profiles for 30% bedrock slope

The drainage response on the 30% hillslopes using the HSB model and the RE model is depicted in Figures 2.3d and 2.3e respectively. Figure 2.3e displays numerical irregularities more clearly than for the 5% RE hillslopes: practically all slopes now show small wiggles in the σ values. When Figures 2.3d and 2.3e are compared, we again see a very good agreement in the shape of storage profiles in the spatial as well as the temporal dimension (ignoring the numerical oscillations). Unlike for the 5% hillslopes we now obtain the best match for the convergent and straight hillslopes, although the RE model shows a slightly more diffused pattern. On the divergent slopes the HSB model has structurally higher storage values than the RE model, but the shape of the storage profiles and the timing of the storage peaks in the χ, τ-domain are in good agreement. This was also ascertained in [*Paniconi et al.*, 2003] for simulations on slopes with a straight profile shape (i.e. no profile curvature). This behavior may be caused by the relatively large effect of the unsaturated zone on these slopes due to low storage values.

2.5.5 Comparison of storage profiles for 5% and 30% bedrock slope

When Figures 2.3d and 2.3e (30% hillslopes) are compared to Figures 2.3b and 2.3c (5% hillslopes), we notice that the former two show overall higher σ values. This is caused by the fact that on all 30% hillslopes despite high gradients in storage values the effect of diffusion on storage and flow is relatively small when compared to the effect of increased convection due to high values for bedrock slope. The small response times on the 30% hillslopes do not allow for diffusion to take full effect. This results in an increased accumulation of storage in the 30% case. On the 5% hillslopes however, these counter balancing processes of convection and diffusion are more dominated by diffusion. A clear indication thereof is that hillslope 1 for 30% bedrock slope generates overland flow, whereas no overland flow occurs on the 5% hillslopes (see Figures 2.3d and e: the saturated area is enclosed by a black line). The HSB model generates overland flow for $46 \leq \tau \leq 125$, the RE model for $72 \leq \tau \leq 122$, and the KW model for $42 \leq \tau \leq 166$. The KW results also show a small saturated area on hillslope 4 for 30% bedrock slope for $81 \leq \tau \leq 100$. The large saturated area in the KW simulations is caused by the low flow values at the outlet. Due to the absence of a flow component driven by gradients in water tables in the KW model, water accumulates at the outlet when the plan shape is convergent or when the local bedrock slope is small. In general the effect of an increased storage accumulation is clearest for the convergent slopes where the width function intensifies the accumulation process, and less pronounced for the divergent slopes where also due to the width function diffusion remains a relatively important process. Thus, the resemblance of the σ profiles of both models for the 5% compared to the 30% slopes is clearest for divergent slopes. When the storage profiles of the 5% slopes (Figures 2.3b and c) are compared to those of the 30% slopes (Figures 2.3d and e) and the KW results (Figure 2.3a), we notice that the profiles for the steep slopes show a better match to the KW profiles than the 5% profiles. Illustrative of this is the comparison of slope numbers 2, 3 and 4 in Figures 2.3a, b, and d, also indicating that diffusion on the 30% slopes has less impact on flow and storage of soil water than on the 5% slopes, as expected.

2.5.6 Comparison of hydrographs for 5% and 30% bedrock slope

In Figure 2.4 we analyze the (dimensionless) hydrographs of both simulation settings (i.e. 5% and 30% bedrock slope) and three models (i.e. KW, HSB and RE) for the nine characteristic hillslopes. We note that the KW model has the fastest response for all hillslope types and all bedrock slopes. The HSB hydrograph shows a fast initial climb for hillslope 1 in particular, which originates from the fact that the HSB model produces more overland flow than the RE model on the 30% slopes, thus draining more rapidly initially. Furthermore it appears that for slope numbers 5, 6, 8 and 9 the KW, HSB and the RE model show a remarkably good match. The hydrographs of slopes 2, 3 and 7 show that the HSB and RE results match well, but despite the dimensionless representation the 5% and 30% results differ slightly, indicating that the effect of diffusion varies for different bedrock slopes. The shape of the hydrographs of the RE and the HSB model are remarkably similar in shape but somewhat displaced‘ in time, indicating a delayed yield of the RE model probably caused by the capillarity effect of the soil.

2.6 Discussion and conclusions

In this paper we have generalized the hillslope-storage Boussinesq model to non-constant bedrock slope and we have conducted an comparison of a Richards equation based (RE) model, taken as a benchmark, with the generalized hillslope-storage Boussinesq (HSB) and hillslope-storage kinematic wave (KW) models in order to investigate within which settings application of the KW and HSB models is valid. In relation to the validity of applying a KW model we can conclude that it is limited to simulation settings in which hydraulic diffusion has a marginal impact on storage. The impact is determined by water table gradients and bedrock slope. When water table gradients are high and bedrock slope is relatively small, diffusive components are predominant, which is the case for the convergent hillslopes and gentle bedrock slopes in this study. On these hillslopes the KW model shows the poorest match to the HSB and RE models. For the straight and divergent slopes with a high bedrock slope, the ratio between water table gradient and bedrock slope is low, making convection the predominant process and a kinematic wave approximation increasingly accurate. Gradients in storage profiles or water tables are determined by a combination of slope inclination, plan shape, and profile curvature. When the flow process is divided into a convective and a diffusive part, we conclude that the relevance of the diffusive component does not solely depend on slope steepness, but also on water table gradients. The importance of this last conclusion is that it refutes a widespread belief that has been based on analysis of straight, unit-width slopes, namely that bedrock slope alone determines the validity of the KW assumption. A new criterion to determine validity of the KW assumption should therefore be developed.

The most general conclusion with respect to the validity of the HSB model is that it provides a broadly accurate description of subsurface storage profiles and subsurface flow in a hillslope of arbitrary geometrical shape, in the same way as the HSB equation for straight slopes was found to be accurate [*Paniconi et al.*, 2003].

On a more specific case by case basis, a dimensionless representation enabled us to investigate the influence of diffusion in different simulation settings. We conclude that the results of the three models on the 5% and 30% slopes in dimensionless representation show the best agreement in terms of storage profiles as well as hydrographs on divergent slope types due to a relatively low influence of diffusion, and the poorest agreement on convergent slopes because of high diffusivity. For convergent slope forms the KW model loses its ability to accurately describe water tables and hydrographs, whereas the HSB model remains close to the RE solution in all simulations. Analyzing the shape of the RE and HSB hydrographs in particular, we see that the shapes are very similar but the RE hydrograph is delayed. This is caused by capillarity effects of the soil. An extension of the HSB and KW model with a component describing the unsaturated zone is expected to improve model results significantly.

A basic assumption underlying the hillslope-storage concept is that subsurface flow can be described by saturated flow processes only. This implies that the unsaturated zone is not expected to have a large influence on the flow process. A second assumption is that movement of water through the soil down the hillslope is parallel to the underlying impervious layer (i.e. second Dupuit-Forchheimer assumption). This requires marginal head differences perpendicular to the hillslope bedrock. Both assumptions are only valid for relatively shallow, highly conductive soils. This limits the application of models based on the Boussinesq equation to these settings. When the application of the HSB or KW model is valid, the advantages of these models compared to RE models are significant, and include computational efficiency, numerical robustness, scope for analytical or other simplified formulations, and low-dimensionality (implying easier parameterization and calibration).

For the model simulations presented in this paper, soil properties (e.g. hydraulic conductivity, soil depth, drainable porosity) are considered to be spatially uniform over the hillslope domain and constant in time. Ongoing research is focussed on investigating the impact of spatio-temporal variation of the model parameters and extension of the model to incorporate processes as overland flow and macropore flow.

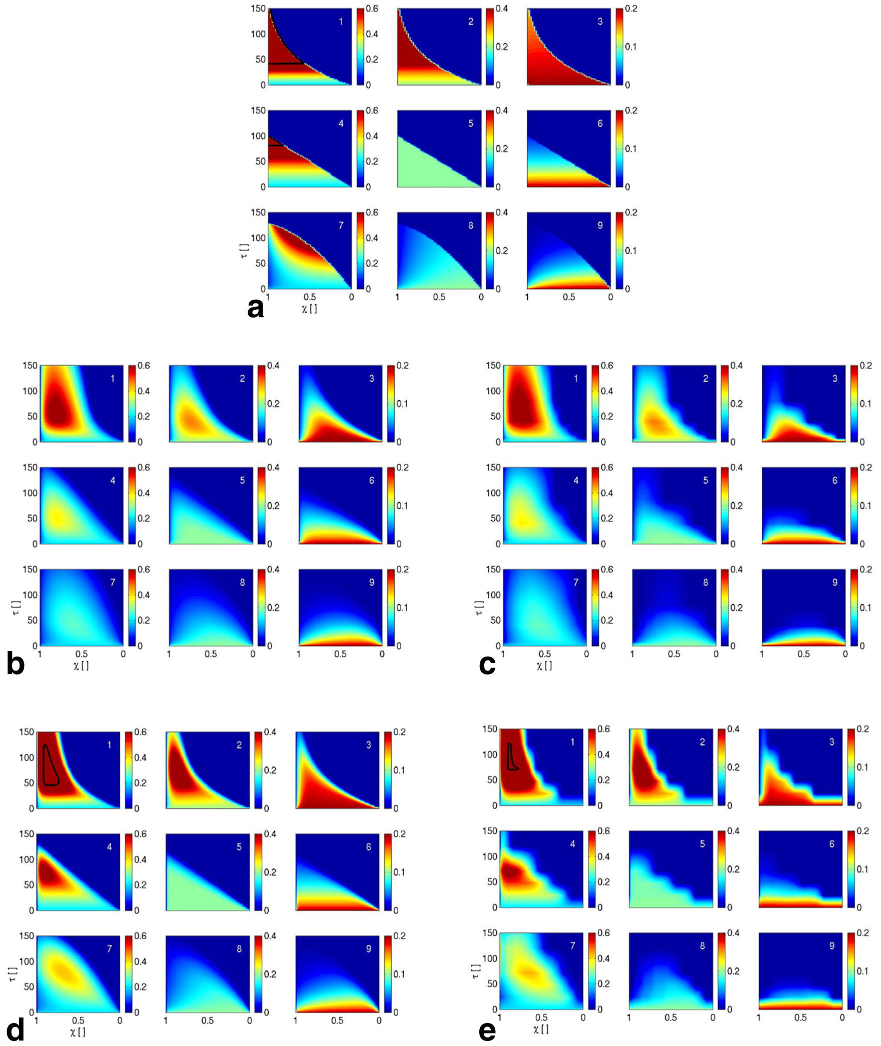

Figure 2.3: Dimensionless storage patterns for free drainage scenarios for a) the KW model (5% and 30% bedrock slope), b) the HSB model, (5% bedrock slope), c) the RE model, (5% bedrock slope), d) the HSB model, (30% bedrock slope), and e) the RE model, (30% bedrock slope). The black lines in Figures a), c), and d) indicate and enclose the saturated areas in the χ, τ-domain. In Figure a) the saturated area only occurs for a bedrock slope of $i = 30\%$.

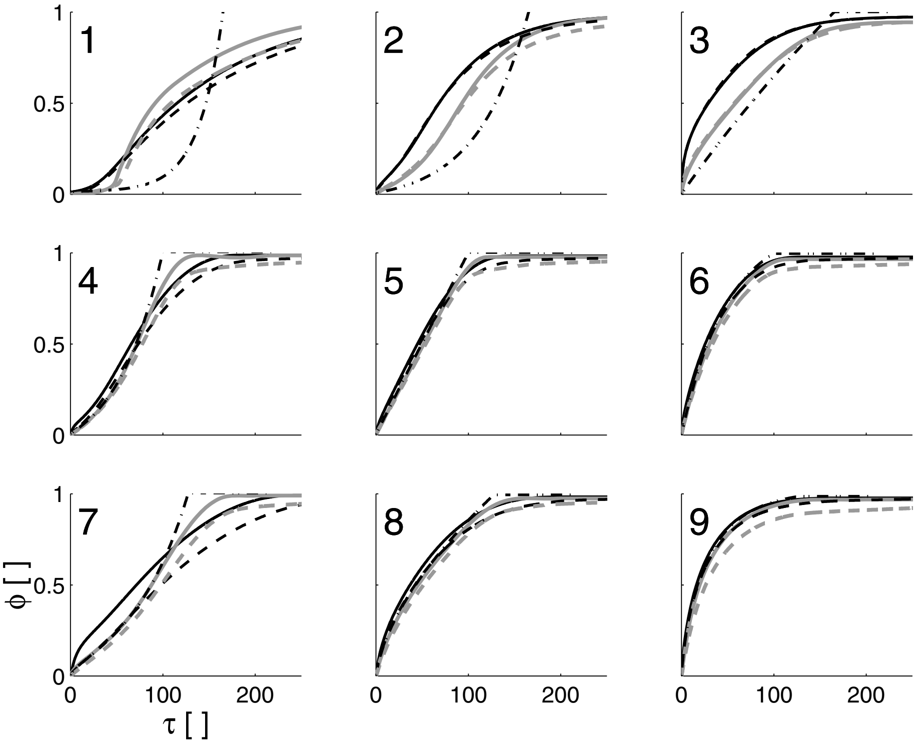

Figure 2.4: Dimensionless hydrograph for a free drainage scenario of the KW (5% and 30%), HSB and RE model for nine characteristic hillslopes for 5% and 30% bedrock slope. Black lines correspond to the results for 5% bedrock slope, and gray lines to those for 30%. Solid lines correspond to the HSB results, and dashed lines to the RE results. The black dash-dotted lines corresponds to the results of the KW model for 5% and 30% bedrock slope.

Chapter 3

Storage-dependent drainable porosity for complex hillslopes

Abstract

In hydraulic groundwater theory, the parameter drainable porosity f (a storage coefficient that accounts for the effect of the unsaturated zone on water table dynamics) is usually treated as a constant. For shallow unconfined aquifers the value of this parameter, however, depends on the depth to the water table and the water retention characteristics of the soil. In this study, an analytical expression for f as a function of water table depth is derived under the assumption of quasi steady-state hydraulic equilibrium, in this way accounting in part for the effects of the unsaturated zone on groundwater dynamics. The derived expression is implemented in the nonlinear hillslope-storage Boussinesq (HSB) model [*Troch et al.*, 2003] to simulate the drainage response of complex hillslopes. The model's behavior is analyzed by comparison to (i) the HSB model with a constant value for f, and (ii) measurements of water tables and outflow hydrographs on a 6.0x2.5x0.5 m laboratory hillslope experiment. The comparison is conducted for a pure drainage case on two different hillslope shapes (linearly convergent and divergent) and for three different slope inclinations (5%, 10%, and 15%). Comparison (i) is run in an uncalibrated and a fully calibrated mode and it enables us to evaluate the effect of a dynamic, state-dependent value for f on model output. Comparison (ii) allows us to test the HSB model on several hillslope configurations and to analyze whether the concept of a storage-dependent f enhances the model performance. The comparison of the HSB models to the measurements from the laboratory hillslopes shows that it is possible to capture the general features of the outflow hydrograph during a drainage experiment using either one of the HSB models. Overall the original (constant f) HSB model, with one fitting parameter more than the revised HSB model, shows a slightly better fit on the hydrographs when compared to the revised (variable f) HSB model. However the peak outflow values (the first few minutes after initiation of the experiments) are better captured by the revised HSB model. The revised HSB model's performance in simulating water table movements is much more accurate than that of the original HSB model. The improved match of the revised HSB model to piezometric measurements is worth stressing because the ability to model water tables is a key attribute of the model, making it possible to investigate phenomena such as saturation excess runoff. Also noteworthy is the good match between the revised HSB model and the outflow measurements, without any calibration, for the divergent slopes. The changing values of the

calibrated drainable porosity parameter for the original HSB model as different configurations are simulated (slope angle, plan shape, initial conditions), together with the ability of the revised HSB model to more accurately simulate water table dynamics, clearly demonstrates the importance of regarding drainable porosity as a dynamic, storage-dependent parameter.

This chapter is based on the paper “Hilberts, A.G.J., P.A. Troch and C. Paniconi, Storage-dependent drainable porosity for complex hillslopes, *Water Resources Research, 41*, W06001, doi:10.1029/2004WR003725, 2005.”

3.1 Introduction

Within its range of validity, Richards equation [*Richards*, 1931] provides the most accurate description of flow processes through variably saturated porous media. However, in catchment and hillslope hydrological modeling practices, the application of Richards' equation is generally cumbersome due to difficulties in the parameterization of the equation, and due to the typically large computational time that is required for solving the equation. For this reason much research has been devoted to investigating the possibility of using simpler models (analytical and numerical) that still reflect the true physical behavior of a catchment or a part thereof (e.g., *Beven* [1981]; *Duffy* [1996]; *Fan and Bras* [1998]; *Hogarth et al.* [1999]; *Ogden and Watts* [2000]; *Parlange et al.* [2001]; *Stagnitti et al.* [1986]; *Troch et al.* [2002, 2003]; *Woods et al.* [1997]; *Zecharias and Brutsaert* [1988]). The drainable porosity parameter (also in some cases referred to as specific yield) is introduced in hydraulic groundwater equations for the purpose of mass conservation, i.e., matching the modeled outflow volumes to groundwater table dynamics, thereby accounting in some way for capillarity and unsaturated zone effects. It is generally treated as a parameter with a constant value. However, studies carried out under nearly-saturated conditions (e.g. *Abdul and Gillham* [1989]; *Gillham* [1984]), and preliminary results from our recent experimental work on a laboratory hillslope suggest that this parameter varies in time and space, which indicates the influence of storage dynamics in the unsaturated zone on the hydraulic groundwater model. Moreover, in *Paniconi et al.* [2003] and *Hilberts et al.* [2004] (where comparisons are made with a three-dimensional Richards based model) it is shown that the water table dynamics and outflow rates are sensitive to this parameter value. The preliminary experimental results mentioned above, and the conclusions from the comparison to a three-dimensional Richards equation based model in the papers motivate us to search for an appropriate (analytical) expression that links the drainable porosity to the state of the (unconfined) aquifer. Our intention is to investigate the possibility of capturing some of the unsaturated zone's influence on groundwater movement by introducing a physically-based description of the drainable porosity parameter.

In the literature we find two slightly different definitions of drainable porosity or specific yield for unconfined aquifers. *Johnson* [1967] and *Bear* [1972] define specific yield as (i) the ratio of the volume of water that a saturated rock or soil will yield by gravity to the total volume of the rock or soil. These authors consider the yield starting from complete saturation to complete gravitational drainage, and it is thus regarded as an aquifer property. In *Luthin* [1966], *Freeze and Cherry* [1979], *Neuman* [1987], and *Dingman* [2002] however, specific yield is defined as (ii) the volume of stored groundwater released per unit area per unit decline of water table. This definition implies a parameter that is dependent on the state (water table position) of the system. *Bear* [1972] summarizes by noting that the parameter as defined under (ii) is the drainable porosity and is sometimes used to denote the "instantaneous" specific yield. In this paper, Bear's definition for drainable porosity as defined in (ii) is adopted, and it can therefore be expressed as

$$f = \frac{v}{\triangle h'} \tag{3.1}$$

where v is the amount of water drained (i.e. drainage volume per unit surface area) $[L]$, and h' is the water table elevation above an arbitrary horizontal datum $[L]$. The vertical water table height is indicated with a prime because the coordinate system will in this paper be changed to water tables measured perpendicular to the bedrock. Although often treated as such, drainable porosity is not a static soil characteristic: it typically changes during the course of a rainfall or drainage event (e.g. *Moench* [2003]; *Szilagyi* [2004]; *Tritscher et al.* [2000]; *Weiler and McDonnell* [2004]). It has been reported that the drainable porosity is a function of soil moisture conditions in the unsaturated zone above the water table [*Bear*, 1972; *Hillel*, 1980; *Luthin*, 1966]. More specifically, *Kim and Bierkens* [1995] (in reply to *Su* [1994]) suggested to regard the drainable porosity parameter that was used in a Boussinesq-type model as a function of the groundwater level under the assumption of hydraulic equilibrium conditions in the unsaturated zone. In *Bierkens* [1998] drainable porosity was directly linked to the depth to the water table for the case of horizontal bedrock. In *Nachabe* [2002] the concept is put forward that for shallow unconfined aquifers the drainable porosity (i.e., transient or instantaneous specific yield) can be significantly influenced by capillarity effects, especially in early stages of drainage experiments. Other studies that have examined capillary fringe effects on subsurface dynamics, both theoretically and experimentally, include *Parlange and Brutsaert* [1987], *Parlange et al.* [1990], *Fink et al.* [2001], *Walter et al.* [2000], and *Nielsen and Perrochet* [2000]. *Nachabe* [2002] describes a relationship between drainable porosity and depth to the water table, including effects of delayed drainage for rapidly moving water tables using a Brooks-Corey parameterization for the unsaturated zone. Except for *Bierkens* [1998] and *Nachabe* [2002], the literature provides little theoretical work that quantitatively links drainable porosity to moisture content, suction head, or water table height. Moreover, the classical techniques and methods to determine drainable porosity experimentally are a topic of discussion. Different methods often lead to results that differ by as much as an order of magnitude in the early stages of drawdown experiments [*Heidari and Moench*, 1997; *Moench*, 1994; *Neuman*, 1987; *Nwankwor et al.*, 1992].

Tritscher et al. [2000] showed the dependency of drainable porosity on the degree of saturation under a variety of conditions. Both this study and *Nachabe* [2002] draw the conclusion that the drainable porosity can be strongly influenced by water table depth. In *Tritscher et al.* [2000], the authors report differences as high as a factor 100 between the drainable porosity values for the deepest versus the shallowest water tables. In view of these previous studies, the question arises as to how varying values of drainable porosity affect the (modeled) water table movements and outflow patterns.

In this paper we first derive an analytical expression for drainable porosity as a function of water table depth. By assuming a vertical hydrostatic soil water pressure distribution in the unsaturated zone, we express drainable porosity as a storage-dependent variable (that is, as a function of water table depth and the hydraulic parameters of the soil) for horizontal and sloping bedrock types.

The derived expression is then implemented in the physically based nonlinear "hillslope-storage Boussinesq" (HSB) model as developed by *Troch et al.* [2003], *Paniconi et al.* [2003], and *Hilberts et al.* [2004]. This implementation enables us to test the validity of the derived equation and also allows for an analysis of the effect of variability in the drainable porosity value on the dynamic hydrological behavior of a physically-based model. The model results are evaluated by comparing them to i) the results of the original (constant f) nonlinear HSB model to explicitly assess the effect of storage-dependent drainable porosity, and ii) to measurements of water tables and outflow rates on a scaled hillslope laboratory experiment of 6.0x2.5x0.5m. By comparison to laboratory measurements we are able to assess whether the HSB model is capable of reproducing water table movements and outflow patterns, and if the concept of storage-dependent drainable porosity offers any advantages in terms of accuracy when compared to the original HSB model.

3.2 Drainable porosity and groundwater storage

3.2.1 Storage in the saturated and unsaturated zone for a horizontal bedrock

In an unconfined aquifer a drainage event causes the water table to move downward, thereby decreasing the size of the saturated zone and enlarging the unsaturated zone. Consequently, drainage of groundwater can result in a decrease in groundwater level directly and in changes in storage in the unsaturated zone. Assuming there is no recharge, we can define the drainable porosity as the change in total storage with respect to a unit change in water table depth. However, the choice of the length of a "unit change" is undefined and arbitrary. A clearer definition is obtained when taking the limit case in Equation 3.1 of f for $\triangle h' \rightarrow 0$, from which we obtain the expression

$$f(\psi, h') = \frac{\mathrm{d}s}{\mathrm{d}h'} \tag{3.2}$$

where $\psi = \psi(z)$ is pressure head $[L]$, t is time $[T]$, and $s = s(\psi, h')$ is the total storage of soil moisture $[L]$ (see Figure 3.1) which can be expressed as:

$$s(\psi, h') = s_1(\psi) + s_2(h') \tag{3.3}$$

where $s_1(\psi)$ is the total available storage of soil moisture above the water table $[L]$ and $s_2(h')$ is the total available storage of water in the saturated zone $[L]$. The available soil moisture storage above the water table can be expressed as

$$s_1(\psi) = \int_{h'}^{Z} (\theta(\psi) - \theta_r)\mathrm{d}z \tag{3.4}$$

where $\theta(\psi)$ is the soil water content $[-]$, z is the vertical coordinate (positive upward) $[L]$, Z is the location of the ground surface above a horizontal datum, and θ_r is the residual soil moisture content $[-]$. The integration of Equation 3.4

is taken over $(Z - h')$ which corresponds to the depth of the unsaturated zone above the water table. The storage of groundwater in the saturated zone is given by :

$$s_2(h') = (\theta_s - \theta_r)(h' - z_0) \tag{3.5}$$

where z_0 is the height of the bedrock above a given horizontal datum $[L]$ and θ_s is the moisture content at saturation. Note that we implicitly assume that water that is released as a result of compressibility of the groundwater and the porous matrix is negligible compared to the water that is released as a result of the emptying of the pore space (i.e., specific storage coefficient is equal to 0).

3.2.2 Integration of soil moisture curves for a horizontal bedrock

To solve Equation 3.4 we require a relationship between soil moisture content θ and suction head ψ, and a relationship between ψ and z. To solve Equation 3.2 we need an expression for storage s_1 in terms of water table depth h'. Under the assumption of zero vertical flux, and that the suction head profile changes from one steady-state situation to another over the time it takes to impose $\mathrm{d}h'$ (quasi steady-state assumption), the relationship between ψ and z is that of hydraulic equilibrium:

$$\psi = h' - z \tag{3.6}$$

This assumption is valid either when the movement of the water table is relatively slow, so that an equilibrium state can be reached above the water table [*Luthin*, 1966], or for shallow systems where redistribution of soil moisture is rapid [*Bierkens*, 1998]. The constitutive relationship between θ and ψ used in this study is the van Genuchten function [*van Genuchten*, 1980]:

$$\theta(\psi) = \theta_r + (\theta_s - \theta_r)\left\{\frac{1}{1 + (\alpha\psi)^n}\right\}^m \tag{3.7}$$

where α $[L^{-1}]$, n (> 0) $[-]$, and m $[-]$ are van Genuchten parameters. Combining Equations 3.6 and 3.7 we obtain

$$\theta(h') = \theta_r + (\theta_s - \theta_r)\left\{\frac{1}{1 + (\alpha(h' - z))^n}\right\}^m \tag{3.8}$$

Troch [1992] found that for the $\theta(\psi)$-relationship it is possible to assume that the relationship between m and n is given by

$$m = 1 + 1/n \tag{3.9}$$

instead of the more common definition $m = 1 - 1/n$ (e.g., *van Genuchten* [1980]), without losing the ability to aptly fit the soil moisture retention data for a wide range of soil types. Using Equations 3.8 and 3.9 in 3.4, we obtain a simple mathematical expression for the unsaturated zone storage s_1, given the position of the water table h':

$$
\begin{aligned}
s_1(h') &= \int_{h'}^{Z} \{\theta_s - \theta_r\} \left\{ \frac{1}{1+(\alpha(h'-z))^n} \right\}^m \mathrm{d}z \\
&= (Z - h')\,(\theta_s - \theta_r)\left(1 + (\alpha\,(h' - Z))^n\right)^{(-1/n)} \qquad (3.10)
\end{aligned}
$$

The total storage can now be expressed as

$$
\begin{aligned}
s(h') &= s_1(h') + s_2(h') \\
&= (Z - h')\,(\theta_s - \theta_r)\left(1 + (\alpha\,(h' - Z))^n\right)^{(-1/n)} \\
&\quad + (\theta_s - \theta_r)(h' - z_0) \qquad (3.11)
\end{aligned}
$$

3.2.3 Drainable porosity for a horizontal bedrock

The first order derivative of s with respect to h' yields the drainable porosity (see Equation 3.2):

$$
f(h') = (\theta_s - \theta_r)\left\{1 - (1 + (\alpha(h' - Z))^n)^{-(\frac{n+1}{n})}\right\} \qquad (3.12)
$$

Equation 3.12 is an analytical expression that relates drainable porosity to local water table depth and is dependent on the soil moisture retention characterization through the van Genuchten parameters. An analogous expression was also derived by *Bierkens* [1998] based on the integration described by *Troch* [1992]. Note that the derived expression assumes zero vertical flux. Generalizing to non-zero fluxes is possible (e.g., *Rockhold et al.* [1997]), although in this case we would not obtain closed form solutions for the storage-dependent drainable porosity.

3.2.4 Drainable porosity for a sloping bedrock

To implement the derived expression for drainable porosity for horizontal bedrock into Boussinesq-type hillslope models (e.g., *Boussinesq* [1877]; *Troch et al.* [2003]), the coordinate system has to be modified such that the water table depth is taken perpendicular to the bedrock. This can be done by substituting

$$
h' - z_0 = \frac{h}{\cos(i)} \qquad (3.13)
$$

$$
Z - h' = \frac{D - h}{\cos(i)} \qquad (3.14)
$$

into Equation 3.11, where D $[L]$ and $h(x,t)$ $[L]$ are the soil depth and the water table height measured perpendicular to the bedrock and $i = i(x)$ $[-]$ is the bedrock slope at coordinate x $[L]$ parallel to the bedrock (see Figure 3.2). From Equation 3.13 we obtain

$$
f(h) = \frac{\mathrm{d}s}{\mathrm{d}h} = \frac{\mathrm{d}s}{\mathrm{d}h'} \cdot \frac{\mathrm{d}h'}{\mathrm{d}h} = \frac{f(h')}{\cos(i)} \qquad (3.15)
$$

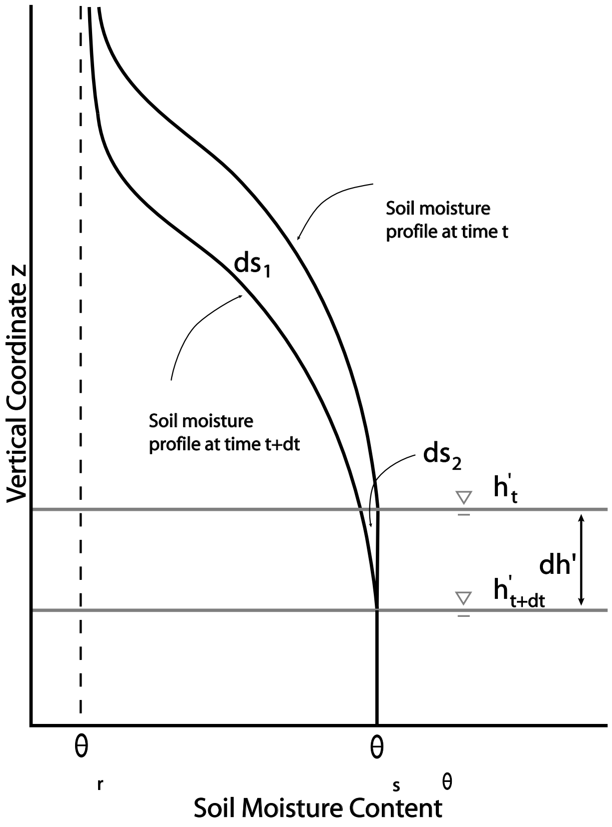
Vertical Coordinate z
Soil moisture profile at time t
ds_1
Soil moisture profile at time t+dt
ds_2
h'_t
dh'
h'_{t+dt}
θ_r
θ_s
θ
Soil Moisture Content

Figure 3.1: Sketch of hypothetical soil moisture profiles and corresponding changes in saturated and unsaturated storage, in relation to water table depth h' at two time instances (t and $t + \mathrm{d}t$).

Substitution of Equations 3.12, 3.13, and 3.14 into 3.15 yields the expression for drainable porosity that will be implemented into the HSB model:

$$\begin{aligned} f(h) &= (\theta_s - \theta_r) \\ &\cdot \left\{ 1 - \left(1 + \left(\alpha \left(\frac{h - D}{\cos(i)} \right) \right)^n \right)^{-\left(\frac{n+1}{n}\right)} \right\} \end{aligned} \tag{3.16}$$

By choosing this coordinate system we thus assume that the saturated zone fluxes are parallel to the bedrock (the extended Dupuit-Forchheimer assumption [*Childs*, 1971]), and that the relationship between outflow and water table fluctuations is characterized by drainable porosity, which in turn is dependent on the water table height and the soil water retention characteristics.

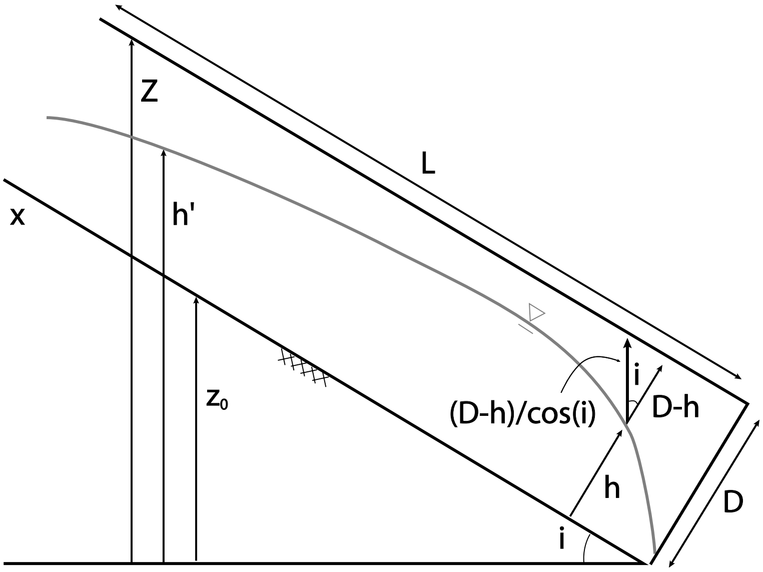

Figure 3.2: Sketch of a sloping unconfined aquifer with bedrock slope (i), water table elevation h', soil surface elevation Z, and bedrock elevation z_0, together with water table height h, depth to water table $(D-h)$, hillslope length (L), and soil depth (D) defined with respect to a reference frame perpendicular to the bedrock and parallel to coordinate x.

3.2.5 Interpretation

Under the assumption that leads to Equation 3.16 (i.e. no recharge and hydrostatic pressure distribution in the unsaturated zone), we can analyze the behavior of this expression. To interpret it let us first analyze the limit values of the function. For shallow unconfined aquifers under humid conditions (i.e. relatively high water tables), h will approach D. This limit case yields:

$$\lim_{h \uparrow D} f(h) = 0$$

For very deep aquifers with deep groundwater tables, D approaches ∞ and therefore:

$$\lim_{D \to \infty} f(h) = \theta_s - \theta_r$$

The drainable porosity for completely saturated soils is very close to 0 because an infinitesimal change in water table location will not result in any outflow, due to the binding of water in the capillary fringe. As the water table drops, the marginal effect of capillarity decreases and as a result drainable porosity values initially increase. This was also noted by *Kim and Bierkens* [1995] and *Nachabe* [2002]. When water tables are deep, a drop in water table will result in a downward shift of the soil moisture profile without a significant change of shape of the profile. Consequently the change in unsaturated storage $(\mathrm{d}s_1/\mathrm{d}h)$

will then approach 0, and the drainable porosity converges to $\mathrm{d}s_2/\mathrm{d}h = \theta_s - \theta_r$. In Figure 3.3 the drainable porosity from Equation 3.16 for a characteristic sand, loam, and clay soil is plotted as a function of the depth to the water table. The van Genuchten parameters used to produce these results are given in Table 3.1. Figure 3.3 shows that for nearly saturated conditions drainable porosity for all soil types goes to zero. For deep groundwater tables, the drainable porosity converges asymptotically to $\theta_s - \theta_r$. Because sandy soil has a low retention capacity, and consequently the range in which capillarity has a significant effect on storage is small, the maximum of f is reached relatively quickly (in terms of depth to the water table) in comparison to loam and clay soils.

3.3 Implementation of storage-dependent drainable porosity into the HSB model

The mass balance equation for a three-dimensional hillslope reads:

$$\frac{\partial S}{\partial t} = -\frac{\partial\{wq\}}{\partial x} + Nw \tag{3.17}$$

where $w = w(x)$ $[L]$ is the hillslope width at x, N is the recharge to the groundwater table $[LT^{-1}]$, $q = q(h)$ $[L^2T^{-1}]$ is the Darcy flux, and $S = S(x,t)$ $[L^2]$ is the total storage in a hillslope at time t and position x along the slope. The Darcy flux reads

$$q = -kh\left(\frac{\partial h}{\partial x}\cos i(x) + \sin i(x)\right) \tag{3.18}$$

where k $[LT^{-1}]$ is the hydraulic conductivity. The storage S is defined as [*Fan and Bras*, 1998; *Troch et al.*, 2003]

$$S = \gamma wh \tag{3.19}$$

Table 3.1: Van Genuchten parameters (regular and modified) for sand, loam, clay, and the laboratory sand.

		Regular ($\mathbf{m = 1 - 1/n}$)		
Parameter	**Sand**	**Loam**	**Clay**	**Lab sand**
$\theta_\mathbf{s}$ (-)	0.26	0.37	0.47	0.32
$\theta_\mathbf{r}$ (-)	0.01	0.05	0.16	0.05
α (1/cm)	-0.0324	-0.0161	-0.0066	-0.0630
n (-)	6.6600	2.6632	1.8601	4.4545
		Modified ($\mathbf{m = 1 + 1/n}$)		
Parameter	**Sand**	**Loam**	**Clay**	**Lab sand**
$\theta_\mathbf{s}$ (-)	0.26	0.38	0.48	0.32
$\theta_\mathbf{r}$ (-)	0.01	0.06	0.19	0.05
α (1/cm)	-0.0301	-0.0090	-0.0020	-0.0532
n (-)	5.9940	1.7608	1.1830	3.7708

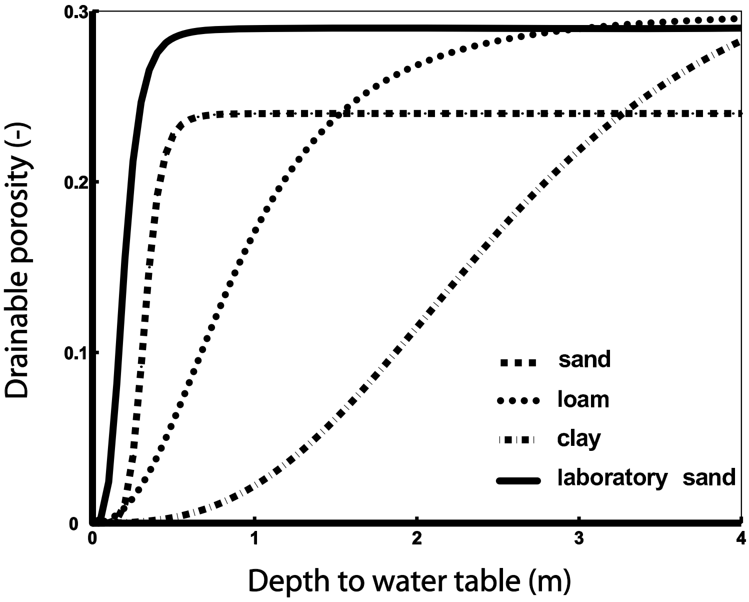

Figure 3.3: The relation between drainable porosity f and the depth to the water table under the assumption of hydrostatic pressure head conditions for four different soil types. The corresponding parameter values are given in Table 3.1.

where $\gamma = \gamma(x,t)$ $[-]$ can be regarded as the specific yield according to the definition of *Bear* [1972], and is defined as:

$$\gamma = \frac{1}{h}\int_{h=0}^{h} f \mathrm{d}h \tag{3.20}$$

which by using Equation 3.15 can also be expressed as:

$$\gamma = \frac{1}{h}\int_{h=0}^{h} \mathrm{d}s = \frac{s(h)-s(0)}{h} \tag{3.21}$$

Note that in the given context the term specific yield (γ) represents a porosity, whereas drainable porosity is actually a storage-coefficient. Note also that for a constant drainable porosity, f and γ have the same value. Substitution of Equations 3.19, 3.20, and 3.21 into 3.17 yields

$$wf\frac{\partial h}{\partial t} = -\frac{\partial\{wq\}}{\partial x} + Nw \tag{3.22}$$

or

$$\frac{\partial h}{\partial t} = -\frac{1}{wf}\frac{\partial\{wq\}}{\partial x} + \frac{N}{f} \tag{3.23}$$

which is the governing equation for the HSB model [*Troch et al.*, 2003]. Note that the parameter f is now a function of h. Equation 3.23 may be expanded, using Equation 3.18, into [*Hilberts et al.*, 2004]

$$\begin{aligned}\frac{\partial(wq)}{\partial x} &= -\left\{kw\frac{\partial h}{\partial x}+kh\frac{\partial w}{\partial x}\right\}\left\{\frac{\partial h}{\partial x}\cos i(x)+\sin i(x)\right\}\\ &- kwh\left\{\frac{\partial^2 h}{\partial x^2}\cos i(x)-\frac{\partial h}{\partial x}\frac{\partial i(x)}{\partial x}\sin i(x)+\frac{\partial i(x)}{\partial x}\cos i(x)\right\}\end{aligned} \tag{3.24}$$

Upon substitution of Equations 3.16 and 3.24 in 3.23 we obtain an expression for $\partial h/\partial t$ that is explicit in h and that reads

$$\begin{aligned}\frac{\partial h}{\partial t} &= \frac{1}{(\theta_s-\theta_r)\left\{1-\left(1+\left(\alpha\left(\frac{h-D}{\cos(i)}\right)\right)^n\right)^{-\left(\frac{n+1}{n}\right)}\right\}}\\ &\cdot\left\{N+\frac{1}{w}\left\{\left\{kw\frac{\partial h}{\partial x}+kh\frac{\partial w}{\partial x}\right\}\left\{\frac{\partial h}{\partial x}\cos i(x)+\sin i(x)\right\}\right\}\right\}\\ &+ \frac{1}{(\theta_s-\theta_r)\left\{1-\left(1+\left(\alpha\left(\frac{h-D}{\cos(i)}\right)\right)^n\right)^{-\left(\frac{n+1}{n}\right)}\right\}}\\ &\cdot\left\{kh\left\{\frac{\partial^2 h}{\partial x^2}\cos i(x)-\frac{\partial h}{\partial x}\frac{\partial i(x)}{\partial x}\sin i(x)+\frac{\partial i(x)}{\partial x}\cos i(x)\right\}\right\}\end{aligned} \tag{3.25}$$

The outflow from the hillslope is calculated using the mass-conservative scheme:

$$Q(t)=\int_{x=0}^{L}\left(-wf\frac{\partial h}{\partial t}+Nw\right)\mathrm{d}x \tag{3.26}$$

3.4 Experimental setup

3.4.1 The laboratory hillslopes and the drainage experiment

The concept of storage dependent drainable porosity is analyzed by comparing the results of the HSB model to measurements of water tables and outflow rates from a drainage experiment in a laboratory setup. The experiments are conducted for two distinct hillslope configurations: linear convergent and linear divergent. A constant and uniform rainfall rate is applied by a rainfall generator to both the convergent and divergent hillslope, until a steady-state water table is reached. Then the rainfall generator is stopped and from this steady-state initial condition the drainage experiment is started. For each hillslope shape we investigate the hydrological response for 5%, 10%, and 15% bedrock slope. The two hillslopes, their dimensions, and the location of the piezometers on the slopes are shown in Figure 3.4. Two versions of the HSB model will be evaluated: the original HSB model, where drainable porosity and conductivity are constant, and the revised, more general HSB model where drainable porosity is a state dependent parameter, calculated according to Equation 3.16.

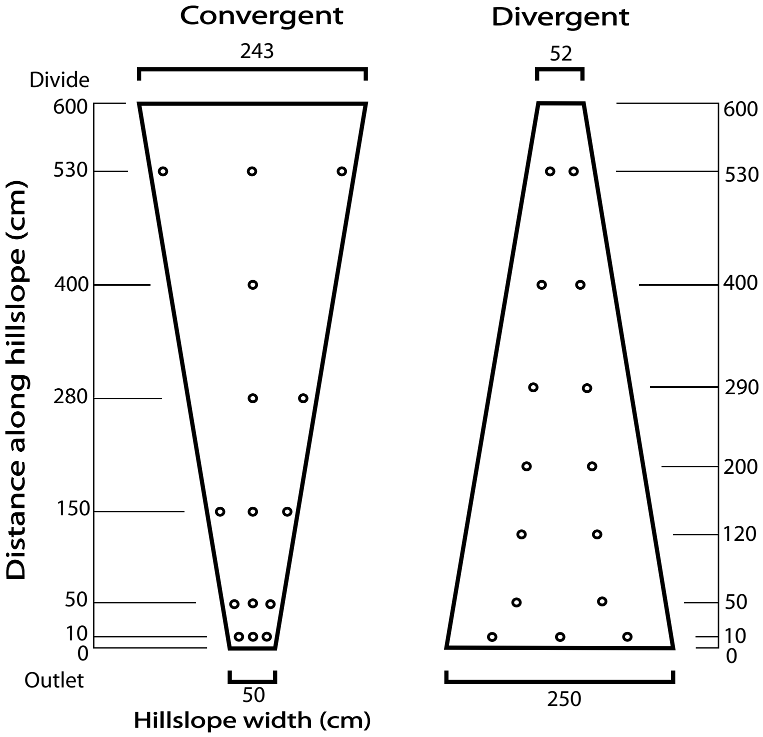
Convergent
Divergent
243
52
Divide
600
530
400
280
150
50
10
0
Outlet
50
Hillslope width (cm)
Distance along hillslope (cm)
600
530
400
290
200
120
50
10
0
250

Figure 3.4: Plan view of the convergent and divergent laboratory slopes and the position of the piezometers (indicated by small circles).

Both HSB models are first run in an uncalibrated mode with the hydraulic conductivity k set to the value that was measured on a core sample in the laboratory, and for the original HSB model the drainable porosity is set to $\theta_s - \theta_r$. In the second experiment the two models are run in a fully calibrated mode. The methods used to determine the parameter values for the two models are described in Sections 2.4.4 and 3.4.4.

3.4.2 Boundary conditions

All sides of the hillslope, except the outlet and the soil surface, are made impermeable by means of plastic sheets. At the outlet a highly permeable filter is placed at 0.05m above the 'bedrock', for a total height of 0.20m. The outlet is thus subject to a Dirichlet-type boundary condition, with the pressure head set to 0.05m.

Every 24 seconds automated water table readings are obtained from the piezometers. All piezometers are connected to a Campbell data logger with a multiplexer. Outflow rates are measured every minute using a calibrated vessel with a floating device. To reduce the noise in the signals, the water table readings are averaged over 2-minute intervals and the outflow rates over 10-minute

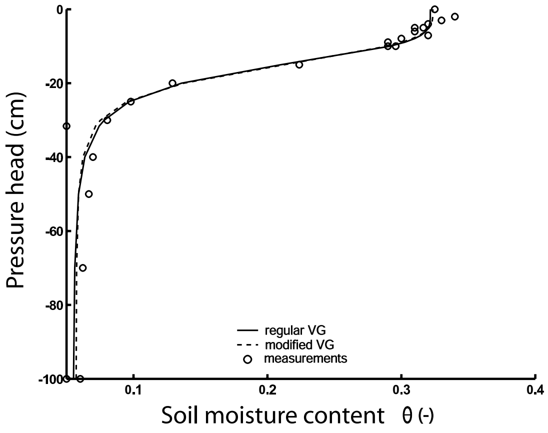

Figure 3.5: The retention curve of the sandy soil used in the laboratory experiments. Circles indicate measurements, the solid line depicts the regular van Genuchten curve, and the dashed line depicts the modified van Genuchten curve.

intervals.

3.4.3 Parameterization of the revised HSB model

For the revised HSB model, the drainable porosity is calculated using Equation 3.16, which is parameterized using the relationship $m = 1 + 1/n$ to determine the van Genuchten parameter values for the coarse sand used in the laboratory experiment. We will hereafter refer to these parameters as the modified van Genuchten parameters, whereas the parameters that are optimized using the regular relationship $m = 1 - 1/n$ will be referred to as the regular van Genuchten parameters. They are given in Table 3.1. The retention curves fitted to the measurements are plotted in Figure 3.5. The soil depth (D) was measured separately for each hillslope shape, and is given in Table 3.2. Because the laboratory bedrock has a negligible leakage and vertical fluxes in the unsaturated zone are assumed to be 0, the sink/source term N is set to 0 for all simulations.

In the uncalibrated runs the hydraulic conductivity k is set to 40 m/d, which is the value that was measured on a laboratory core sample. In the calibrated runs the conductivity is the only fitting parameter in this version of the model, and it is optimized by minimizing the summed absolute difference between measured and modeled outflow rates (i.e. the 1-norm). The calibrated value is given in Table 3.2.

3.4.4 Parameterization of the original HSB model

In the uncalibrated runs the hydraulic conductivity k is set to 40 m/d as above. The value for drainable porosity is set to $(\theta_s - \theta_r)$, which seems the most suitable value for an a priori estimate, since we expect the aquifer to reach full gravita-

Table 3.2: Calibrated conductivity values k (m/d) for the original and revised HSB model, specific yield (γ') values (-), and soil depth D (m) for all six hillslope configurations.

	Original HSB					
	k 5%	**k 10%**	**k 15%**	γ' **5%**	γ' **10%**	γ' **15%**
con	35	40	43	0.12	0.18	0.23
div	30	29	31	0.18	0.26	0.31
	Revised HSB			**All HSB**		
	k 5%	**k 10%**	**k 15%**	**D**		
con	44	49	56	0.48		
div	32	34	31	0.44		

tional drainage under the assumptions of Dupuit-Forchheimer. In the calibrated runs the parameters of the original HSB model are both regarded as fitting parameters. The drainable porosity is calculated as [*Paniconi et al.*, 2003]:

$$\gamma' = \frac{V_c}{V_i} \tag{3.27}$$

where V_c is the cumulative outflow from the laboratory drainage experiment, and V_i is the volume of soil (pore space plus solid matrix) occupied by the water in the saturated zone at time zero. Note that based on the definitions given in Section 3.1, γ' is better described as the specific yield ([*Bear*, 1972; *Johnson*, 1967]) of the aquifer under study, and it can be regarded as an estimate for γ as given in Equation 3.20. Note also that for a constant value for f (as was assumed in *Troch et al.* [2003], *Paniconi et al.* [2003], and *Hilberts et al.* [2004]) the three parameters collapse into the same value: $\gamma' = \gamma = f$. The calculated specific yield values are given in Table 3.2. The optimal value for conductivity is then found by minimizing the 1-norm of the difference between measured and modeled outflow rates. The optimal parameter values are also given in Table 3.2.

3.4.5 Parameter interpretation

The revised HSB model has four additional unsaturated zone parameters: θ_s, θ_r, α, and n compared to one (γ') in the original HSB model. These four modified van Genuchten parameters are all determined a priori on the basis of soil water retention characteristics (which can be derived for most soil types using pedotransfer functions or are otherwise relatively easy to estimate from soil core samples). The original HSB model involves the parameter specific yield (γ'), which can be calculated a posteriori on the basis of hydrographs and initial groundwater storage. As stated in the introduction of this paper, the value of drainable porosity (or specific yield in the case of the original HSB model) is not unique for a given soil or hillslope. As is apparent from Table 3.2, it will vary with slope angle and plan shape of the hillslope, and with other factors as well (profile shape, initial water table level and moisture status, etc.). Using the modified van Genuchten parameterization to describe the drainable porosity removes a parameter from the model that has a poor physical basis (γ'), and replaces it with a storage dependent parameter that is clearly physically defined (f) and that does not need to be calibrated on outflow data and piezometric measurements, but instead can be calculated based on the soil water retention characteristics (measured a priori) and the simulated depth to the water table. Thus our approach has potential for hydrological analysis in ungauged basins.

3.5 Results

3.5.1 Uncalibrated models

The outflow of the original HSB model, the revised HSB model, and laboratory measurements are shown in Figure 3.6. Note that the y-axis is scaled differently for the different bedrock slope angles. Figure 3.6 shows that the convergent hillslopes drain more slowly than the divergent ones, which is primarily caused by a smaller outlet width [*Troch et al.*, 2003]. Furthermore we notice that for the 5% slopes the fluxes for the original HSB model are clearly overestimated, especially for the convergent slope. The revised HSB model shows a much better fit. For the 10% convergent hillslope we notice that the original HSB model has an almost perfect fit, whereas the revised HSB model slightly underestimates the fluxes at early times and overestimates for large times. For the 10% divergent slope both models show a good fit to the data. For the 15% convergent slope the revised HSB model again underestimates the fluxes at early times and slightly overestimates for large times. The original HSB model displays the same pattern, although the underestimation at early times is smaller and the overestimation for large times is larger. For the 15% divergent slope, both models show slightly underestimated fluxes.

In Figure 3.7 the water table profiles are plotted for the six hillslope configurations at times 0, 60, 120, and 300 minutes. The initial conditions (which are steady-state profiles as a result of the applied rainfall) show higher saturation degrees on the upper parts of the three convergent slopes when compared to the divergent ones, due to the difference in outflow width. We notice that the original HSB model systematically overestimates the water table height for all slope shapes and all bedrock slope angles, especially at early times. The revised HSB model is clearly more accurate, even though it still overestimates the water table values. The improvement of the revised HSB model is most evident at early times, when a low value for the drainable porosity in the revised HSB model causes the water tables to drop relatively quickly. For large times the simulated water table profiles for the two models converge.

3.5.2 Calibrated models

Table 3.2 gives the optimized conductivity values for both models and the calibrated specific yield values for the original HSB model. Figure 3.8 shows the

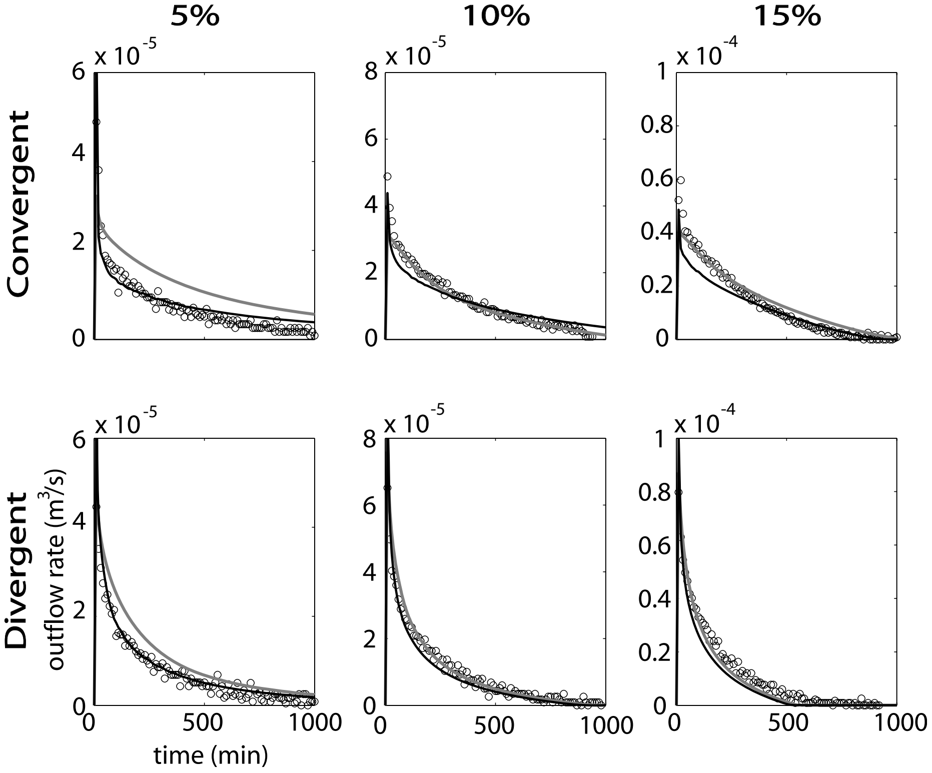

Figure 3.6: Outflow rates for the uncalibrated HSB models for the six hillslope configurations. Measured values are shown as black circles, the original HSB model is the grey line, and the revised HSB model is the black line.

outflow of the original HSB model, the revised HSB model, and laboratory measurements. Figure 3.9 shows the evolution of the space-averaged drainable porosity value as function of time for the revised model.

The specific yield value increases for steeper slopes, as expected since less water is retained in the unsaturated zone on steep hillslopes, due to increased gravitational drainage. The relatively low values for the 5% hillslopes explain the large overestimation of the uncalibrated original HSB model on these hillslopes in Figure 3.6. Noteworthy is that the specific yield value for the 15% divergent slope ($\gamma' = 0.31$) exceeds the value $(\theta_s - \theta_r) = 0.29$. This indicates that more water has drained than is estimated based on the initial saturated storage (V_i), from which we can conclude that also water from the initial unsaturated zone has drained.

With regard to the optimized conductivity values, we notice that the values are slightly higher for the convergent slopes and lower for the divergent slopes when compared to the laboratory determined value of 40 m/d. This may be caused by the higher initial water table values for the convergent slopes when compared to the divergent slopes, thereby increasing the average conductivity

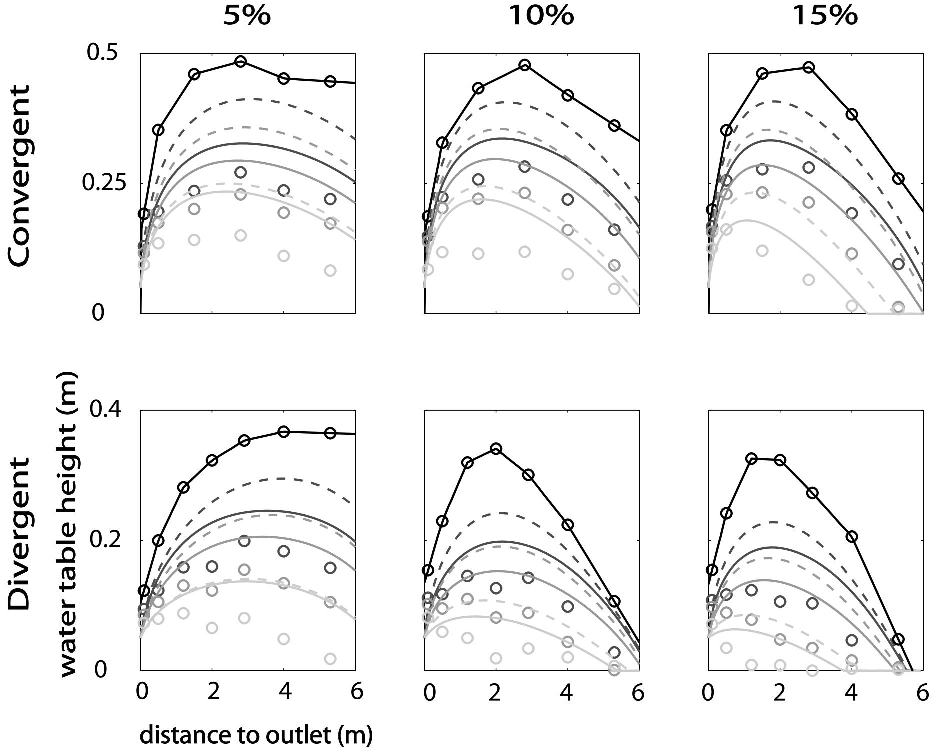

Figure 3.7: Water table profiles for the uncalibrated HSB models at time 0 (black), at 60 minutes (dark grey), at 120 minutes (grey) and at 300 minutes (light grey) for the six hillslope configurations. The measured values are the circles, the original HSB model are the dashed lines, and the revised HSB model the solid lines.

for these slopes.

Overall we notice that compared to the hydrographs in Figure 3.6, the fit of both models has improved (not greatly though), as expected. The overall fit of the revised HSB model is slightly poorer compared to the original HSB model. However, at early times when the impact of capillarity on storage and flow is highest due to high saturation degree, the fit has improved. For the 5% convergent slope we see that the match is good at the beginning of the drainage experiment, but is overestimated at large times. An improvement in the fitting of the tail part of the hydrograph is achieved at the expense of the goodness-of-fit at early times: the drop of the flux rate is then too sharp. The fact that this sharp decrease in modeled fluxes is not reflected in the measurements may indicate that there is some recharge from the unsaturated zone during the early stages of drainage, due to the applied rainfall just before the experiment. For the 10% slope the fit to the data is very good for small times and the overestimation for large time is small. For the 15% slope the fit to the data is good for small times, but there is underestimation of flux for large times. The 5% divergent slope shows an almost perfect fit. For the 10% and the 15% divergent slopes, the fluxes initially drop too quickly, but for larger times the fit improves. The space-averaged drainable porosity in Figure 3.9 shows a quick convergence towards $\theta_s - \theta_r$ for the hillslopes that drain quickly (i.e. divergent and steep slopes), and show slow convergence for slowly draining slopes. When convergence is reached, the advantages of the revised HSB model vanish, because effectively f then remains constant.

It is noteworthy in this context that although the time and space averaged value of f may in some cases be (almost) equal to the value of γ', the modeled states and fluxes can be very different for the two models. A low value of f at early times causes the water tables to drop quickly (and fastest where the water tables are closest to the surface), thereby changing the water table profiles fundamentally from the original HSB model. Even when the values of f and γ' are equal afterwards, the outflow behavior and water table dynamics remain different for the two models. The opposite effect can also be noticed: the averaged value of f and the value of γ' can in some cases be different, whereas the modeled outflow for both models can be almost indistinguishable. This effect can for example be seen in Figure 3.8 for the 5% divergent slope, where the time and space averaged value of drainable porosity is equal to $f = 0.25$, and for the original HSB model $\gamma' = 0.18$, whereas the modeled outflow is very much alike.

In Figure 3.10 the water table profiles are plotted for the six hillslope configurations at times 0, 60, 120, and 300 minutes. As in Figure 3.6, we notice that both models overestimate the water table values. Once again the revised HSB model is clearly more accurate. However, due to the calibration of the original HSB model (i.e. the lower values of specific yield), the differences between both models have decreased slightly although the differences between the original and revised HSB models for early times still range up to 0.10m.

3.6 Discussion and conclusions

In this paper we have presented, for horizontal and sloping bedrock aquifers, an analytical expression for storage-dependent drainable porosity (for horizontal and sloping bedrock), thereby incorporating some of the effects of the unsaturated zone on groundwater storage and fluxes. The assumption underlying the derivation is that during drainage the pressure head in the unsaturated zone is permanently in vertical hydraulic equilibrium. The derived expressions (i.e. Equations 3.12 and 3.16) link drainable porosity directly to the depth to the water table, thereby transforming it from a fitting parameter into a state-dependent parameter. The derived expression is then incorporated into the HSB model and compared (in terms of water table height and outflow values) to the results of the original (constant f) HSB model and to a series of laboratory measurements. The validation of the model is conducted on a convergent and a divergent hillslope, for 5%, 10%, and 15% bedrock slope inclination (i.e. 6 different hillslope configurations). Two simulation settings were analyzed: an uncalibrated model run, where the model parameters were determined based on conductivity and water retention measurements on soil cores; and a fully calibrated run, where the optimized parameter values (i.e. specific yield and conductivity in the case

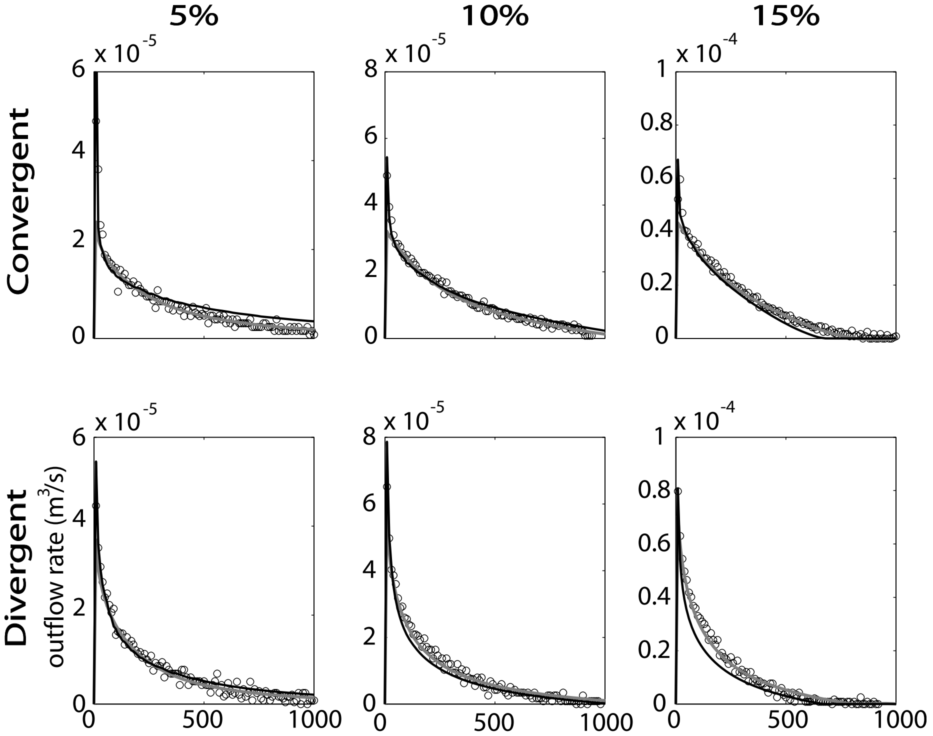

Figure 3.8: Outflow rates for the calibrated HSB models for the six hillslope configurations. Measured values are shown as black circles, the original HSB model is the grey line, and the revised HSB model is the black line.

of the original HSB and only conductivity in the case of the revised HSB) were used.

The comparison of the HSB models to the measurements from the laboratory hillslopes shows that it is possible to capture the general features of a drainage experiment using either one of the HSB models. Overall the original HSB model (having one fitting parameter more than the revised HSB model) shows a slightly better fit on the hydrographs when compared to the revised HSB model. The peak outflow values however (the first few minutes after initiation of the experiments) are better captured by the revised HSB model. The revised HSB model's performance in simulating water table movements is much more accurate than that of the original HSB model. The improved match of the revised HSB model to piezometric measurements is worth stressing because the ability to model water tables is a key attribute of the model, making it possible to investigate phenomena such as saturation excess runoff.

The difference between the original and the revised HSB model performance on outflow results is most clearly visible for the uncalibrated model runs on gentle slopes: the large overestimation of fluxes by the original HSB model here

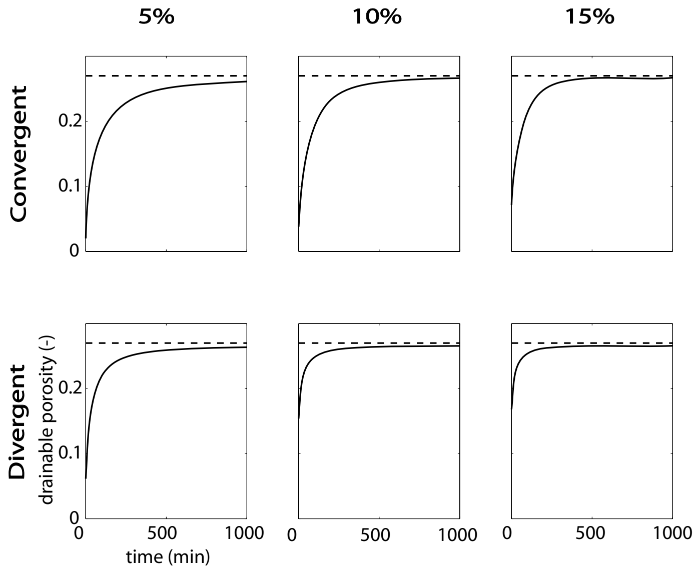

Figure 3.9: Space-averaged drainable porosity values for the calibrated revised HSB models for the six hillslope configurations. The dashed line indicates the value $(\theta_s - \theta_r)$.

clearly advocates the calculation of f as a storage-dependent parameter. Also remarkable is the good match between the revised HSB model and outflow measurements without any calibration for the divergent slopes. The fact that the performance of the original HSB model is not independent of slope inclination and initial conditions, together with the ability of the revised model to more accurately simulate water table dynamics, clearly demonstrates the importance of regarding drainable porosity as a function of storage.

A further comment on the storage-dependent drainable porosity concept worth mentioning is that even when the time and space averaged value of f is equal to the calibrated value of γ', the dynamic behavior of both models can be significantly different. A low value of f at early times can change the water table profiles such that the hydrographs for both models remain different thereafter. The opposite also holds: even when the averaged value of f and the value of γ' differ significantly, the outflow behavior may be almost identical.

In relation to the hydrographs we notice that for some drainage experiments the fluxes as modeled with the revised HSB model drop too quickly at early times during drainage, although the cumulative modeled outflow is generally in accordance with the measurements. Since changing the van Genuchten parameters would influence the cumulative volumes, one can conclude that for the revised HSB model it is not possible to obtain a better fit for the hydrographs by tuning these parameters. This leads to the conclusion that in the early stages of our drainage experiments, the assumptions underlying the drainable porosity expression might not be completely valid. Since the experiment is started right

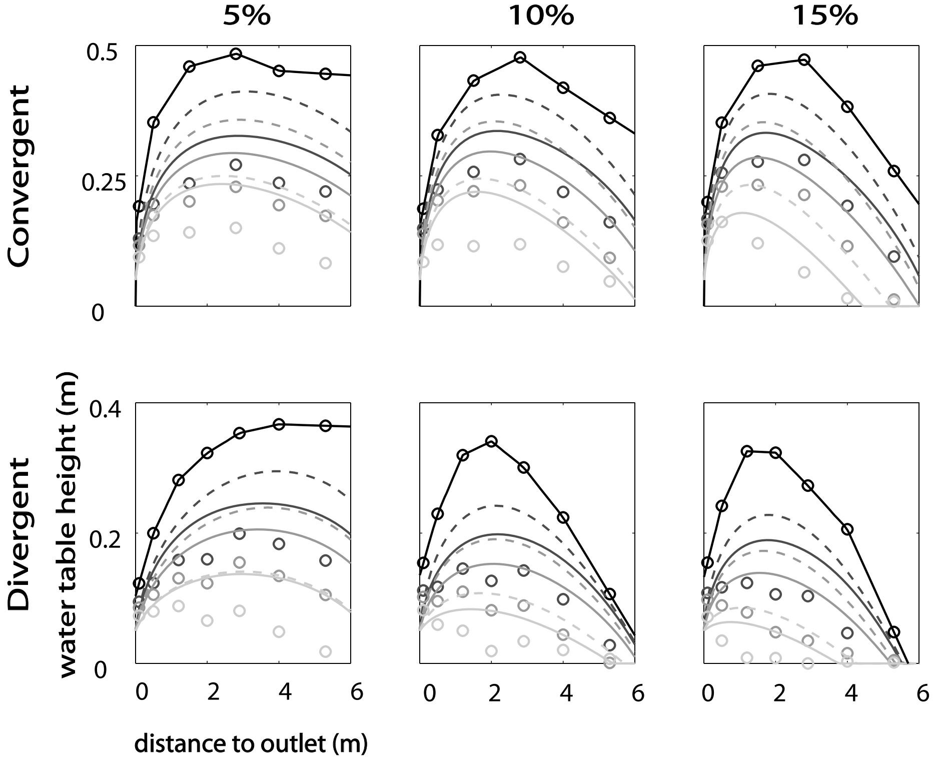

Figure 3.10: Water table profiles for the calibrated HSB models at time 0 (black), at 60 minutes (dark grey), at 120 minutes (grey) and at 300 minutes (light grey) for the six hillslope configurations. The measured values are the circles, the original HSB model are the dashed lines, and the revised HSB model the solid lines.

after a rainfall event, it is probable that there is still some vertical downward flux in the unsaturated zone, violating our assumption of zero recharge and hydraulic equilibrium in the unsaturated zone.

In *Vachaud and Vauclin* [1975] it is concluded that the capillary fringe plays an important role in the flow of water. Incorporating the capillary fringe as an integral part of the Boussinesq aquifer (i.e. substituting h by $h + \psi_c$, where ψ_c is the capillary fringe) will improve the simulated water tables. The substitution effectively implies changing from the assumption that transport only occurs below the water table (underlying Boussinesq-type models) into the assumption that transport only takes place in the saturated zone.

Ongoing work is aimed at generalizing the expression for drainable porosity such that it can be calculated as a storage-dependent parameter in case of non-zero steady-state fluxes in the unsaturated zone. Analytical integration of the corresponding soil moisture profiles is then not possible, but semi-analytical solutions may be derived by means of piecewise integration of the soil hydraulic characteristics (see *Rockhold et al.* [1997]). In the case of non-zero recharge we may also have to consider hysteresis phenomena in the soil water retention characteristic. It is expected that a more general expression would improve the revised HSB model's performance, especially just after initiation of the drainage experiments. Moreover, it would enable us to extend the analysis of the concept of storage-dependent drainable porosity to recharge scenarios, rendering the revised HSB model suitable for rainfall-runoff simulations in poorly gauged catchments. Future work will also evaluate these concepts by comparison to a three-dimensional Richards equation based model and to field data.

Chapter 4

An attempt to explain the high and low frequency behavior of the complex drainable porosity in a tidal aquifer

Abstract

In *Cartwright et al.* [2005] and in a preceding paper by *Nielsen and Perrochet* [2000], an investigation is conducted to assess the effects of an oscillating water table on the effective porosity. Both papers present results from a thorough laboratory experiment and numerical simulations. We wish to comment on some of the findings and conclusions in *Cartwright et al.* [2005] with regards to the effect of capillarity, and the response at very high and very low oscillation frequencies. We also present some results from a simple numerical solution to a non-hysteretic one-dimensional Richards equation model, and compare these to the original data and the modeling results presented in *Cartwright et al.* [2005].

This chapter is based on the paper "Hilberts, A.G.J and P.A. Troch, Comment on "Influence of capillarity on a simple harmonic oscillating water table: Sand column experiments and modeling" by N. Cartwright et al., in press, *Water Resources Research*, doi:10.1029/2006WR005042, 2006."

4.1 The frequency response and the influence of capillarity

In *Cartwright et al.* [2005] a complex effective porosity,n_ω, is defined as

$$n\frac{\mathrm{d}h_{tot}}{\mathrm{d}t} = n_\omega \frac{\mathrm{d}h}{\mathrm{d}t} \tag{4.1}$$

$$|F| = \frac{|\eta|}{|\eta_0|} \tag{4.2}$$

and

$$F(\omega) = |F|e^{-i\phi} = \frac{1}{1 + i\omega\frac{n_\omega D}{K}} \tag{4.3}$$

where h_{tot} is the equivalent height of the total storage of soil moisture, h is the water table height (calculated according to Equation 12 from *Nielsen and Perrochet* [2000]), t is time, $n = (\theta_s - \theta_r)$, θ_s is the saturated soil moisture content, θ_r is the residual soil moisture content, $|\eta|$ and $|\eta_0|$ are respectively the amplitudes of the water table height and driving head, ϕ is the phase shift between measured water table height $h(t)$ and driving head $h_0(t)$, D is the average water table height, K is the saturated hydraulic conductivity, $\omega = 2\pi/T$ is the angular frequency, T is the period of the oscillation, $i = \sqrt{-1}$, and n_ω is the effective porosity which is a complex number. Equation (4.3) can be reformulated as

$$n_\omega = (\frac{1}{F(\omega)} - 1)\frac{K}{i\omega D} \tag{4.4}$$

From equation 1 in the paper by *Cartwright et al.* [2005] the authors draw the conclusion that for low frequencies, n_ω should converge towards $n = (\theta_s - \theta_r)$ since the phase lag will approach 0, thereby eliminating the imaginary part of n_ω. An alternative motivation for the same conclusion follows from the limit case behavior of Equation 5 in *Cartwright et al.* [2005], however, this function is the result of a function fit to the data which is extrapolated quite far outside the range of measured values, and no physical basis for the function form is given. For high frequencies, they note that $|n_\omega|$ decays linearly on a double-logarithmic scale and they mention a curious relationship between the decay and the van Genuchten parameters. In this comment we state that, under the influence of capillarity, n_ω can converge to other values than n for low frequencies. For high frequencies we attempt to explain the sharp decay of $|n_\omega|$ with ω, and we present a quantitative analysis of the processes involved.

4.1.1 Low frequency response

First, the conclusion that n_ω converges to $(\theta_s - \theta_r)$ for low frequencies is only expected to hold when the water table is not in the proximity of the soil surface: for these frequencies it can be expected that h_0 and h will be in phase with equal amplitude, indeed causing the complex n_ω to converge towards n. However, when the water table fluctuations occur sufficiently close to the soil surface, the temporal changes in total storage h_{tot} will be very small compared to the changes in h, causing the value of n_ω in Equation 4.1 to approach a value lower than $(\theta_s - \theta_r)$ (e.g., [*Hilberts et al.*, 2005]). In *Cartwright et al.* [2005] it is mentioned that the presented experiments are unaffected by the proximity of the water table to the soil surface. However, Table 2 and Figure 3 indicate that for the glass-beads soil this assumption is dubious. Table 2 shows that the minimal average driving head level is about 50 cm above the base of the column (total height of 180 cm) which leaves approximately 130 cm unsaturated zone depth on average. Figure 3 shows that the glass-beads soil (i.e. $d_{50} = 0.082$ mm) at pressure head $\psi = -130$ cm is still not fully drained. We expect therefore that the proximity to the soil surface is quite strongly affecting the values of n_ω for the glass-beads soil. This also seems to be indicated by the results in Table 2, from which we can conclude that the highest value for $|n_\omega|$ of the glass-beads soil is 0.013 even though the value of the oscillation frequency is very low (viz. 2.4910^{-4} s^{-1}, which corresponds to an oscillation period $T = 7$ hours).

A second issue is that the limit case $\lim_{\omega\to 0}(n_\omega)$ cannot be determined from Equation 4.4, since it has no solution. Also equation 4.1 offers no solution for the limit case where frequencies approach 0, since the derivatives $\mathrm{d}h_{tot}/\mathrm{d}t$ and $\mathrm{d}h/\mathrm{d}t$ will approach 0, leaving the relationship between n_ω and n undetermined.

In relation to the response at very low frequencies, Figure 7 in *Cartwright et al.* [2005] indicates that the value of $|n_\omega/n|$ for a numerical solution to Richards equation for the glass-beads soil (i.e., solid circles in their figure) converges to 1 relatively quickly, i.e., $|n_\omega|$ converges to n. Here, we compare the results of a simple numerical solution of a non-hysteretic Richards equation model to the results of *Cartwright et al.* [2005]. For our simulations we use identical soil parameter settings as in *Cartwright et al.* [2005], (i.e., for the glass-beads soil $K = 2.8 \cdot 10^{-5}$ m/s, $\theta_s = 0.38$, $\theta_r = 0.06$, $\alpha = 0.68$ 1/m, and $\beta = 10$, where α and β are van Genuchten parameters), and we used an oscillation amplitude $|\eta_0| = 0.15$ m, an average driving head $D = 0.50$ m, and a column depth of 1.8 m. In our Figure 4.1, the results of these simulations, together with the original data listed in Table 2 of *Cartwright et al.* [2005], are plotted as a function of ω. Note that the data that derive from the paper by *Nielsen and Perrochet* [2000] are left out because the average water table height significantly deviates from that in *Cartwright et al.* [2005] and this paper.

Figure 4.1 illustrates that for the glass-beads soil (black circles) even for very low frequencies (e.g., $\omega = 6.2832 \cdot 10^{-6}$ rad/s or $T \simeq 11.6$ days), the value for $|n_\omega/n|$ based on our modeling exercise is still clearly lower than 1, viz. $|n_\omega/n| = 0.24$. If we compare this to Figure 7 in *Cartwright et al.* [2005], it can be seen that for the same frequency (i.e., $n\omega H_\psi/K = 0.1091$, where H_ψ is the equivalent capillary fringe height) the indicated value of $|n_\omega/n|$ based on their model result is much higher (approximately 0.9). However, for the fine and course sand (respectively diamonds and squares in the figures), $|n_\omega/n|$ converges to 1 as indicated by *Cartwright et al.* [2005].

Figure 4.2 shows the same data as Figure 4.1, however, the x-axis is scaled according to *Cartwright et al.* [2005]. When we compare Figure 4.2 to Figure 7 of *Cartwright et al.* [2005], we notice a clear distinction: where Figure 7 shows a clear overestimation of $|n_\omega/n|$ for approximately $n\omega H_\psi/K < 10^1$ for all three soil

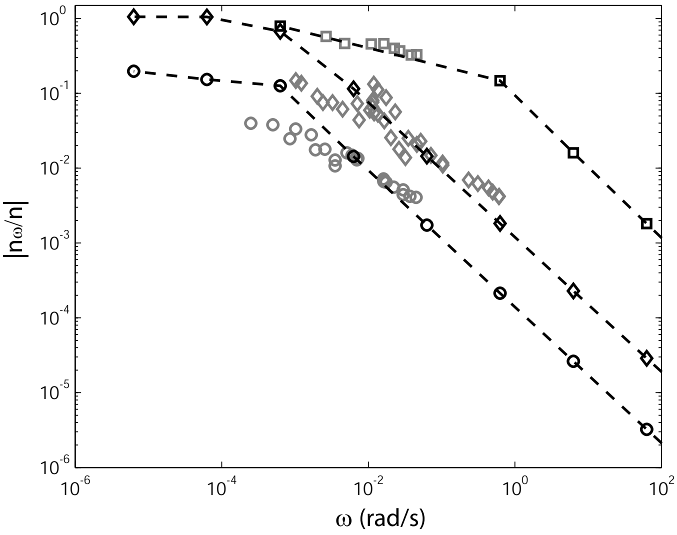

Figure 4.1: The frequency response of $|n_\omega/n|$ for the three soil types used in this study (viz., glass-beads (circles), fine sand (diamonds) and coarse sand (squares)). The grey symbols are the data from *Cartwright et al.* [2005], and the black lines and symbols are the results of the modeling exercise in this paper.

types, Figure 4.2 shows lower drainable porosity values for the coarse sand and the glass-beads soil than presented in the Richards model results in *Cartwright et al.* [2005]. For the coarse sand, the fit to the measurements is better than for the other soil types and better that presented in *Cartwright et al.* [2005]. An explanation for the good performance for the coarse sand is yet to be found. Based on our model results, we cannot dismiss a non-hysteretic Richards equation model for all soil types, since it performs reasonably well when confronted with the measurements for the coarse sand. However, the authors agree with Cartwright and co-workers in that an improved match can be obtained by incorporation of the effects of hysteresis into modeling practise (e.g., [*Werner and Lockington*, 2003]).

4.1.2 High frequency response

Also for high frequencies, Equations 4.1 and 4.4 prove troublesome: for the limit case $\lim_{\omega\to\infty}(n_\omega)$, Equation 4.4 has no solution. For high frequency oscillations of the driving head, the amplitude of the water table oscillations will converge to 0, causing the right hand side of Equation 4.1 to become 0 which causes n_ω to be undefined.

The data obtained by *Cartwright et al.* [2005] show that the calculated values of $|n_\omega/n|$ decay apparently linearly (on a double- logarithmic scale) for higher

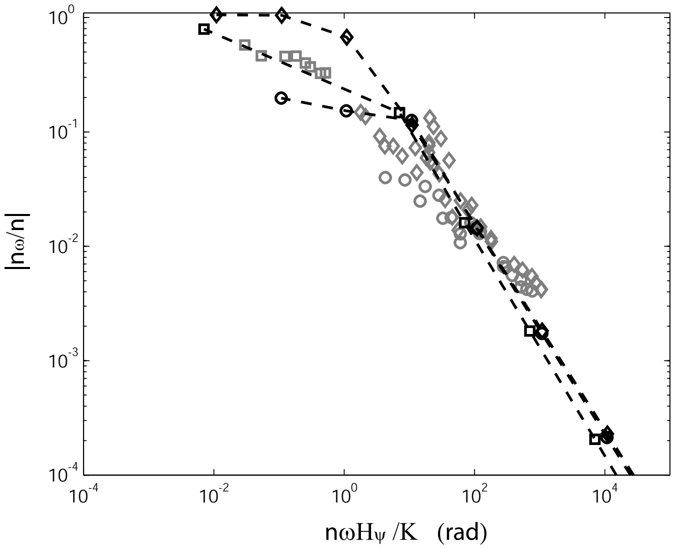

Figure 4.2: The frequency response of $|n_\omega/n|$ for the three soil types used in this study, scaled according to *Cartwright et al.* [2005]. The colors and symbols are as defined in Figure 4.1.

frequencies, with a computed slope of $-2/3$. The results of the Richards equation modeling exercise in the same paper show a slope of approximately -1 (see Figure 6). The high frequency response of our modeling exercise shown in Figures 4.1 and 4.2 indicates that all three slopes show a very similar decay, which ranges from -0.90 to -0.93.

The decay of $|n_\omega|$ for increasing frequencies can be ascribed to the inability of a part of the unsaturated zone to reach a new equilibrium situation for high frequency oscillations. If there is an equilibrium initial condition in the unsaturated zone and h_0 is increased rapidly, merely a small part of the unsaturated zone will become saturated before h_0 starts to drop. However, at higher elevations above the water table, where conductivities get increasingly smaller, the response to changes in h_0 gradually become negligible. For increasing frequencies of $h_0(t)$, $|\eta|$ will become smaller, as will the changes in the unsaturated zone storage close to the soil surface. For small $|\eta|$ and large ω, the fluctuations of $h(t)$ will mainly occur within the nearly saturated part of the retention curve (i.e., the capillary fringe), causing the value of $|n_\omega|$ to drop rapidly. In *Cartwright et al.* [2005], in paragraph [21] it is stated that this drop occurs due to an increased influence of capillarity for higher frequencies, and therefore $|n_\omega| << n$. Here, we propose a more quantitative explanation for the observed decay of $|n_\omega|$ with increasing frequencies.

4.1.3 An attempt to explain the modeled and measured high frequency decay of $|n_\omega$—

We shall assume that the response of the unsaturated zone is restricted to the domain over which water table fluctuations take place (viz., over a range $2|\eta|$). This assumption implies that above $D+|\eta|$ no changes in soil moisture conditions take place (i.e., $\theta(z > D + |\eta|, t) = \theta(z > D + |\eta|, t + \mathrm{d}t)$, see Figure 4.3). The assumption is expected to become more valid for increasing frequencies. The integrated soil moisture in the profile (or total storage) at time t can be calculated as

$$s(t) = h(t)(\theta_s - \theta_r) + \int_{h(t)}^{Z} (\theta(t, z) - \theta_r)\mathrm{d}z \tag{4.5}$$

where Z is the location of the soil surface. Substitution of $t + \mathrm{d}t$ into Equation 4.5 allows us to express the change in storage from time t to $t + \mathrm{d}t$

$$ds = \mathrm{d}h(\theta_s - \theta_r) - \int_{h(t)}^{h(t+\mathrm{d}t)} (\theta(t, z) - \theta_r)\mathrm{d}z \tag{4.6}$$

where $\mathrm{d}h = h(t + \mathrm{d}t) - h(t)$ is the water table change over a time increment $\mathrm{d}t$. As stated before, we assume that there is an equilibrium soil moisture profile above the lowest water table height $h = D - |\eta|$ that returns each cycle (at $t = kT$, where $k = 0, 1, 2, ...$). According to the integration described in *Hilberts et al.* [2005] which uses an alternative van Genuchten parameterization (viz., $m = 1 + 1/\beta$), Equation 4.6 can then be expressed as

$$ds = \mathrm{d}h(\theta_s - \theta_r)\left[1 - \left(1 + (\alpha'\mathrm{d}h)^{\beta'}\right)^{-1/\beta'}\right] \tag{4.7}$$

where α', and β' are the modified van Genuchten parameters. The parameter values for the three soils used in this study are listed in Table 4.1. Equation 4.7 describes the total storage change over a time interval $\mathrm{d}t$, which is equal to $n\mathrm{d}h_{tot}$ from Equation 4.1. Combination of Equations 4.1 and 4.7 allows us to derive a simple expression for $|n_\omega|$ for high frequencies:

$$|n_\omega| = (\theta_s - \theta_r)\left[1 - \left(1 + (\alpha'\mathrm{d}h)^{\beta'}\right)^{-1/\beta'}\right] \tag{4.8}$$

Given that the total water table change $\mathrm{d}h = 2|\eta|$, the value of $|n_\omega|$ can be calculated using Equation 4.8 and the results of the numerical solution to Richards equation. The results are shown in Figure 4.4.

Table 4.1: The modified (i.e., $m = 1 + 1/\beta$) van Genuchten parameters for the three soil types used in this study.

Parameter	Glass-bead	Fine sand	Coarse sand
$\theta_\mathbf{s}$ (-)	0.38	0.38	0.41
$\theta_\mathbf{r}$ (-)	0.06	0.09	0.08
α' (1/cm)	-0.0066	-0.0163	-0.11
β' (-)	9.33	8.27	20

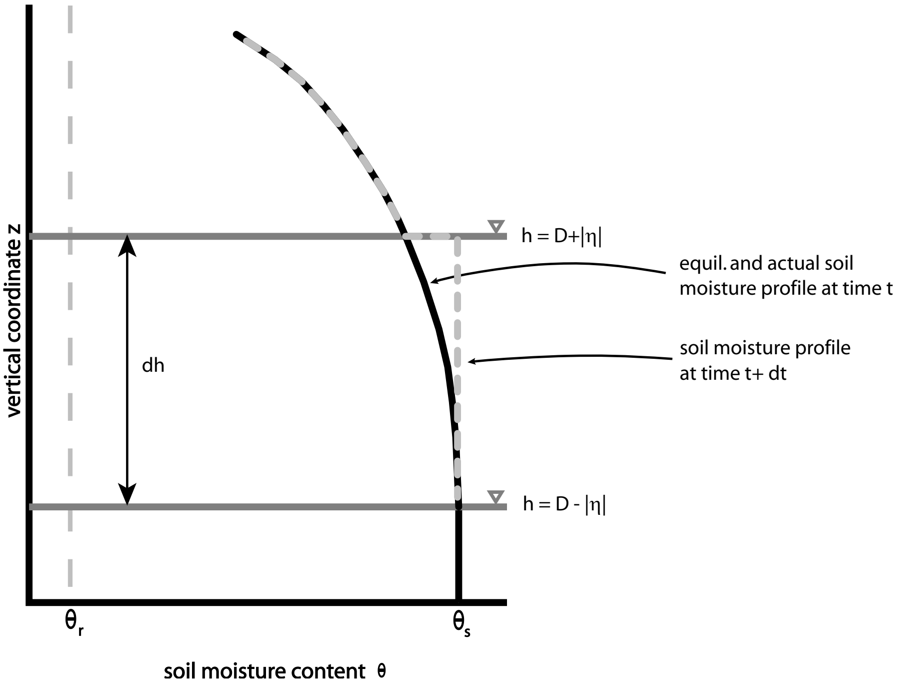
vertical coordinate z
h = D+|η|
equil. and actual soil moisture profile at time t
soil moisture profile at time t+ dt
dh
h = D - |η|
θr
θs
soil moisture content θ

Figure 4.3: Sketch of the assumed soil moisture profile response (from time t to $t + \mathrm{d}t$) as a result of oscillations in the pressure head with amplitude $|\eta|$.

We note that the value of $|n_\omega/n|$ based on Equation 4.8 (in grey) are clearly underestimated compared to the values obtained using Equation 4.4 (in black). This indicates that the assumption of a static soil water profile above $D + |\eta|$ is too conservative: a larger part of the unsaturated zone than assumed (probably a significant part of the capillary fringe) will respond to the oscillations in the driving head. However, the slope of the grey curves show convergence towards a slope of approximately 0.90 that we observed in our modeling results. Also *Cartwright et al.* [2005] makes note of slopes equal to $(1 - 1/\beta)$ in their modeling results, which is very close to 0.90 for the given parameters. Their Section 7 is devoted to this curious relationship between the van Genuchten parameters and the slopes of the curves for high frequencies, for which no apparent cause was found. Based on Equation 4.8, we expect a power-law relationship between $\mathrm{d}h$ and $|n_\omega|$, where the slope of this curve is $(-1/\beta')$. Furthermore, from analysis of the results of our modeling exercise we find that ω and $\mathrm{d}h$ also have an approximate power-law relationship for high frequencies. This implies that ω and the modeled $|n_\omega|$ also have a power-law relationship, of which the slope is determined by β'. However, since we lack a functional relationship between $\mathrm{d}h$ and ω, we cannot present an analytical expression for the modeled $|n_\omega|$ as a function of ω.

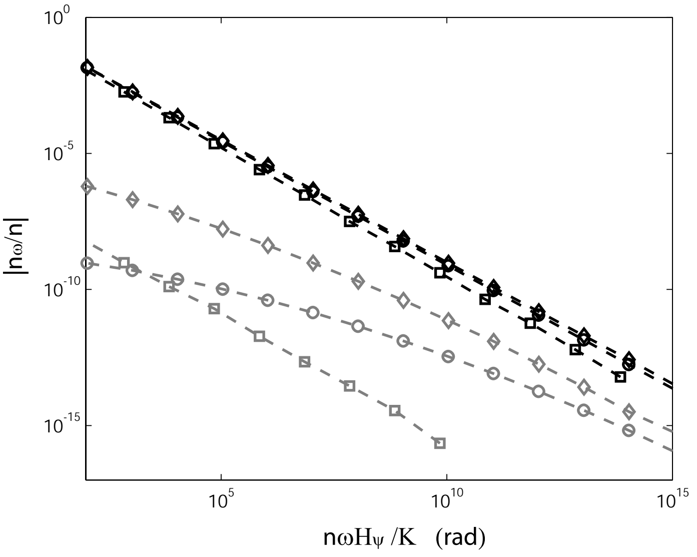

Figure 4.4: The high-frequency response of $|n_\omega/n|$ for the three soil types used in this study, scaled according to *Cartwright et al.* [2005]. The symbols are as defined in Figure 4.1, however, the black lines indicate results based on Equation 4.4 whereas grey lines indicate results based on Equation 4.8.

4.2 Criteria to determine the influence of capillarity

In paragraph [26] of *Cartwright et al.* [2005] it is mentioned that the effects of capillarity become important when the distance from the water table to the sand surface is approximately half the value of the equivalent saturated capillary fringe height (H_ψ) for the cases that were investigated. Table 1 in their paper lists 1.50 m, 0.60 m, and 0.085 m for H_ψ for respectively the glass-beads soil, the fine sand, and the course sand. For deep water tables, the uptake of water as a result of an increase of the pressure head dh (or yield in case of drainage) will be $(\theta_s - \theta_r)\mathrm{d}h$. The effect of capillarity (or rather, the unsaturated storage effect) becomes noticeable when the change in water table height dh does no longer lead to constant uptake or yield of water but is reduced instead. This effect is reflected in the shape of the differential soil moisture capacity function, which is defined as the derivative of the soil moisture profile with respect to the pressure head (i.e., $\mathrm{d}\theta/\mathrm{d}\psi$). The point where the uptake or yield is no longer constant (viz. $\theta_s - \theta_r$) is the point at which $\mathrm{d}\theta/\mathrm{d}\psi$ is no longer 0, because at this point the yield changes depend on the actual suction head as well as the suction head changes. The differential soil moisture capacity for the three soil types investigated in this study is depicted in Figure 4.5.

The suction head for which the capillarity effect were noticeable according to *Cartwright et al.* [2005] were approximately 0.75 m, 0.30 m, and 0.043 m.

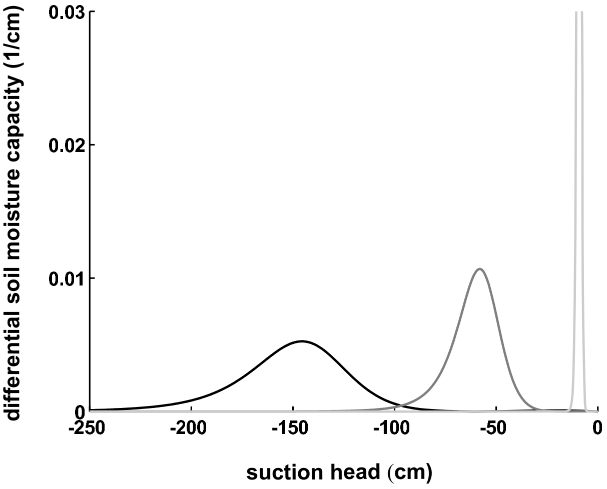

Figure 4.5: The differential moisture capacity functions for the three soil types used in *Cartwright et al.* [2005] (black = glass-beads soil, dark shaded grey = fine sand, and light shaded grey = coarse sand).

These values correspond nicely to the suction heads at which the differential soil moisture capacity starts to rise in Figure 4.5 (going from $\psi = 0$ towards smaller ψ, i.e., the drying direction). Inspection of the differential soil moisture capacity may form an easy and elegant way to assess the expected effects of unsaturated storage on water table changes.

Chapter 5

Low-dimensional modeling of hillslope subsurface flow: the relationship between rainfall, recharge, and unsaturated storage dynamics

Abstract

We present a coupling between the one-dimensional Richards equation for vertical unsaturated flow and the one-dimensional hillslope-storage Boussinesq equation (HSB, see [*Troch et al.*, 2003]) for lateral saturated flow along complex hillslopes. Here, the capillary fringe is included in the flow domain as an integral part of the Boussinesq aquifer. The coupling allows quantitative investigation of the role of unsaturated storage in the relationship between rainfall and recharge. The coupled model (HSB-coupled) is compared to the original HSB model (HSB-original) and a three-dimensional Richards equation (RE) based model (taken to be the benchmark) on a set of seven synthetic hillslopes, ranging from convergent to divergent. Using HSB-original the water tables are overestimated and the outflow rates are generally underestimated, and there is no delay between rainfall and recharge. The coupled model, however, shows a remarkably good match with the RE model in terms of outflow rates, and the delay between rainfall and recharge is captured well. We also see a clear improvement in the match to the water tables, even though the values are still overestimated for some hillslope shapes, in particular the convergent slopes. We show that, for the hillslope configurations and scenarios examined in this paper, it is possible to reproduce hydrographs and water table dynamics with a good degree of accuracy using a low-dimensional hydrological model.

This chapter is based on the paper "Hilberts, A.G.J., P.A. Troch, C. Paniconi and J. Boll, Low-dimensional modeling of hillslope subsurface flow: the relationship between rainfall, recharge, and unsaturated storage dynamics, in review, *Water Resources Research*, doi:10.1029/2006WR004964, 2006."

5.1 Introduction

Our understanding of hillslope subsurface flow processes and their effect on catchment response to atmospheric forcing is incomplete and has been the subject of much research for several decades. Among the first to reveal the importance of hillslope subsurface flow with regard to catchment stormflow were *Hewlett and Hibbert* [1967] and *Dunne and Black* [1970]. They concluded that for humid climates water table dynamics in hillslopes have a large effect on channel stormflow through the formation of areas of saturation along the channel network, often called saturated source areas, which cause saturation-excess overland flow. Since then many studies have investigated subsurface flow processes experimentally (e.g. *McGlynn et al.* [2004]; *O'Loughlin* [1981]; *Torres et al.* [1998]; *Woods et al.* [1997]) and through modeling. The two-part paper by *Freeze* [1972a], where storm flow processes are examined using a three-dimensional Richards-based model to describe subsurface processes, is one of the first (computer) modeling studies of hillslope processes, and since then many have followed.

In addition to the rather complex, three-dimensional models that are often used in these modeling studies (e.g., [*Abbott et al.*, 1986; *Wigmosta et al.*, 1994]), several simplified low-dimensional models have been proposed, because of the computational expense and parameterization difficulties associated with the former type of model. Efforts include *Beven and Kirkby* [1979], who describe the original version of TOPMODEL, *Duffy* [1996] who develops a two-state variable integral-balance (hillslope) model, *Reggiani et al.* [1998], who describe the "Representative Elementary Watershed" (REW) model, and *Sloan* [2000] who describes a storage-discharge type model which is derived from hydraulic groundwater theory. Among the simplified models, many studies have focused on analysis of the Boussinesq equation (e.g. *Brutsaert* [1994]; *Chapman* [2005]; *Childs* [1971]; *Szilagyi et al.* [1998]). Most of these studies were conducted on straight hillslopes, sometimes using linearized versions of the Boussinesq equation, aiming at an increased fundamental understanding of the flow and storage dynamics in hillslopes.

In recent work by the authors, the Boussinesq equation was generalized to account for the three-dimensional soil mantle in which the flow processes take place [*Hilberts et al.*, 2004; *Paniconi et al.*, 2003; *Troch et al.*, 2003]. The effect of slope shape (i.e. convergent, divergent, straight) and bedrock curvature on storage and outflow processes was examined for drainage and recharge scenarios, and compared to the three-dimensional Richards equation (RE) based model of *Paniconi and Wood* [1993]. A general conclusion of our recent work with the hillslope-storage Boussinesq (HSB) model is that the modeled outflow rates compared relatively well to results of the RE model, but capturing the water table dynamics was less successful. Results from a recent laboratory experiment [*Hilberts et al.*, 2005] indicated that this may be caused by the strong effect of capillarity (or, more precisely, the unsaturated storage) on groundwater dynamics, especially for shallow soils as typically encountered on hillslopes.

The capillary fringe is an (almost) entirely saturated transition zone between the unsaturated zone and groundwater, of which the effects on groundwater flow are often ignored. However, the literature provides evidence that in the capillary fringe, fluxes can have considerable lateral components, thereby adding to lateral groundwater flow (e.g., *Jayatilaka and Gillham* [1996]; *Luthin and Miller* [1953]). These flow processes were investigated numerically (e.g., *Luthin and Day* [1955]; *Vachaud and Vauclin* [1975]), and experimentally (e.g., *Berkowitz et al.* [2004]), and all of these studies clearly show large lateral flow components in the capillary fringe. *Vachaud and Vauclin* [1975] demonstrated that the fluxes in the capillary fringe are of the same order of magnitude as groundwater fluxes, and that they often have a large lateral component. They estimated that, for their experiment, roughly 14% of the lateral flux takes place above the water table.

The effect of capillarity on water table dynamics, which in hydraulic groundwater models is usually accounted for through parameters such as specific yield, effective porosity or drainable porosity, has been noted in previous studies such as *Hooghoudt* [1947], who referred to it as the "Wieringermeer effect", and later by *Gillham* [1984], *Abdul and Gillham* [1989], *Parlange et al.* [1990], *Kim and Bierkens* [1995] and *Nielsen and Perrochet* [2000]. However, only few have tried to account for the effect. In a benchmark paper by *Parlange and Brutsaert* [1987], the capillarity effect on groundwater systems is modeled, assuming a deep profile for which $\theta = \theta_r$ holds at the land surface. Assuming instantaneous equilibrium in the unsaturated zone, an analytical expression to account for capillarity effects is derived that can be added to the Boussinesq equation. In *Barry et al.* [1996] the equations derived in *Parlange and Brutsaert* [1987] are extended to include higher-order capillarity effects, and they are used to investigate the inland propagation of oscillations in water tables for a coastal aquifer. *Nachabe* [2002] derives an analytical expression to account for dynamic capillarity effects, which also includes delayed recharge due to rapidly dropping water tables. In *Hilberts et al.* [2005] an analytical expression is derived to account for capillarity effects under equilibrium in shallow groundwater systems, and its influence on hillslope dynamics is investigated. All of these studies are mainly applicable in situations where recharge is negligibly small. To extend the investigation of the effect of unsaturated zone storage on saturated flow to recharge scenarios, a coupling of the saturated zone model to a dynamic unsaturated zone model is needed, and the impact of the capillary fringe on water table dynamics needs to be incorporated.

Hydrological studies at the hillslope and catchment scale, as well as land surface modeling, have put much emphasis on the processes that occur in the soil layer close to the soil surface. This is because the interactions of the unsaturated zone with the atmospheric boundary layer are known to have an important effect on surface fluxes, and therefore also on climate [*Koster et al.*, 2003]. It is well-known that subsurface flow processes are currently not well-simulated in land surface models [*Liang et al.*, 2003]. A more thorough understanding of the interactions between (shallow) groundwater and soil moisture in the unsaturated zone is needed if we are to improve model results significantly [*Koster et al.*, 2000].

Several authors have described a coupling of separate models for unsaturated and saturated flow under a diversity of assumptions. *Pikul et al.* [1974] coupled a one-dimensional Boussinesq model to a one-dimensional RE model for the unsaturated zone. The coupled system was solved as a boundary value problem, and the drainable porosity for the saturated zone model was taken to be a constant (viz. $\theta_s - \theta_m$), where θ_s [$-$] is saturated soil moisture content and θ_m [$-$] is "the minimum soil moisture content below the depth from which moisture may be removed directly by evapotranspiration." As no functional form is given for θ_m, its value is somewhat arbitrary [*Vachaud and Vauclin*, 1975]. A very similar approach was used by *Kim et al.* [1999], but also here no relationship describing the drainable porosity was given. *Smith and Hebbert* [1983] coupled a Boussinesq model to a kinematic wave model for the unsaturated zone. To calculate the recharge from the unsaturated zone to the saturated zone, they assumed that the soil moisture pulses in the unsaturated zone have attenuated when they reach the groundwater table. The coupled system was solved as a system of ordinary differential equations. A similar approach was taken by *Beven* [1982], however in this work two kinematic wave models were coupled. *Liang et al.* [2003] described a coupling between a one-dimensional RE model for the unsaturated zone and a generalized bucket-model for lateral subsurface flow, which was linked to the VIC model [*Wood et al.*, 1992]. The coupled system was also solved as a boundary value problem. However, in none of the mentioned papers that deal with coupling of models, the actual functional interactions between the saturated zone and the unsaturated zone are investigated.

In this work the one-dimensional Richards equation is coupled to the HSB equation. In the coupled model, the capillary fringe is treated as an integral part of a Boussinesq aquifer, i.e., lateral groundwater transport takes place over the entire saturated depth (and not only below the atmospheric pressure plane). By introducing the unsaturated zone matric pressure head as a system-state and reformulating the derived equations in state-space notation, we solve the coupled system simultaneously as a set of ordinary differential equations, and obtain a functional state-dependent expression for the drainable porosity. With a Richards equation representation for the unsaturated zone and a functional form for the drainable porosity, this coupled model allows us to investigate more accurately the interactions between the saturated and unsaturated zone and the relationship between rainfall intensity, unsaturated storage (and drainable porosity), and recharge. We assume that a single (space-averaged) soil moisture profile can sufficiently describe the unsaturated zone processes, which is an assumption that is done to retain the coupled model's low-dimensionality. A similar assumption underlies the work of *Boussinesq* [1877], where recharge was assumed uniform over a hillslope. The coupled HSB model's behavior is compared to the original HSB model of *Troch et al.* [2003] and the three-dimensional RE model of *Paniconi and Wood* [1993] (which is taken to be a benchmark model) for a set of seven synthetic hillslopes.

5.2 Governing equations

5.2.1 Unsaturated and saturated zone of the coupled model

If we assume that the soil water movement in the unsaturated zone is predominantly vertical, it can be described using the one-dimensional Richards equation:

$$\frac{\partial \theta}{\partial t} = \frac{\mathrm{d}\theta}{\mathrm{d}\psi} \cdot \frac{\partial \psi}{\partial t} = \frac{\partial q_v}{\partial z} \tag{5.1}$$

where $\theta = \theta(x, z, t)$ $[-]$ is the volumetric soil moisture content, $\psi = \psi(x, z, t)$ $[L]$ is the matric pressure, t is time, z is the vertical coordinate, positive downward (see Figure 5.1), and q_v is the vertical soil moisture flux [L/T], expressed as

$$q_v(z, t) = -K(\psi)(-\frac{\partial \psi}{\partial z} + 1) \tag{5.2}$$

where $K(\psi)$ $[L/T]$ is the hydraulic conductivity as a function of matric pressure. To describe $\theta(\psi)$ and $K(\psi)$ we use the *van Genuchten* [1980] relationships:

$$\theta(\psi) = \theta_r + (\theta_s - \theta_r)\left(\frac{1}{1 + (\alpha\psi)^n}\right)^m \tag{5.3}$$

$$K(\psi) = k\frac{\left(-1 + \left(1 - \left(\left(1 + (\alpha\,\psi)^n\right)^{-m}\right)^{m^{-1}}\right)^m\right)^2}{\left(1 + (\alpha\,\psi)^n\right)^{m/2}} \tag{5.4}$$

where k $[L/T]$ is the saturated hydraulic conductivity, θ_r $[-]$ is the residual soil moisture content, n $[-]$, m $[-]$, and α $[1/L]$ are fitting parameters, and $m = 1 - 1/n$. To integrate the soil water retention curve, an alternate parameterization is more convenient:

$$\theta(\psi) = \theta_r + (\theta_s - \theta_r)\left(\frac{1}{1 + (\alpha'\psi)^{n'}}\right)^{m'} \tag{5.5}$$

where n', m', and α' are again fitting parameters, and $m' = 1 + 1/n'$ (see *Troch* [1992] and *Hilberts et al.* [2005]). Both parameterizations of the unsaturated zone are used in our modeling approach. The conventional parameterization is used to describe the relationships between pressure head, soil moisture content, and hydraulic conductivity for Richards' equation, whereas the alternate parameterization in a later stage is used to determine the value for the state-dependent drainable porosity (see Section 5.2.2).

The saturated zone dynamics are modeled with the HSB model [*Hilberts et al.*, 2004; *Paniconi et al.*, 2003; *Troch et al.*, 2003]:

$$w\gamma\frac{\partial h}{\partial t} = -\frac{\partial (wq)}{\partial x} + N\cos(i)w \tag{5.6}$$

where $w = w(x)$ [L] is the hillslope width at x [L] running along the bedrock slope (positive in the upslope direction), γ $[-]$ is the drainable porosity, $h = h(x, t)$ [L] is the water table height perpendicular to the bedrock, t [T] is time, $N = N(x, t)$ [L/T] is the vertical recharge to the groundwater table, and $q = q(x, t)$ [L^2/T] is the lateral Darcy-flux which is assumed to be parallel to the bedrock (i.e. Dupuit-Forchheimer assumption):

$$q(x, t) = -kh\left(\frac{\partial h}{\partial x}\cos(i) + \sin(i)\right) \tag{5.7}$$

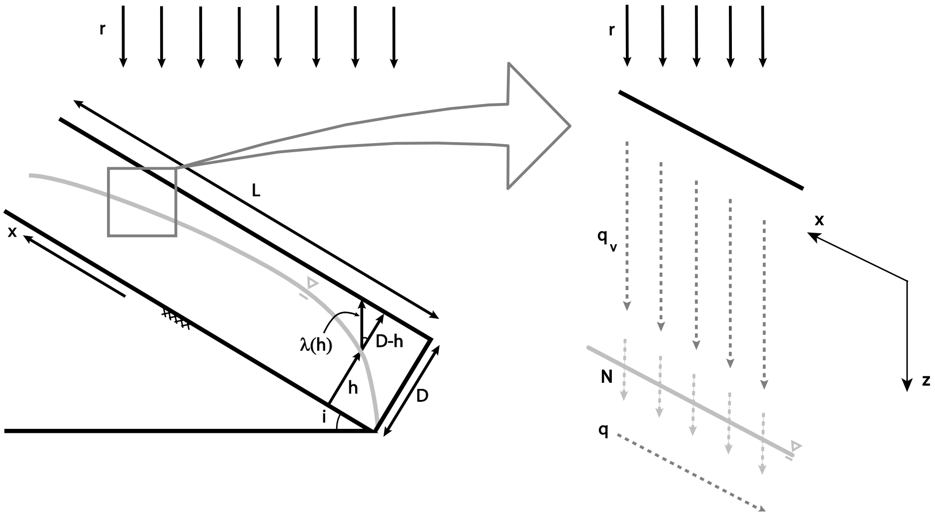

Figure 5.1: Definition sketch showing a hillslope cross-section with relevant parameters, and the coordinate systems for the unsaturated zone (vertical flow) and saturated zone (lateral flow).

where $i = i(x)$ $[-]$ is the bedrock slope. In Figure 5.1 both the hillslope coordinate system and the vertical coordinate system are depicted.

5.2.2 Interactions between the saturated and the unsaturated zone

Using the unsaturated zone model, it is possible to calculate the recharge N based on the position of the water table and the actual soil moisture profile. Mass conservation requires that for each location on the hillslope the following relationship holds

$$N(x,t) = r(t) - \frac{\partial}{\partial t}\left(\int_0^{\frac{(D-h)}{\cos(i)}} (\theta(x,z,t) - \theta_r)\mathrm{d}z\right) \tag{5.8}$$

where D $[L]$ is the soil depth and $r(t)$ $[L/T]$ and $N(x,t)$ $[L/T]$ are the vertical rainfall rate and recharge rate, respectively. Note that all terms in Equation 5.8, including the integration boundaries, are in vertical coordinates. *Chapman* [2005] argued that although many studies use rainfall and recharge rates perpendicular to the bedrock, it is more realistic to consider the vertical fluxes. Furthermore, *Chapman* [2005] shows that both approaches yield similar results in terms of average water table height as long as the recharge/conductivity ratio is relatively small.

For notational convenience we will use

$$\lambda(h) = \frac{(D-h)}{\cos(i)} \tag{5.9}$$

to indicate the depth to the water table in the vertical coordinate. Equation 5.8 can then also be formulated as

$$\begin{aligned} N(x,t) = r(t) - \frac{\partial}{\partial t}(\int_0^\lambda (\theta_e(x,z,t) - \theta_r)\mathrm{d}z) \\ -\frac{\partial}{\partial t}(\int_0^\lambda (\theta(x,z,t) - \theta_e(x,z,t))\mathrm{d}z) \end{aligned} \tag{5.10}$$

where $\theta_e(x,z,t)$ is the soil moisture profile under hydraulic equilibrium conditions at t for a given water table position and zero recharge. The changes in unsaturated storage are now expressed as storage changes relative to the hydraulic equilibrium storage profiles. This is done to avoid a singularity in the coupled model, as will be explained in Section 5.2.4. Equation 5.10 can be written as

$$\begin{aligned} N(x,t) = r(t) - \frac{\partial h'}{\partial t}\frac{\mathrm{d}}{\mathrm{d}h'}\left(\int_0^\lambda (\theta_e(x,z,t) - \theta_r)\mathrm{d}z\right) \\ -\frac{\partial}{\partial t}\left(\int_0^\lambda (\theta(x,z,t) - \theta_e(x,z,t))\mathrm{d}z\right) \end{aligned} \tag{5.11}$$

where $h' = h/\cos(i)$ is the vertical water table height above the bedrock. Because $\partial h'/\partial t = 1/\cos(i)\partial h/\partial t$, and $\mathrm{d}/\mathrm{d}h' = \cos(i)\mathrm{d}/\mathrm{d}h$, Equation 5.11 is equivalent to:

$$\begin{aligned} N(x,t) = r(t) - \frac{\partial h}{\partial t}\frac{\mathrm{d}}{\mathrm{d}h}\left(\int_0^\lambda (\theta_e(x,z,t) - \theta_r)\mathrm{d}z\right) \\ -\frac{\partial}{\partial t}\left(\int_0^\lambda (\theta(x,z,t) - \theta_e(x,z,t))\mathrm{d}z\right) \end{aligned} \tag{5.12}$$

The term $\mathrm{d}/\mathrm{d}h\left(\int_0^\lambda (\theta_e(x,z,t) - \theta_r)\mathrm{d}z\right)$ is the change of storage in the unsaturated zone (in hydraulic equilibrium) with respect to a change in water table height, which in *Hilberts et al.* [2005] was denoted $-\mathrm{d}s_1/\mathrm{d}h$ and for which an analytical expression was derived:

$$\begin{aligned} &\frac{\mathrm{d}}{\mathrm{d}h}\left(\int_0^\lambda (\theta_e(x,z,t) - \theta_r)\mathrm{d}z\right) \\ &= -(\theta_s - \theta_r)\left(1 + (-\alpha'\lambda)^{n'}\right)^{-(\frac{n'+1}{n'})} \end{aligned} \tag{5.13}$$

where α' and n' are modified van Genuchten parameters defined by Equation 5.5.

The second term within the square brackets in Equation 5.11 can be expanded by applying Leibniz' rule:

$$\begin{aligned} \frac{\partial}{\partial t}\left(\int_0^{\lambda}(\theta(x,z,t)-\theta_e(x,z,t))\mathrm{d}z\right) = \\ -\frac{1}{\cos(i)}\frac{\partial h}{\partial t}\cdot(\theta(x,\lambda,t)-\theta_e(x,\lambda,t)) \\ +\int_0^{\lambda}\frac{\partial\theta}{\partial t}\mathrm{d}z-\int_0^{\lambda}\frac{\partial\theta_e}{\partial t}\mathrm{d}z \end{aligned} \tag{5.14}$$

Note that both the equilibrium and the actual soil moisture content are at full saturation at the position of the water table (i.e., $\theta(x,\lambda,t)=\theta_e(x,\lambda,t)=\theta_s$), which allows Equation 5.14 to be further reduced. The changes in the equilibrium profile depend directly on the changes in water table height (i.e., the profile is displaced according to the displacement of the water table):

$$\begin{aligned} \int_0^{\lambda}\frac{\partial\theta_e(x,z,t)}{\partial t}\mathrm{d}z &= \int_0^{\lambda}\frac{\mathrm{d}\theta}{\mathrm{d}\psi}\frac{\partial\psi_e(x,z,t)}{\partial t}\mathrm{d}z \\ &= \int_0^{\lambda}\frac{\mathrm{d}\theta}{\mathrm{d}\psi}\frac{\partial h'(x,t)}{\partial t}\mathrm{d}z \\ &= \frac{1}{\cos(i)}\int_0^{\lambda}\frac{\mathrm{d}\theta}{\mathrm{d}\psi}\frac{\partial h(x,t)}{\partial t}\mathrm{d}z \end{aligned} \tag{5.15}$$

where ψ_e is the equilibrium pressure head. Upon combination of Equations 5.12, 5.13, 5.14, and 5.15, Equation 5.8 becomes:

$$\begin{aligned} N(x,t) = r(t) + \frac{\partial h}{\partial t}(\theta_s-\theta_r)\left(1+(-\alpha'\lambda)^{n'}\right)^{-(\frac{n'+1}{n'})} \\ -\int_0^{\lambda}\frac{\partial\theta}{\partial t}\mathrm{d}z+\frac{1}{\cos(i)}\int_0^{\lambda}\frac{\mathrm{d}\theta}{\mathrm{d}\psi}\frac{\partial h}{\partial t}\mathrm{d}z \end{aligned} \tag{5.16}$$

For a Boussinesq-type aquifer (i.e., without any retention effects of the unsaturated zone), the drainable porosity parameter in Equation 5.6 is a constant

$$\gamma = (\theta_s-\theta_r) \tag{5.17}$$

Substitution of Equations 5.16 and 5.17 into 5.6 yields the expression for the saturated zone model, and taking the derivative of Equation 5.2 with respect to z and substituting this into Equation 5.1 yields the unsaturated zone model. Together these form a coupled system with a state-dependent drainable porosity, without inclusion of the capillary fringe in the Boussinesq flow domain:

$$\begin{aligned} wf\frac{\partial h}{\partial t} &= -\frac{\partial (wq)}{\partial x} + w\cos(i) \\ &\cdot \left\{ r - \int_0^{\lambda} \frac{\partial \theta}{\partial t}\mathrm{d}z + \frac{1}{\cos(i)} \int_0^{\lambda} \frac{\mathrm{d}\theta}{\mathrm{d}\psi}\frac{\partial h}{\partial t}\mathrm{d}z \right\} \qquad (5.18) \\ C\frac{\partial \psi}{\partial t} &= -\frac{\partial K(\psi)}{\partial z}(1 - \frac{\partial \psi}{\partial z}) + K(\psi)\frac{\partial^2 \psi}{\partial z^2} \qquad (5.19) \end{aligned}$$

where $f = f(h)$ is the drainable porosity after *Hilberts et al.* [2005], modified such that recharge rate is vertical instead of perpendicular to bedrock:

$$f(h) = (\theta_s - \theta_r)\left\{ 1 - \cos(i)\left(1 + (-\alpha'\lambda)^{n'}\right)^{-(\frac{n'+1}{n'})} \right\} \qquad (5.20)$$

and $C = C(\psi)$ is the differential moisture capacity:

$$C(\psi) = \frac{\mathrm{d}\theta}{\mathrm{d}\psi} \qquad (5.21)$$

5.2.3 Governing equations with inclusion of the capillary fringe

The conclusions of *Paniconi et al.* [2003] are that the high outflow rates and the relatively low water table values for the RE model compared to the HSB models indicate that the HSB models are draining too slowly. Given the findings from this study and the importance of the capillary fringe on lateral groundwater flow and water table dynamics that as reported in the literature reviewed earlier, we will include the capillary fringe in our coupled model.

When a capillary fringe ψ_c is introduced as an integral part of the aquifer, the governing equations for the coupled model are not greatly altered . If we define

$$h^* = h - \psi_c \qquad (5.22)$$

to be the saturated depth over which lateral transport takes place $[L]$, and we substitute this expression into Equations 5.18 and 5.19, the equations essentially remain the same. In Equation 5.18 the integral boundary becomes $\lambda = (D - \overline{h})/\cos(\overline{i}) - \psi_c$, and Equation 5.19 does not change. However, flow equation 5.7 changes to

$$q(x,t) = -kh^*\left(\frac{\partial h}{\partial x}\cos(i) + \sin(i)\right) \qquad (5.23)$$

and the drainable porosity f (Equation 5.20) is now calculated based on the new value for λ.

We will refer to the model based on Equations 5.18, 5.19, and 5.23 as HSB-coupled, and this model's behavior will be compared to the original HSB model and an RE based model.

We will test the hypothesis that the term within accolades in Equation 5.18 can be approximated using a single soil moisture profile derived for the entire hillslope, analogous to the assumption underlying the original work of *Boussinesq* [1877] that recharge is uniform . If this hypothesis leads to acceptable levels of accuracy, it allows for a significant reduction in the dimensionality of the model. This hypothesis implies that $\theta(x, z, t)$ is assumed equal for all x, and the integration over the profile $\theta(x, z, t)$ therefore is conducted using boundaries based on a hillslope-averaged water table height:

$$\lambda = \lambda(\overline{h^*}) = \frac{(D - \overline{h^*})}{\cos(\bar{i})} \tag{5.24}$$

where

$$\begin{aligned}\overline{h^*}(t) &= 1/(\overline{w}L)\int_0^L w(x)h^*(x,t)\mathrm{d}x\\ \bar{i} &= 1/(\overline{w}L)\int_0^L w(x)i(x)\mathrm{d}x\\ \overline{w} &= 1/L\int_0^L w(x)\mathrm{d}x\end{aligned}$$

where $\overline{h^*}$ is the average height of the saturated zone (the capillary fringe included), $\overline{w}$ is the average width, $\bar{i}$ is the average bedrock slope, and L $[L]$ is the hillslope length measured along the bedrock. By introducing a state vector $\mathbf{X} = [h(x,t), \psi(z,t)]$, and discretizing in the spatial coordinates z and x (see Figure 5.1), Equations 5.18 and 5.19 can be solved simultaneously as a set of ordinary differential equations.

5.2.4 An alternate derivation involving singularity

The most obvious manner to expand Equation 5.8 would be to directly regard soil moisture profile changes with respect to θ_r. Applying Leibniz' rule in this case yields:

$$N(x,t) = r(t) - \int_0^\lambda (\frac{\partial\theta(x,z,t)}{\partial t})\mathrm{d}z + \frac{\partial h}{\partial t}(\theta(x,\lambda,t)) - \theta_r) \tag{5.25}$$

The third term on the right hand side of Equation 5.25 would normally be brought to the left hand side, thereby altering the constant parameter γ in Equation 5.6 to become a state-dependent parameter $f(h)$. However, since $\theta(x,\lambda,t) = \theta_s$, upon combination of Equations 5.25 and 5.6 a singularity arises on the left hand side of Equation 5.6:

$$f = (\theta_s - \theta(x,\lambda,t)) \tag{5.26}$$

and since at the water table $\theta(x,\lambda,t) = \theta_s$, it causes a singularity in Equation 5.6.

In the derivation of Section 5.2.2 this singularity is avoided by regarding the changes of soil water profile with respect to equilibrium profile, for which the drainable porosity is expressed analytically and subsequently corrected by an extra source term (viz. $\int_0^\lambda \frac{\mathrm{d}\theta}{\mathrm{d}\psi}\frac{\partial h}{\partial t}\mathrm{d}z$) that accounts for changes in equilibrium profile.

5.2.5 The three-dimensional Richards equation-based model

The governing equation for the three-dimensional RE model is [*Paniconi and Wood*, 1993]:

$$\eta(\psi)\frac{\partial \psi}{\partial t} = \nabla \cdot (K(\psi)(\nabla\psi + \mathbf{e}_z)) \tag{5.27}$$

where $\eta = S_w S_s + \theta_s(dS_w/d\psi)$ is the general storage term, S_w is the water saturation defined as θ/θ_s , S_s is the aquifer specific storage coefficient, $\mathbf{e}_z$ is the vector $(0, 0, 1)^T$ (positive upward), and the hydraulic conductivity tensor is $K(\psi)$ as in Equation 5.4. The nonlinear retention characteristics are described using the van Genuchten relationship given in Equation 5.3. The RE model used in this work is the subsurface module of a coupled surface-subsurface numerical model using a tetrahedral finite element discretization in space, a weighted finite difference scheme in time, and Newton or Picard iteration to resolve the nonlinearity [*Paniconi and Putti*, 1994; *Putti and Paniconi*, 2004].

5.3 Interpretation

5.3.1 Interpretation of the equations for the coupled model

In the coupled model (Equation 5.16) the unsaturated zone affects the water table dynamics in two distinct ways. First, the unsaturated zone replenishes the groundwater (viz. the third and fourth terms on the right hand side of Equation 5.16). These terms together indicate the total change in soil moisture storage for a certain depth to the water table λ. Second, the soil moisture profile in the unsaturated zone determines the available storage capacity in the soil above the water table, which is reflected in the second term on the right hand side of Equation 5.16, thereby directly influencing the drainable porosity.

In Figure 5.2 hypothetical soil moisture profiles for times t and $t + \mathrm{d}t$ (and corresponding depth to water table values $\lambda(\overline{h}(t))$ and $\lambda(\overline{h}(t+\mathrm{d}t)))$ are depicted for a drainage and a rainfall scenario. The solid lines give the actual soil moisture profiles (at two different times), the dashed lines are the equilibrium soil moisture profiles, the black lines correspond to the profiles at $t = t$, and the grey lines correspond to those at $t + \mathrm{d}t$. For convenience let us name the term within accolades in Equation 5.18:

$$N^*(x,t) = r(t) - \underbrace{\int_0^\lambda \frac{\partial\theta}{\partial t}\mathrm{d}z}_{actual} + \underbrace{\frac{1}{\cos(i)}\int_0^\lambda \frac{\mathrm{d}\theta}{\mathrm{d}\psi}\frac{\partial h}{\partial t}\mathrm{d}z}_{equilibrium} \tag{5.28}$$

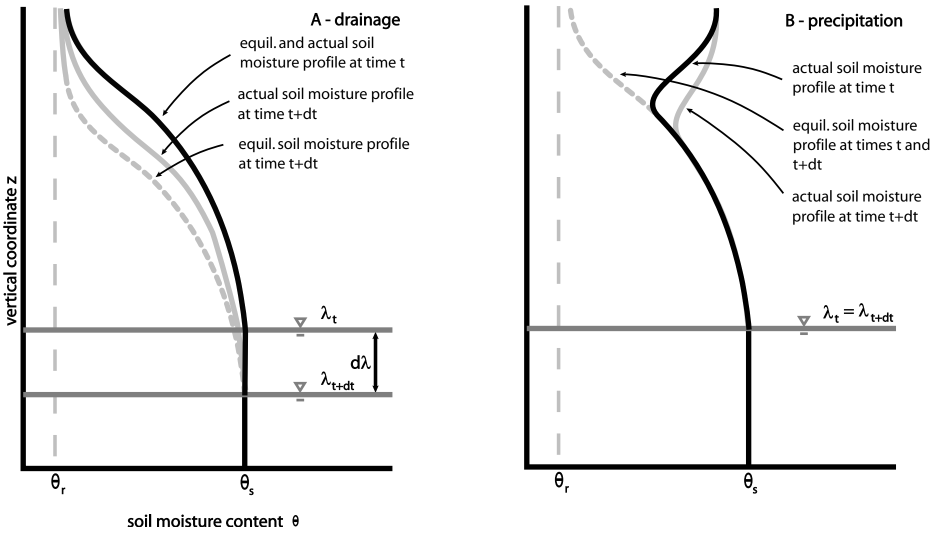
A - drainage
equil. and actual soil moisture profile at time t
actual soil moisture profile at time t+dt
equil. soil moisture profile at time t+dt
vertical coordinate z
λt
dλ
λt+dt
θr
θs
soil moisture content θ
B - precipitation
actual soil moisture profile at time t
equil. soil moisture profile at times t and t+dt
actual soil moisture profile at time t+dt
λt = λt+dt
θr
θs

Figure 5.2: Sketch of soil moisture profile, and changes in soil moisture content for a drainage (A) and a recharge (B) scenario at times t and $t + \mathrm{d}t$

For a drainage scenario (Figure 5.2a) starting from hydraulic equilibrium, the total change in actual soil moisture content (the second term on the right hand side of Equation 5.28) is always equal to or greater (i.e., less negative) than the total change in equilibrium soil moisture storage (the third term). Note that because initially all the soil moisture changes will be negative for a drainage experiment, the absolute value of the second term will be smaller than the value of the third term. Therefore, for a short time at the onset of a drainage experiment, N^* will be negative. Later in the drainage process the water tables will drop more slowly and the unsaturated zone replenishes the saturated zone, causing N^* to become positive. The drainable porosity f (Equation 5.20) accounts for the changes in equilibrium profile and is smaller than $(\theta_s - \theta_r)$, and greater than zero. In the case where the actual profiles collapse into the equilibrium profiles N^* becomes zero, and the solution converges to the solution derived in *Hilberts et al.* [2005] but modified for vertical drainage.

In the case of rainfall, the value and sign of N^* depends strongly on the water table height, the soil moisture conditions and the rainfall rate. When the water table is steady (i.e., $\lambda(\overline{h}(t)) = \lambda(\overline{h}(t + \mathrm{d}t))$) and the unsaturated zone is initially relatively dry, most water from rainfall will be stored in the unsaturated zone. In Equation 5.28 this means that the third term on the right hand side becomes zero, the first and second term become equal, thereby causing N^* to be zero. When the unsaturated zone initially is relatively wet (Figure 5.2b), only part of the water coming from rainfall will be stored in the unsaturated zone, and the remainder will recharge the groundwater. In case the water table is dropping, and a soil moisture pulse is traveling towards the water table, a mix of the responses above will occur.

5.3.2 The relationship between rainfall, recharge, and unsaturated storage

The interaction between rainfall and recharge rates is illustrated in Figure 5.3, showing the (simplified) response of the unsaturated and saturated zones to a constant rainfall rate. We distinguish three stages: stage A, where a soil moisture wave due to rainfall is traveling towards a static water table in an initially relatively dry profile, stage B where the soil moisture pulse reaches the water table and causes the water table to rise, and stage C where the water table has reached a new equilibrium under recharge. In stage A all the rain water that infiltrates is stored in the unsaturated zone and recharge is zero. Stage B shows the situation just after the soil moisture front has reached the groundwater, causing a rapid rise in water table height. Note that during this stage of rising water tables, the recharge is higher than the rainfall rate. For a static water table, the flux across the water table surface would be equal to the rainfall rate, but since the water table is rising and thereby “taking up” water from the unsaturated zone, the recharge is higher than the rainfall rate. The phenomenon of the unsaturated and saturated zones competing for unsaturated storage just above the water table was also mentioned in studies such as *Duffy* [1996], *Seibert and McDonnell* [2002], and *Weiler and McDonnell* [2004]. When a new steady-state water table position is reached (i.e., stage C), the water table is static, and the flux across it is equal to the rainfall rate.

Since the increased recharge of stage B is due to movement of the water table $\partial h/\partial t$, and is therefore brought to the left hand side of Equation 5.6, the term determines the value of drainable porosity f. The second term on the right hand side of Equation 5.16 can thus be either regarded as an input term, or as a correction term for the storage coefficient γ in Equation 5.6.

5.4 Model comparison setup

5.4.1 The models and hillslopes

We compare the coupled HSB (HSB-coupled) model’s response to that of the three-dimensional Richards equation (RE) model described in Section 5.2.5, and the original uncoupled HSB model (HSB-original) described in *Troch et al.* [2003] and given by Equation 5.6. The original HSB model is run in an uncalibrated mode assuming that the value of drainable porosity is $\gamma = (\theta_s - \theta_r)$, which can be considered a reasonable and conservative a priori estimate for a sandy soil when precise retention characteristics are unknown. Moreover, this is the value of γ one would obtain for a perfectly draining soil, which corresponds to a Boussinesq aquifer. We test the model’s response under rainfall and during drainage on a set of seven artificial hillslopes that were also used in *Troch et al.* [2003], consisting of three convergent, three divergent, and one straight hillslope. The hillslope outlines are based on the nine geometries described in *Troch et al.* [2002], but have non-curved bedrock, thus the three straight slopes in *Troch et al.* [2002] collapse into a single slope, yielding seven hillslopes as depicted in Figure 5.4. The aquifer properties are given in Section 5.4.3. The hillslopes have a length of

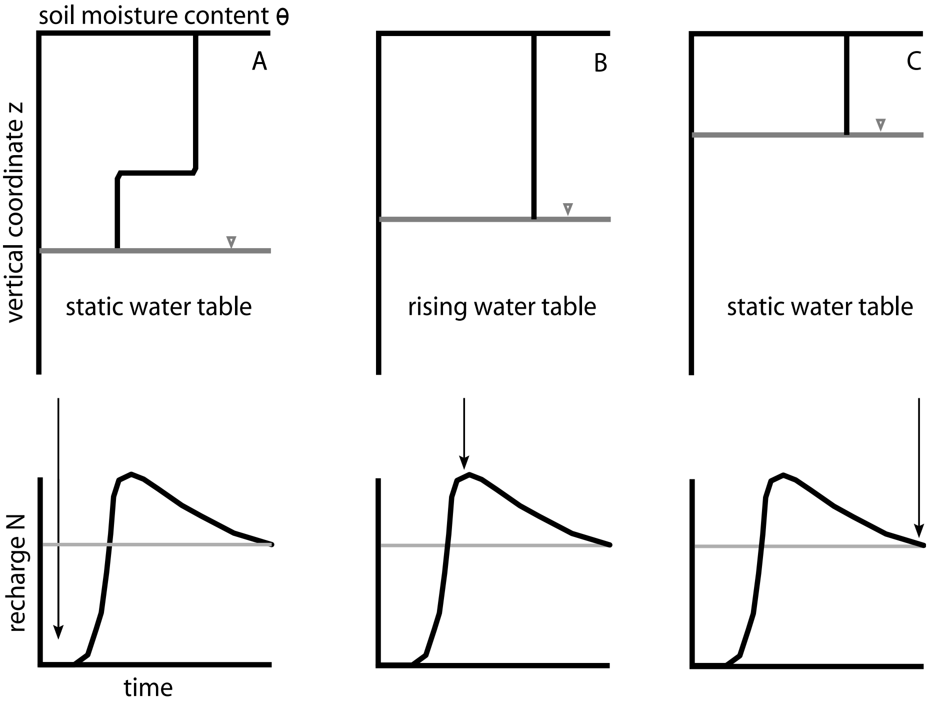

Figure 5.3: Schematic representation of the interactions between soil moisture dynamics (as a result of rainfall) and recharge rates, before (A), during (B), and after (C) a soil moisture pulse reaches the water table.

100m and range in width from 50m to 1.72m. A sandy soil of 3m depth overlies an impervious bedrock layer. On these hillslopes the models are compared under a constant rainfall intensity of 10mm/day for the first 50 days, followed by a free drainage period.

We use a sandy soil in our simulations since its properties correspond best with the original assumptions underlying Boussinesq's theory, developed for highly conductive and relatively shallow soils. Moreover, the effect of capillarity is likely to be smallest for these soil types. Thus, if inclusion of unsaturated zone effects leads to improved results for a sandy soil, we will have demonstrated the importance of unsaturated storage for a "worst-case" scenario, with even more noticeable effects expected for less conductive soil types.

Even though the unsaturated zone varies in depth, the vertical and lateral coordinates are both situated in a static frame of reference and discretized using a fixed number of nodes. The node spacing for the simulations in this work are $\Delta z = 0.075$m and $\Delta x = 1$m.

5.4.2 Boundary and initial conditions

For the saturated zone, it is assumed that the downhill boundary condition is $h(0,t) = 0$, and the uphill boundary condition is a zero-flux boundary as are all

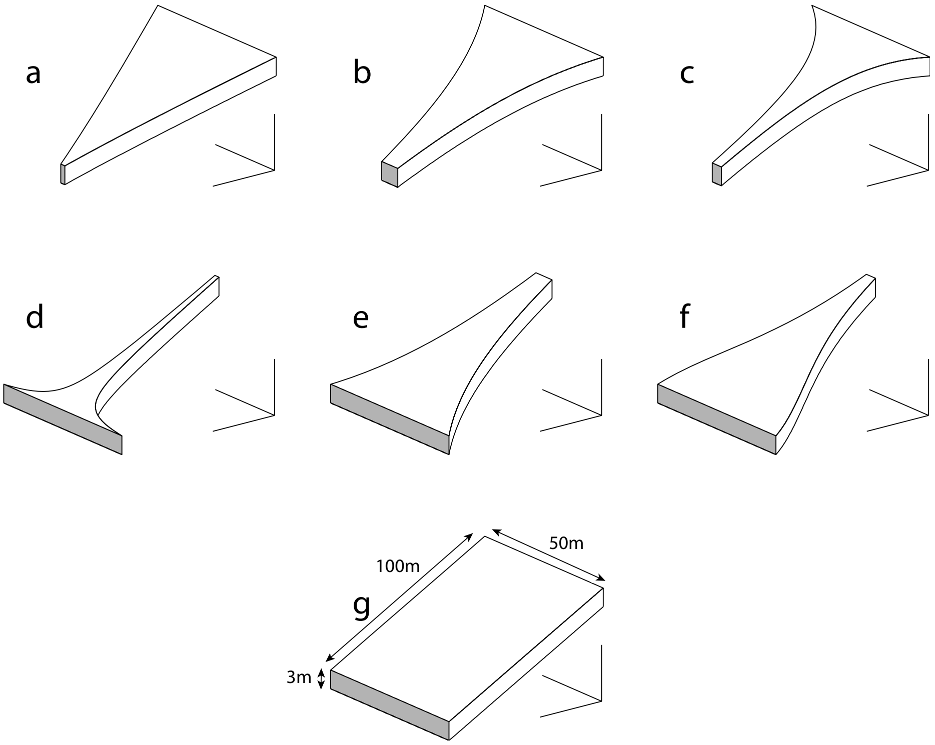

Figure 5.4: Three-dimensional view of three convergent (a,b,c), three divergent (d,e,f), and a straight hillslope (g) used in the model comparison study.

sides and the bedrock. At the upper boundary of the unsaturated zone we assume that the flux across the soil surface is equal to the rainfall rate: $q_v(0,t) = r(t)$. At the lower boundary (i.e., the bedrock) the pressure head is equal to the average water table height $\psi(D/\cos(\bar{i}),t) = \overline{h}(t)/\cos(\bar{i})$ for the coupled HSB model.

The initial condition for all models is a uniform water table $h(x,0) = 0.10$m above the bedrock, measured perpendicular to the bedrock for the coupled and original HSB models and vertical for the RE model, yielding comparable initial conditions (see *Paniconi et al.* [2003] for details). For HSB-coupled and the RE model we furthermore assume that the initial condition in the unsaturated zone is that of vertical hydraulic equilibrium. This yields a positive pressure head at the bedrock $\psi(D/\cos(\bar{i}),t) = \overline{h}(t)/\cos(\bar{i})$ for HSB-coupled, and $\psi(D/\cos(\bar{i}),t) = h(t)/\cos(\bar{i})$ for the RE model. The two formulations for the initial conditions differ slightly because HSB-coupled uses a single unsaturated zone profile, whereas the RE model is fully three-dimensional.

5.4.3 Hillslope and soil parameters

The hillslope plan shapes and dimensions are shown in Figure 5.4. For the simulations a bedrock slope of $i(x) = 5\%$ is used. The sandy soil overlaying

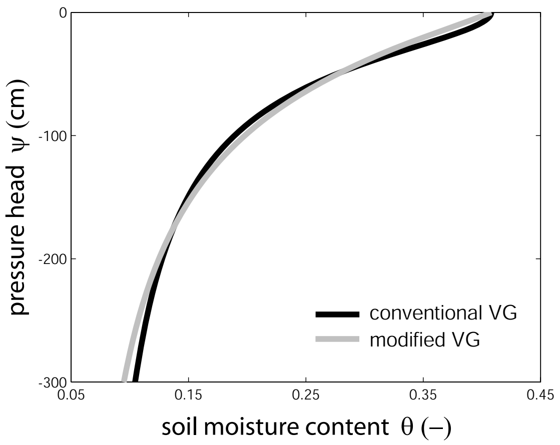

Figure 5.5: The retention characteristics of the sandy soil used in the model comparison. The black line depicts the conventional van Genuchten curve ($m = 1 - 1/n$) and the grey line is the modified van Genuchten curve ($m' = 1 + 1/n'$)

the impervious bedrock has a saturated hydraulic conductivity of $k = 5$m/d, and a aquifer specific storage coefficient $S_s = 0.01\text{m}^{-1}$. Table 5.1 lists the van Genuchten parameters for the conventional parameterization (i.e., $m = 1-1/n$), and for the modified parameterization of *Troch* [1992] and *Hilberts et al.* [2005] (i.e., $m' = 1 + 1/n'$). The corresponding soil water retention characteristics are plotted in Figure 5.5.

5.4.4 Parameterization of the capillary fringe

The capillary fringe is a narrow zone that serves as a transition between the vadose zone and the groundwater zone. The lower limit of the capillary fringe is commonly accepted to be the surface where pressure head is equal to zero, but the upper limit is scarcely definable ([*Hillel*, 1980]), with different authors placing it anywhere between 75% and 100% water saturation. *Berkowitz et al.* [2004] argued that the term "capillary fringe" should be replaced by the term "partially saturated fringe", because just above (and below) the water table we

Table 5.1: Van Genuchten parameters (conventional and modified) for the sandy soil used in the comparison study.

Parameter	**Sand**[a]	**Sand**[b]
$\theta_\mathbf{s}$ (-)	0.408	0.408
$\theta_\mathbf{r}$ (-)	0.054	0.054
α (1/cm)	-0.0254	-0.0081
n (-)	1.9529	1.4154

[a] for conventional $m = 1 - 1/n$
[b] for modified $m = 1 + 1/n$

often find small inclusions of entrapped air or inclusions of partially saturated soil causing the water content to be less than 100%. A range of ψ-values for which $\theta(\psi)$ is "close" to θ_s therefore is a more appropriate definition [*Bear*, 1972]. For the soils in this study the capillary fringe (or partially saturated fringe) is defined as the lowest value of ψ for which the soil moisture value is higher than $0.85 \cdot \theta_s \simeq 0.35$, which corresponds to a capillary fringe $\psi_c \simeq -0.27$m. The value is set at 85% water saturation because this is in good agreement with textbook values (e.g. *Bear* [1972]), and the resulting value for ψ_c is also in the range of values for a sandy soil (e.g. [*Bear*, 1972; *Harr*, 1962].

5.5 Model comparison results

5.5.1 Hydrographs and water tables

We describe the results of the model runs using HSB-coupled and we compare them with HSB-original and the RE model.

Figure 5.6 shows the outflow rates of the RE model, HSB-original, and HSB-coupled. The fit of the hydrographs of both HSB models compared to the RE model, for the rising and falling limbs, is summarized in Table 5.2. From Figure 5.6 we notice that for short times after initiation of the experiment, HSB-original shows higher fluxes than the RE model, which is due to the absence of an unsaturated zone description in this model, causing an instantaneous reaction to rainfall. This is most clearly visible for the divergent slopes (i.e., hillslopes d, e, f), where the hydrographs only climb after approximately 5-10 days for both the RE and the HSB-coupled model, whereas the HSB-original model shows an increase in flux starting at $t = 0$. At later times, however, the HSB-original fluxes are generally underestimated. These findings are supported by the values of the mean absolute errors given in Table 5.2. We see that HSB-original has higher mean absolute error values for all slopes in both the rising and falling limbs, with the exception of slope 3 (rising limb only) where due to a low estimation of the initial flux the errors for HSB-original and HSB-coupled are comparable.

Comparing the hydrographs of HSB-coupled and the RE model, we see a remarkably good agreement on all hillslopes. Also the timing of both hydrographs (i.e., the time at which the hydrograph starts to climb, and the time when peak outflow is reached) matches well. The goodness of fit suggests that a single soil moisture profile yields an adequate approximation of the unsaturated zone processes (as hypothesized in Section 5.2.2) is accepted.

In Figure 5.7 the water tables are shown for HSB-coupled, the RE model, and HSB-original, after 5 days, 20 days, 50 days, and 100 days. Table 5.3 summarizes the mean absolute errors in the water table values for each of these times when compared to the benchmark RE model. The water tables after 5 days are remarkable: whereas HSB-original is performing very poorly (i.e., large overestimation of water tables), the HSB-coupled water tables match almost perfectly on all hillslopes; the modeled water tables are in many cases indistinguishable from the RE results. The water tables after 20 days also show a remarkable match for HSB-coupled for all hillslopes. Looking at the results after 50 and 100

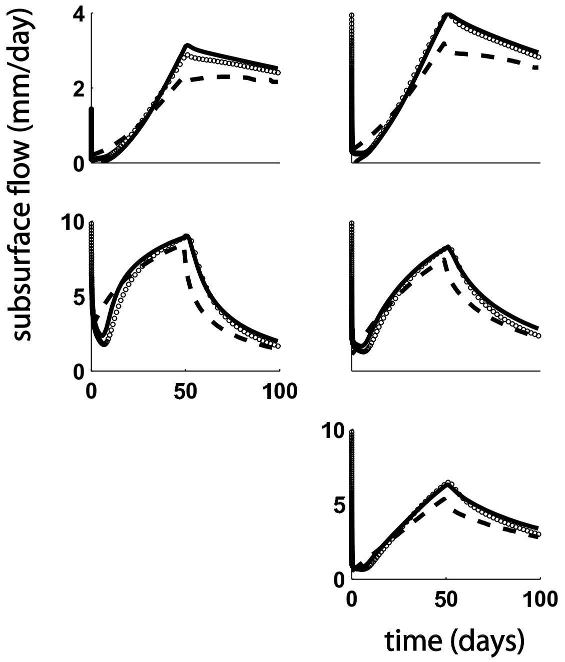

Figure 5.6: Outflow hydrographs as a result of a rainfall rate of 10 mm/day for the first 50 days followed by a pure drainage period, for HSB-coupled (solid lines), HSB-original (dashed lines), and the RE model (circles).

days, we see that both HSB models produce similar water table heights for the convergent slopes, with both models overestimating the water table heights. For the divergent slopes both models again overestimate the water table height, but the match for the HSB-coupled model is much better than that of HSB-original.

Overall we conclude that HSB-coupled is clearly better able to reproduce the hydrographs for all hillslopes, and in particular for the divergent slopes. The same holds for the water table values, except that the advantages of HSB-coupled over HSB-original for the convergent slopes at later times in the experiment is less noticeable. The differences between the HSB-coupled and RE water table profiles, for the convergent slopes in particular, may be caused by errors introduced when using a single soil moisture profile for HSB-coupled. We expect that this error will be largest for convergent slope shapes and steep slope angles, because of the relatively sharp gradients in water tables at later times in the experiment. The validity of using a single soil moisture profile for higher bedrock slopes and more convergent shapes will be investigated in future work, especially considering that overland flow may occur in these simulations, causing very different local responses.

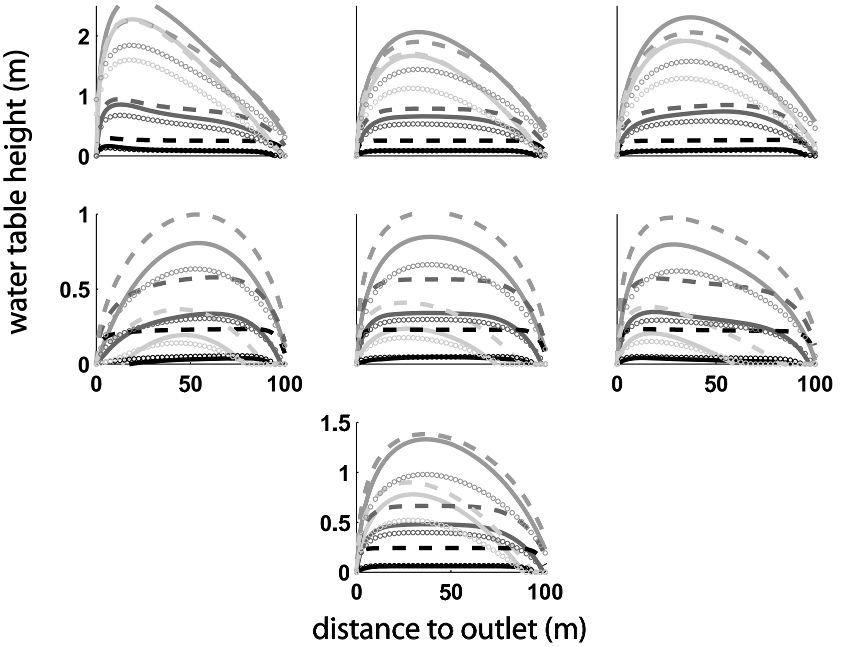

Figure 5.7: Water tables for HSB-coupled (solid lines), HSB-original (dashed lines), and the RE model (circles), after 5 (black), 20 (dark grey), 50 (grey), and 100 days (light grey).

5.5.2 Recharge rates

Figure 5.8 shows the value of the recharge term N in Equation 5.16 and the rainfall rates during the experiment. We see that the values of N are initially negative due to a rapidly dropping water table and little water supply by the unsaturated zone. When the soil moisture front (due to rainfall) approaches the water table (roughly between $t = 2$ and $t = 4$ days), the value of N rises to positive values. The positive recharge rates cause the water tables to rise, thereby taking up water from the unsaturated zone, which in turn causes enhanced recharge rates (roughly between $t = 4$ and $t = 10$ days). As the water table rises, the lateral flux increases and (roughly around $t = 10$ days) the water table and outflow rate start to converge towards steady state. A new equilibrium is reached when $r = N$, which on the divergent hillslopes (d to f) is approached around $t = 50$ days. Because the rainfall rates drop to 0 mm/day at $t = 50$ days, the equilibrium is not fully reached. Just after $t = 50$ days we see that the recharge rates decline quickly, and eventually drop to below $N = 0$ due to the falling water tables.

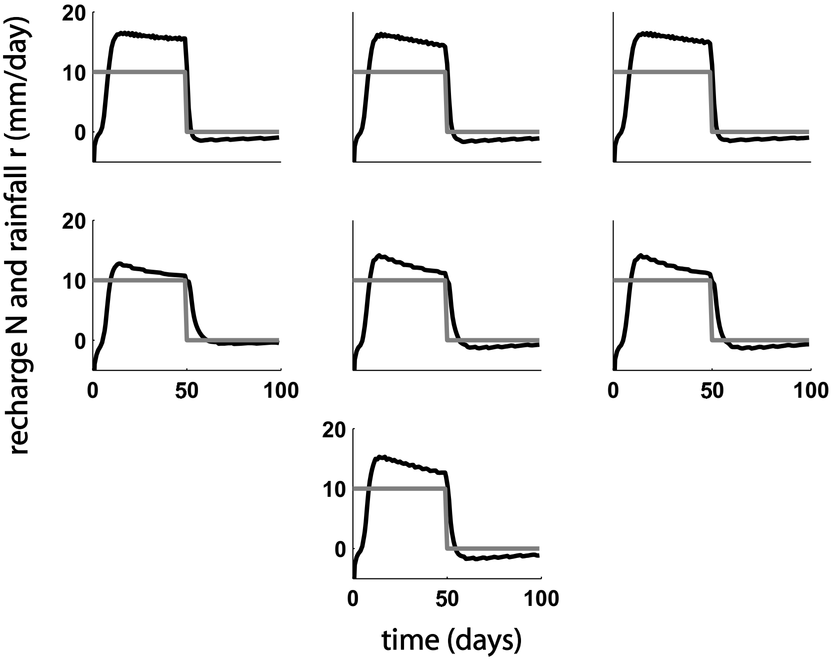

Figure 5.8: Rainfall rates (grey) and recharge rates (black) calculated using Equation (5.16)

5.6 Discussion

In the Introduction we indicated that over the past decades there have been many attempts to model hillslope and catchment hydrological processes. Most of these attempts have been aimed at predicting outflow rates, but recently several model studies have also investigated the water table dynamics (or saturated storage dynamics) that are of crucial importance in determining the location and size of variable source areas, and thereby also to assess the risk for flood peaks in the channel network draining a hillslope or catchment. Examples include *Wigmosta et al.* [1994] and *Ivanov et al.* [2004], who present high-dimensional catchment scale models, and *Seibert and McDonnell* [2002], *Weiler and McDonnell* [2004] and *Brooks et al.* [2006] who present the results of a conceptual modeling study applied to the hillslope scale. Even though these models have been applied successfully in the studies presented, they are all partly or fully conceptual instead of physically based, which makes the investigation of the exact interactions between the saturated and unsaturated zones cumbersome. In this work we have presented a physically based low-dimensional hillslope model. In the test cases we assumed that the conductivity, soil depth and other soil properties are constant in depth and in the direction along the hillslope, but the saturated module of the coupled model and the original HSB model are capable of handling spatial

Table 5.2: The mean absolute errors (mm/day) in the hydrographs of HSB-original and HSB-coupled when compared to the RE model.

			rising limb error (mm/d)				
slope #	**1**	**2**	**3**	**4**	**5**	**6**	**7**
HSB-orig.	0.23	0.36	0.33	0.80	0.58	0.56	0.54
HSB-coup.	0.22	0.32	0.36	0.41	0.36	0.35	0.35
			falling limb error (mm/d)				
HSB-orig.	0.38	0.51	0.44	1.00	0.66	0.61	0.62
HSB-coup.	0.06	0.13	0.16	0.39	0.47	0.51	0.26

variability along these axes. On the other hand, since all variables and properties are assumed to be constant over the width of the hillslope, we cannot account for spatial variability along this axis. In the current version of the coupled formulation we also cannot account for spatial variability in rainfall rate or soil hydraulic properties of the unsaturated zone, because a single soil moisture profile is used to model the unsaturated zone dynamics. Moreover, we assume that groundwater fluxes are parallel to the bedrock, and we do not use an infiltration model, thus the rainfall is assumed to infiltrate fully into the soil column (i.e., no infiltration-excess runoff).

The properties of the sandy soil in our simulations correspond best with the original assumptions underlying Boussinesq's theory, as the equations were derived for highly conductive and relatively shallow soils. Sandy soils have a smaller capillarity effect than silt, loam or clay soils. Hence, the improvement in hydrological simulations when coupling the saturated and unsaturated zones presented here, provides a good test case in terms of saturated properties and retention characteristics. For less conductive soils, we expect greater improvement than achieved for the sandy soil type.

The developed HSB-coupled model is an efficient, parsimonious model that can be used in investigations of variable source areas, which play an important role in the generation of saturated overland flow and floods. Because the described model also outputs pressure heads and soil moisture contents in the

Table 5.3: The mean absolute errors (m) in the water tables of HSB-original and HSB-coupled when compared to the RE model for slope numbers 1 to 7.

				slope number				
model	**time (days)**	**1**	**2**	**3**	**4**	**5**	**6**	**7**
HSB-orig.	5	0.16	0.17	0.17	0.18	0.18	0.18	0.17
HSB-coup.	5	0.01	0.01	0.01	0.02	0.01	0.01	0.01
HSB-orig.	20	0.26	0.26	0.26	0.25	0.26	0.26	0.26
HSB-coup.	20	0.06	0.05	0.06	0.02	0.01	0.02	0.03
HSB-orig.	50	0.34	0.37	0.39	0.30	0.31	0.30	0.35
HSB-coup.	50	0.29	0.27	0.32	0.09	0.09	0.08	0.16
HSB-orig.	100	0.40	0.39	0.44	0.15	0.16	0.14	0.26
HSB-coup.	100	0.35	0.31	0.36	0.07	0.08	0.09	0.17

unsaturated zone, it has potential applications in combination with land-surface models, where unsaturated zone processes and interactions with shallow groundwater are generally not simulated well. Overall, the low dimensionality of the HSB model makes it appealing for poorly gauged catchments, since the required parameters are relatively easily accessible and since the model is much less computationally demanding than a full three-dimensional RE (or analogous) model. Future work includes testing the model in the field, for instance on the experimental hillslope and small catchment described in *Brooks et al.* [2004, 2006], and accounting for hysteresis and macropore flow.

5.7 Conclusions

In this work we have presented a coupling between the one-dimensional Richards equation for unsaturated flow and the one-dimensional hillslope-storage Boussinesq model (HSB, [*Troch et al.*, 2003]) for lateral saturated flow along complex hillslopes. In the model we have included the capillary fringe in the Boussinesq flow domain, i.e., the aquifer depth was taken to be the sum of the water table height and the height of the capillary fringe, ψ_c. We assumed the fluxes in the unsaturated zone to be vertical, and in the saturated zone parallel to the underlying impervious bedrock (i.e., Dupuit-Forchheimer assumption). We assumed that an average soil moisture profile derived for the entire hillslope provides an adequate description of unsaturated zone processes. This assumption, which proves to yield sufficiently accurate results based on the timing of the hydrographs, together with the manner in which the HSB formulation is able to represent a three-dimensional soil mantle as a one-dimensional flow system, makes possible a very efficient low-dimensional model of unsaturated and saturated hillslope dynamics.

The role of the unsaturated zone in transmitting the soil moisture pulses as a result of rainfall is investigated, and the relationships between rainfall, recharge, drainable porosity and unsaturated storage are analyzed. Besides the expected delaying effect of the unsaturated zone on recharge rates, the simulations also showed that the unsaturated zone does not always dampen the rainfall signal, but can also amplify it, causing recharge rates to exceed rainfall rates under certain conditions. This effect is caused by water tables including water from the unsaturated zone into the saturated zone as they rise.

The coupled model (HSB-coupled) was compared (in terms of hydrographs and water table distributions) to the original HSB model (HSB-original) and to a three-dimensional RE model (taken to be the benchmark) on a set of seven synthetic hillslopes, ranging from convergent to divergent. The modeled outflow rates of HSB-original are systematically lower than those of the RE model. For the HSB-coupled model, the outflow rates and the timing of the hydrographs (the time to the first increase in outflow, the time to peak, etc.) very closely matched that of the RE model for all hillslopes at all times. Also the match to the water tables is significantly better than that of HSB-original, especially for the divergent slopes. The correct timing of the HSB-coupled hydrographs suggests that a single soil moisture profile suffices to describe the unsaturated zone dynamics. We conclude that for the hillslope configurations and scenarios examined in this paper it is possible to reproduce hydrographs and water table dynamics with a good degree of accuracy.

Chapter 6

Evaluation of a low-dimensional coupled hillslope-hydrological model using data from a plot-scale experimental site in Troy (ID), USA.

Abstract

In this study we evaluate a low-dimensional coupled saturated-unsaturated hillslope hydrological model described in *Hilberts et al.* [2006] by comparing the outflow response and the space-time evolution of water table heights with measurements obtained from a hillslope plot near Troy (ID), USA. In the model, a one-dimensional Richards model for unsaturated zone dynamics is coupled to the HSB-model for lateral subsurface flow described in *Troch et al.* [2003]. The model was adapted such that available information on the relationship between saturated hydraulic conductivity and depth $k(z)$ could be implemented. The water retention characteristics are determined based on soil core analysis and the $k(z)$-relationship is parameterized based on outflow measurements, and no calibration is conducted. Different boundary conditions and different parameterizations for the $k(z)$-relationship are investigated.

We conclude that the model's hydrograph response is reasonable, showing slight underestimations of most peak flows, and slight overestimations during most recession periods. The timing of the peaks in the hydrographs and the water tables is generally well captured. Also the water table response is well captured, but also here the peaks are generally underestimated. This phenomenon may be caused by the small free pore space during nearly saturated conditions, which causes a very sensitive response of the water tables under these conditions. Thus, the underestimations for peak water table values may be caused by small differences in the calculated precipitation, recharge or subsurface flux. The overestimation of water tables and fluxes during recession periods may be caused by using a single van Genuchten parameterization for the entire soil profile, whereas several soil horizons with slightly different retention characteristics are present. Recent experimental results indicate that also the porosity decreases with depth, which may explain the quick water table responses and decreased outflow rates.

6.1 Introduction

In catchment hydrology, numerical models are widely used to investigate the hydrological response to rainfall events. Over the last decades the hydrological community has acknowledged the importance of variable source areas in the generation of flood peaks (e.g., *Dunne and Black* [1970]; *Freeze* [1972b]; *Niedzialek and Ogden* [2004]), and for this reason an increasing emphasis has been put on hydrological models that are able to accurately simulate the water table dynamics. However, a restriction that modelers have to deal with is the structural lack of appropriate data to parameterize and calibrate/validate the applied models. This restriction in particular applies to distributed, physically-based models, that typically require a large amount of data for this purpose (e.g, *Beven and Moore* [1992]; *Freeze* [1972a]). To overcome this problem, models have been developed that are capable of simulating water table dynamics (e.g., [*Beven and Kirkby*, 1979; *Bierkens*, 1998; *Bronstert*, 1999; *Chapman*, 2005; *Duffy*, 1996; *Reggiani et al.*, 1998; *Smith and Hebbert*, 1983]), but still evaluation of the performance is typically cumbersome due to a lack of distributed measurements of water table dynamics. Only few papers have been published in which model performance is thoroughly evaluated using distributed field measurements (e.g., [*Brooks et al.*, 2006; *Frankenberger et al.*, 1999; *Torres et al.*, 1998]).

Recently, *Hilberts et al.* [2006] developed a low-dimensional coupled saturated-unsaturated hillslope hydrological model (HSB-coupled) that is capable of simulating outflow rates and water table dynamics. The model performs remarkably well when compared to a three-dimensional Richards model applied to hillslopes with different plan and profile shapes. In this study we adapt the model to incorporate available information on the relationship between saturated hydraulic conductivity and depth, and we evaluate the model's performance by comparing model results to distributed measurements from a well-instrumented hillslope-plot experiment. We also investigate the effect of the fixed-head lower boundary condition by comparing it to a free-surface boundary condition (i.e. seepage face) as described in *Chapman* [2005], and we analyze the effect of the parameterization of the relationship between conductivity and depth.

6.2 Model description

The model used in this study (HSB-coupled) couples a one-dimensional Richards equation model to describe the unsaturated zone processes the HSB model of *Troch et al.* [2003] for lateral subsurface flow. In the modeling approach, the capillary fringe is regarded as an integral part of the Boussinesq aquifer. Thus, lateral groundwater fluxes are assumed to take place over the entire saturated domain, instead of only below the water table, which is typically assumed in Boussinesq-type modeling approaches. The model is described as a system of two partial differential equations which are solved simultaneously [*Hilberts et al.*, 2006]. The governing equations read:

$$\begin{aligned} wf\frac{\partial h}{\partial t} &= -\frac{\partial (wq)}{\partial x} + w\cos(i) \\ &\cdot \left\{ r - \int_0^{\lambda} \frac{\partial \theta}{\partial t}\mathrm{d}z + \frac{1}{\cos(i)}\int_0^{\lambda} \frac{\mathrm{d}\theta}{\mathrm{d}\psi}\frac{\partial h}{\partial t}\mathrm{d}z \right\} \end{aligned} \tag{6.1}$$

$$C\frac{\partial \psi}{\partial t} = -\frac{\partial K(\psi)}{\partial z}(1 - \frac{\partial \psi}{\partial z}) + K(\psi)\frac{\partial^2 \psi}{\partial z^2} \tag{6.2}$$

where $w = w(x)$ is the width-averaged hillslope width at distance x from the outlet, $h = h(x,t)$ is the water table height measured perpendicular to the restrictive layer, t is time, $q = -k(h - \psi_c)(\partial h/\partial x \cos(i) + \sin(i))$ is the Darcy flux parallel to the restrictive layer, ψ_c is the capillary fringe value (always negative in sign), k is the saturated hydraulic conductivity, i is the restrictive layer slope angle, $r = r(t)$ is the rainfall rate, $\lambda = \lambda(t)$ is the hillslope-averaged depth to the saturated zone (i.e., the average depth from the soil surface to the top of the capillary fringe), $\theta = \theta(z,t)$ is the corresponding (vertical) soil moisture profile, z is the vertical coordinate (positive downward), $\psi = \psi(z,t)$ is the suction head in the profile, $K = K(\psi)$ is the unsaturated hydraulic conductivity, $f = f(h)$ is the drainable porosity after *Hilberts et al.* [2005], modified such that recharge rate is vertical instead of perpendicular to restrictive layer:

$$f(h) = (\theta_s - \theta_r)\left\{ 1 - \cos(i)\left(1 + (-\alpha'\lambda)^{n'}\right)^{-(\frac{n'+1}{n'})} \right\} \tag{6.3}$$

and the soil water retention function is parameterized using the van Genuchten relationship [*van Genuchten*, 1980]:

$$\theta(\psi) = \theta_r + (\theta_s - \theta_r)\left(\frac{1}{1 + (\alpha\psi)^n}\right)^m \tag{6.4}$$

where θ_s, θ_r, n, and m are fitting parameters. Equation 6.4 is parameterized such that $m = 1 - 1/n$, yielding the regular van Genuchten parameters. An alternative parameterization is also conducted, assuming that $m = 1 + 1/n$, yielding the modified van Genuchten parameters described in *Hilberts et al.* [2005]. The modified parameters will be indicated with a prime (i.e., α', n', and m'), and are used to analytically integrate the soil water retention curve and thereby derive the analytical expression for drainable porosity (Equation 6.3), that is required to solve the system of coupled differential equations (i.e., Equations 6.1 and 6.2).

Equation 6.3 is derived in *Hilberts et al.* [2005], and gives an analytical expression for the drainable porosity, assuming that the unsaturated zone above the water table is in vertical hydraulic equilibrium. The drainable porosity can then be expressed as a function of the depth to the unsaturate zone and the van (modified) Genuchten parameters. Since the unsaturated zone is not in equilibrium due to constantly changing precipitation, the deviations from an equilibrium condition are accounted for through the recharge term within accolades in Equation 6.1. $C = C(\psi)$ is the differential moisture capacity:

$$C(\psi) = \frac{\mathrm{d}\theta}{\mathrm{d}\psi} \tag{6.5}$$

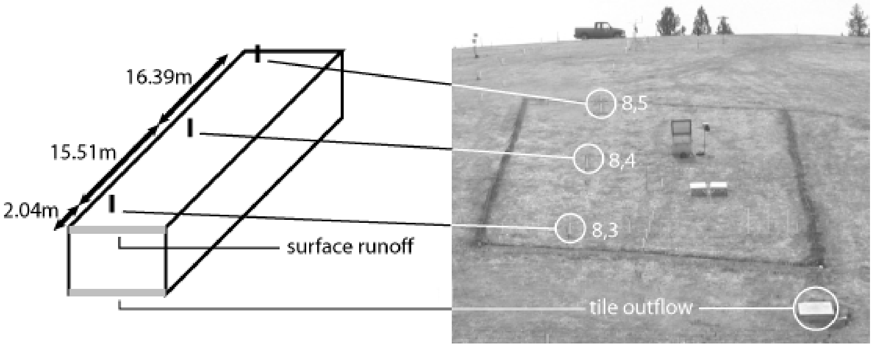

Figure 6.1: The hillslope plot with the location of the piezometers, the tile drains for subsurface flow and surface runoff.

6.3 Site description

The experimental site is located 8 km North of Troy (ID) in the eastern Palouse region and is described in *Brooks et al.* [2004] and *Brooks et al.* [2006]. The hillslope plot has a length of 36m and a width of 18m. The average soil depth is approximately 0.67m. All borders are lined with plastic sheets from the soil surface to the restrictive layer and the side slopes and upslope divide are also covered with metal sheeting to prevent run-on and side losses. A buried tiledrain is installed upslope to prevent upslope subsurface flux from entering the hillslope plot. The soil types are classified as silt-loam, overlying a impermeable fragipan layer. The soil profile consists of three silt-loam horizons with different conductivities and different soil water retention characteristics [*Brooks et al.*, 2004].

At this hillslope plot three (automated) piezometers are installed that monitor on an hourly basis pressure head levels at the depth of the fragipan, i.e., at approximately 0.67m below the soil surface. To monitor air temperature and precipitation, a weather station is located on the hillslope. At the base of the plot a tile drain is installed to separately monitor subsurface flow and overland flow, using two tipping buckets. The locations of the tile drains, and the three piezometers are indicated in Figure 6.1.

6.4 Modeling procedure

6.4.1 Assumptions underlying the modeling procedure

In this work we assume that the hillslope has a constant depth of 0.67m, that the soil hydraulic properties (see section 6.4.2) do not vary in the lateral or vertical direction, except for the saturated hydraulic conductivity, which proved to be a sharply declining function of depth (see *Brooks et al.* [2004]). We also assume that saturated subsurface flow takes place in the lateral direction only (i.e., parallel to the fragipan and downslope), and that the fluxes across the width of the hillslope are negligible. For the unsaturated zone fluxes, it is assumed that the fluxes are vertical. The capillary fringe is regarded as an integral part of the Boussinesq aquifer, since experimental evidence shows that the fluxes in the capillary fringe are typically laterally directed (e.g., [*Berkowitz et al.*, 2004; *Vachaud and Vauclin*, 1975]). The precipitation (see section 6.4.4) is also assumed uniform over the hillslope. For the model runs in this study, we used 73 nodes for the lateral discretization ($\Delta x = 0.50m$), and 68 nodes ($\Delta z = 0.01m$) for the vertical discretization.

6.4.2 Soil parameters

To apply the HSB-coupled model to the hillslope plot, we need to set the soil hydraulic parameters (i.e., α, n, and the $k(z)$-relation), and to define hillslope geometry. We use the double exponential conductivity-to-depth relationship that is derived based on experimental results and that is reported in *Brooks et al.* [2004] and *Brooks et al.* [2006]:

$$K(\psi) = k(z)k_r = (a_1 \exp(-a_2 z) + a_3 \exp(-a_4 z))k_r \tag{6.6}$$

where a_1 to a_4 are fitting parameters, z is the vertical coordinate taken positive downward. We adapted the model code such that this relationship between conductivity and depth could be implemented. The relationship is parameterized using outflow measurements from the tile drain and recordings from piezometer 8, 3 for two time periods: the first being from the 26th March to the 14th of April 2002 [*Brooks et al.*, 2004], the second from the 26th of March to the 26th of April 2003. The parameterization based on the first set yields the parameter values $a_1 = 1.2731 \cdot 10^{-4}$ ms^{-1}, $a_2 = 5.5$, $a_3 = 1.0417 \cdot 10^{-3}$ ms^{-1}, and $a_4 = 50$. The parameterization based on the second set yields the parameter values $a_1 = 1.4363 \cdot 10^{-4}$ ms^{-1}, $a_2 = 7.8$, $a_3 = 2.5382 \cdot 10^{-4}$ ms^{-1}, and $a_4 = 17.60$. Both sets of parameters will be used to evaluate the model response.

The relative conductivity k_r is defined as

$$k_r = ((1 + (\alpha\psi)^n)^{-m})^{1/2}(1 - (1 - (1 + (\alpha\psi)^n)^{-1})^m)^2 \tag{6.7}$$

The lateral conductivity $k = k(h(x,t))$ is defined as the integral of $k(z)$ (see Equation 6.6) over h:

$$\begin{aligned} k(h) &= \frac{1}{h}(\frac{a_1}{a_2}(\exp(-a_2 h) - \exp(-a_2 D)) \\ &+ \frac{a_3}{a_4}(\exp(-a_4 h) - \exp(-a_4 D))) \end{aligned} \tag{6.8}$$

where D is the soil depth. Note that k is varying in space and time through it's dependency on $h(x,t)$. The regular (i.e., $m = 1 - 1/n$) and modified (i.e., $m' = 1 + 1/n'$, see [*Hilberts et al.*, 2005]) van Genuchten parameters for the silt-loam soil are calculated based on core sample measurements and are listed in Table 6.1.

Note that we use a single parameterization to describe the soil water retention characteristics of the entire soil profile, which consists of three horizons with different retention characteristics [*Brooks et al.*, 2004].

Given that $1/\alpha$ can be regarded as a good approximation for the capillary fringe [*Cho and Rooij*, 1999], we estimate its value $\psi_c \simeq -0.25$m, which corresponds to the top 10% of θ-values of the retention curve, which is within the range of values that is normally considered to belong to the capillary fringe (e.g., [*Berkowitz et al.*, 2004]).

6.4.3 Boundary and initial conditions

For the hillslope plot, the divides and the restrictive layer are treated as a zero-flux boundary, except for the outlet, where either a fixed-head ($h = 0$ at the outlet) or a free-surface (i.e., seepage face) boundary condition is assumed. The fluxes across the soil surface are assumed to be equal to the net precipitation, thus no infiltration model is used and all precipitation is assumed to fully infiltrate into the soil.

To investigate the effect of the boundary condition on water table dynamics, we also apply a free-surface boundary condition, allowing a seepage face to develop. The relationships used to describe the boundary condition derive from *Chapman* [2005] and are adapted to suit the small differences in model description between *Chapman* [2005] and *Hilberts et al.* [2006]. *Chapman* [2005] derived

$$H_s = (0.82 + 0.42 \tan i)Q \tag{6.9}$$

where $H_s = h'/L'$ is the dimensionless seepage face pressure head, h' is the seepage face pressure head measured vertically, and L' is the length of the hillslope measured horizontally, $Q = q'/(kL')$ is the dimensionless outflow rate, and q' is the (horizontal) subsurface flux. Reformulating Equation 6.9 in the hillslope-storage Boussinesq coordinate system yields an equation that can be used to describe the free-surface lower boundary condition:

$$\frac{\mathrm{d}h}{\mathrm{d}x} = -\tan i + \frac{1}{\cos^3 i(0.82 + 0.42 \tan i)} \tag{6.10}$$

The equation implies that the water table gradient nea the outlet is solely determined by the restrictive layer slope angle i. In the following we will assume that this relationship can be used to describe the seepage face height, however, the

Table 6.1: The regular ($m = 1 - 1/n$) and modified ($m' = 1 + 1/n'$, see *Hilberts et al.* [2005]) van Genuchten parameters for the silt-loam soil type of the hillslope plot.

parameter	**regular**	**modified**
$\theta_\mathbf{s}$ (-)	0.49	0.49
$\theta_\mathbf{r}$ (-)	0.19	0.19
α (1/cm)	-0.0395	-0.0009
n (-)	1.2627	0.6927

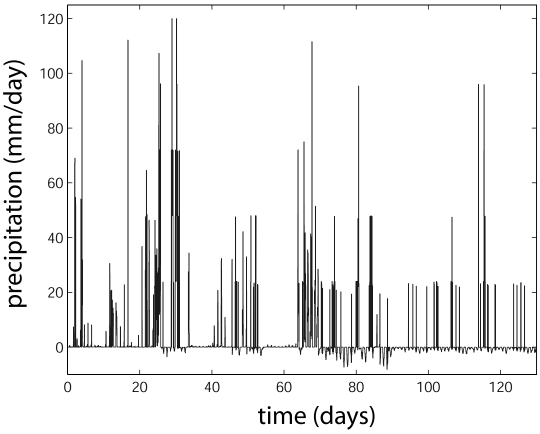

Figure 6.2: Precipitation rates (rainfall + snow melt) for the period 1st of January to 10th of May 2003.

authors are aware of the fact that the relationship is likely to become less accurate as the seepage face height gets closer to the soil surface. After discretization of Equation 6.10, the seepage face pressure head can be calculated based on the adjacent upslope pressure head value.

As an initial condition we use a uniform water table profile that corresponds to 60% saturation. The first 20 days of the simulation are used for the model to spin-up, and allows the effect of the initial conditions to gradually fade away. Analysis of the water table response showed that after 20 days, the effect of the initial condition was not noticeable anymore (not shown here). The outflow rates and temporal evolution of the water tables are not evaluated during the spin-up: the model response is analyzed starting after the spin-up period.

6.4.4 Model inputs

The net precipitation for the HSB-coupled model is calculated as

$$r = q_p - q_{et} \tag{6.11}$$

where q_p is the precipitation rate $[LT^{-1}]$ (i.e., rainfall + snow melt, calculated according to *Brooks* [2003]), and q_{et} is the evapotranspiration rate $[LT^{-1}]$ calculated according to *Thornthwaite and Mather* [1955]. Hourly data of the net precipitation rate from 0.00h on the 1st of January 2003 until 24.00h on the 10th of May 2003 are depicted in Figure 6.2.

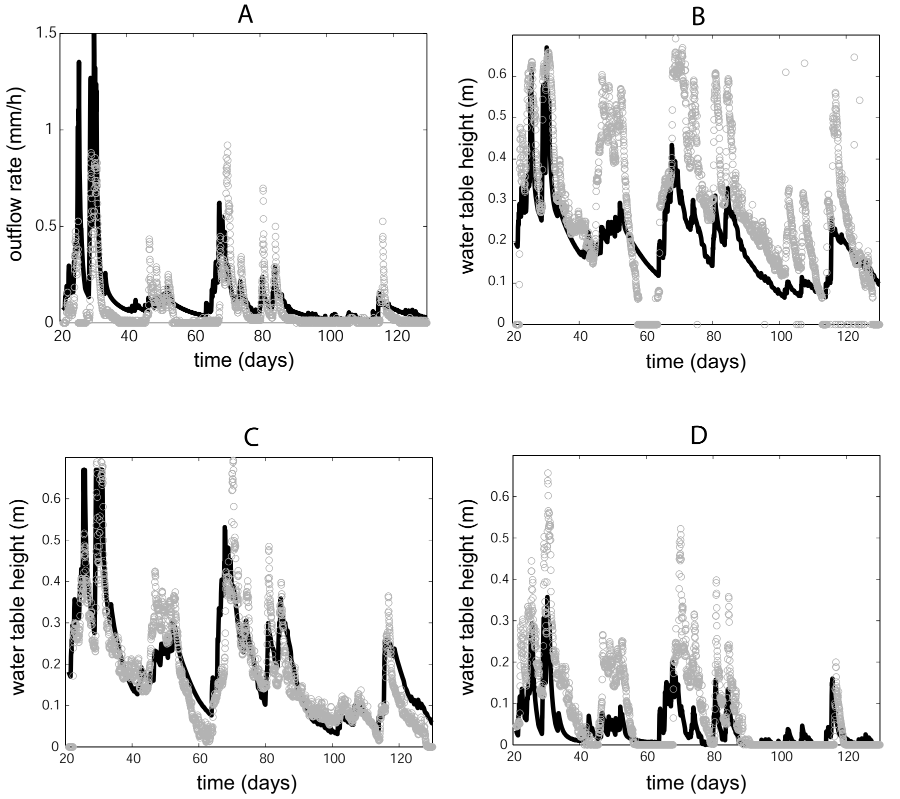

Figure 6.3: Subsurface outflow rates (i.e., tile outflow (A)) and the temporal evolution of the water table heights (B/D) from the 21st January onwards, using a Dirichlet boundary condition. Grey dots indicate measurements and the black lines are the model results.

6.5 Hydrograph response and perched groundwater dynamics

6.5.1 Fixed-head lower boundary condition

Figure 6.3 compares modeled subsurface flow at the outlet and water table dynamics at the three piezometer locations with observations. The hydrograph response (Figure 6.3-A) shows that the timing of the peaks is generally well reproduced, except for the peak at approximately $t = 71$ days. The height of the peak flows is captured well at the beginning of the observation period. However, in later stages of the simulation the height of the peaks is often underestimated. We also note that the recession periods initially show slightly overestimated outflow rates. Note that the overestimation after the peak at approximately $t = 26$ days is due to a malfunction of the tipping bucket from $t = 26$ to $t = 28$ days caused by frost.

Also for the piezometer response (Figures 6.3-B/D) we see that the peaks are generally timed well, and also the peak values are initially captured well, but in later stages of the simulation period, the piezometric levels are underestimated. This is particularly the case for piezometers $8, 3$ (B) and $8, 5$ (D). However, for piezometer $8, 4$ (C) we see a very good agreement between modeled and measured water tables.

6.5.2 Seepage face lower boundary condition

The modeled water tables dynamics in space and time and the outflow rates using a seepage face lower boundary condition (see section 6.4.3) are given in Figure 6.4. We see that the outflow rates (A) are very similar to those of Figure 6.3-A, except for the values for the first two peaks. Also the water table heights in piezometers $8, 4$ (C) and $8, 5$ (D) are almost identical to those in Figure 6.3. However, for the piezometer closest to the outlet (B), we see that compared to the runs with a Dirichlet ($h = 0$m) boundary condition, the water table heights have increased slightly. We note that, even though still underestimated, the peak water tables at $t \simeq 45 - 53$ days are more accurately simulated. Also the peak water table value at $t \simeq 68$ days is better simulated using a seepage face.

6.6 Discussion

In relation to the peak water table values, we note that especially for nearly saturated conditions the empty pore space is limited due to the effect of capillarity. This effect was already noted by *Hooghoudt* [1947] and referred to as the "Wieringermeer-effect". In the modeling approach, this effect is reflected in small values for drainable porosity [*Hilberts et al.*, 2005]. The small amount of empty pore space causes a very sensitive response of the water tables under these conditions. Thus, the underestimations for peak water table values may be caused by very small differences in the calculated lateral volume flux, precipitation or recharge.

The slight underestimation of the peak values and the simultaneous overestimation of recession values for water tables and outflow rates may be a result of using a single van Genuchten parameterization for the entire soil profile. Recent experimental results indicate that not only the saturated hydraulic conductivity is much smaller for the soil layer closest to the fragipan, but also the porosity decreases with depth. Lower porosity values in the layer closest to the fragipan will cause the available pore space (drainable porosity) to be smaller, which in turn causes a quicker water table response and decreased outflow rates [*Paniconi et al.*, 2003].

Also the relationship between saturated hydraulic conductivity and depth, which in *Brooks et al.* [2004] is estimated from data obtained during low precipitation rates compared to those in this paper, is likely to affect the underestimated outflow rates and water table heights. In section 6.4.2, two different parameterizations of the conductivity-to-depth relationship are given. Both parameterizations are derived using data collected over a comparable time span. The second set of parameters is used here to illustrate the effect of different,

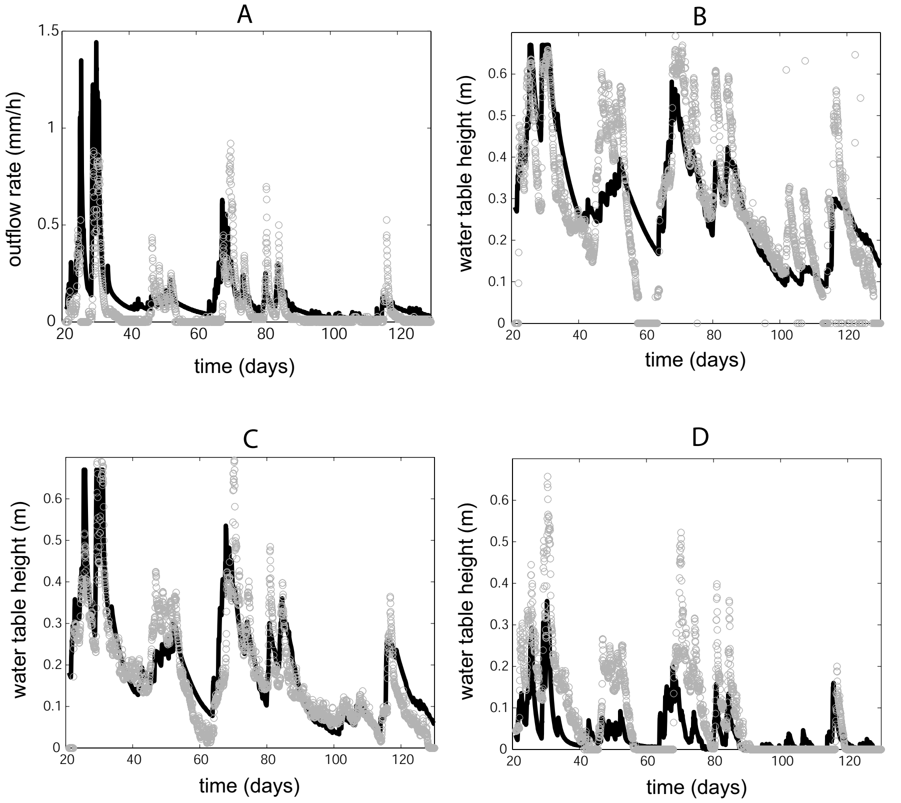

Figure 6.4: Subsurface outflow rates (A) and water table heights (B/D) from the 21st January onwards, using a seepage face boundary condition. Grey dots indicate measurements and the black lines are the model results.

but equivalent parameterizations of the $k(z)$-relationship. The results obtained using this set of parameters for two different types of boundary conditions (i.e., fixed-head and seepage face) are given in Figure 6.5.

We note that the recession periods of the hydrograph are slightly better captured using this parameterization, but the differences are very small. For all piezometers we see that the peak water tables are modeled more accurately, e.g., the peaks at approximately $t = 45 - 53$ and $t = 68$ days. However, the increased accuracy for peak water tables goes at the expense of reduced accuracy during recession periods. Also for this parameterization we note that different boundary condition only significantly affect the most downslope piezometer: for piezometers $8,4$ and $8,5$ (C and D) the results for the different boundary conditions are indistinguishable.

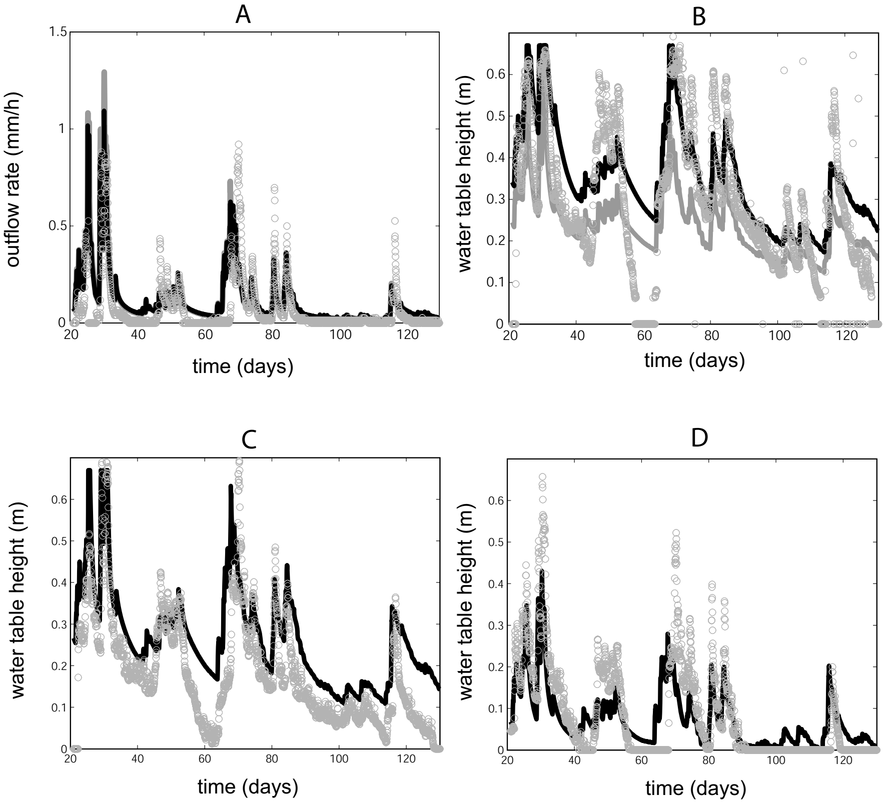

Figure 6.5: Subsurface outflow rates (A) and water table heights (B/D) from the 21st January onwards, for an alternative $K(z)$-parameterization, using a Dirichlet (grey lines) and a seepage face (black lines) boundary condition. Grey dots indicate measurements.

6.7 Conclusions

In this paper we evaluate the low-dimensional HSB-coupled model described in *Hilberts et al.* [2006] by comparing the outflow response and the temporal evolution of the water table heights with measurements obtained from a well-instrumented hillslope plot of approximately 18x36m near Troy (ID), USA. The HSB-coupled model was adapted such that the available information on the double-exponential relationship between saturated hydraulic conductivity and depth could be implemented. Apart from the parameterization of the van Genuchten relationship and the relationship between conductivity and depth, which are determined a priori, no calibration is conducted. In the modeling procedure we assume a) a constant soil depth, b) that the soil hydraulic properties do not vary in the lateral or vertical direction, except for the saturated hydraulic conductivity, c) that the fluxes in the unsaturated zone are vertical, d) that fluxes in the saturated zone take place in the lateral direction only (i.e., parallel to the fragipan and directed downslope), e) that the fluxes across the width of the hillslope are negligible, and f) that the precipitation is uniform over the hillslope. The capillary fringe is regarded as an integral part of the Boussinesq aquifer.

We analyze the effect of using a free-surface downslope boundary condition instead of a Dirichlet boundary condition, and we investigate what the effects are of using a different parameterization for the relationship between saturated hydraulic conductivity and depth.

We conclude that the models hydrograph response is reasonable, showing slight underestimations of most peak flows, and slight overestimations during most recession periods. The timing of the peaks in the hydrographs and the water tables is generally good. Also the water table response is well captured, but also here the peaks are generally underestimated. This phenomenon may be caused by the low drainable porosity values during nearly saturated conditions, which causes a very quick response of the water tables under these conditions. Thus, the underestimation for peak water table values may be caused by small differences in the calculated precipitation and recharge. The overestimation of water tables and fluxes during recession periods may be caused by using a single van Genuchten parameterization for the entire soil profile, whereas several soil horizons with slightly different retention characteristics are present. Recent experimental results indicate that also the porosity decreases with depth, which may explain the quick water table responses and decreased outflow rates.

Chapter 7

Summary and conclusions

7.1 Principal conclusions

In **Chapter 2** a generalized HSB model is presented that enables handling of non-constant bedrock slopes, and a comparison to a three-dimensional RE model and a hillslope-storage KW model is conducted for 5% and 30% bedrock slope and nine different characteristic hillslopes. In relation to the validity of the KW model we conclude that it is limited to applications where the effects of hydraulic diffusion are limited, which is determined by bedrock slope and water table gradients. Water table gradients are determined by bedrock slope, hillslope plan shape, and profile curvature. When water table gradients are high and bedrock slope is small, the effect of diffusion is most prominent. On these hillslopes the KW model compares least favorable to the RE model. For increasing degrees of divergence the water table gradients decrease. Also for increasing bedrock slopes, the effect of diffusion becomes less noticeable, due to the fact that the soil drains too quickly for diffusion to take full effect. Therefore, the KW model compares best to the RE model for high bedrock slopes and divergent slope shapes. It is noteworthy to mention that a convergent plan shape or a concave profile shape may cause the KW model to perform relatively poorly, even when bedrock slopes are high.

Regarding the comparison between the HSB and the RE model we conclude that the water tables (or storage profiles) compare well on all hillslopes. Also the hydrographs show good agreement, however, the RE hydrograph is delayed, which is caused by the delayed recharge effects of the unsaturated zone.

In **Chapter 3** the effects of the unsaturated zone on groundwater storage and fluxes are partly accounted for by introduction of an analytical expression for the parameter drainable porosity for horizontal and sloping bedrock. The expression is derived for drainage experiments and links drainable porosity directly to the depth of the unsaturated zone, and provides a physical basis for the interpretation of the parameter. The expression is implemented in the HSB model, and the results obtained using this model are compared to measurements from a scaled hillslope in a laboratory setup, and to results from the uncalibrated and calibrated original HSB model. On the outflow rates the original HSB model, having two fitting parameters, performs better than the revised HSB model, except for the initial peak outflow rates that occur during the first few minutes after initiation of the experiments. For the uncalibrated hydrographs, the best performing model depends on the bedrock slope; the original HSB model shows the best agreement for the 10% and 15% slopes, and the revised HSB model for the 5% slope. The revised HSB model shows a much more accurate simulation of the water table profiles for all runs.

It is concluded that the simulated water table dynamics improve when the capillary fringe is incorporated in the Boussinesq aquifer. Since the dynamic effects of the unsaturated zone appear to affect the outflow response at early times, it is concluded that a dynamic representation of these processes is expected improve the models accuracy.

Chapter 4 describes an application of the theory described in Chapter 3 to a tidal aquifer study described in *Cartwright et al.* [2005]. *Cartwright et al.* [2005] shows the effects of oscillating water tables in a tidal aquifer on the value of the drainable porosity. The drainable porosity in *Cartwright et al.* [2005] is a complex number that expresses the attenuation and delay between the driving head (representing the driving tidal influence), and the water table height in an aquifer. A curious phenomenon for high frequency oscillations is noted, namely the linear decay on a double logarithmic scale of the absolute value of complex drainable porosity with increasing frequencies, and the relationship between the slope of the linear decay and the parameter β, which is a water retention parameter. In this chapter, we show that for low-frequency oscillations, the value of drainable porosity does not necessarily converge to $(\theta_s - \theta_r)$, but instead may converge to lower values when the oscillations take place close to the soil surface or in the zone of influence of the capillary fringe. For the curious phenomena at high-frequencies, we formulate a possible explanation by assuming that only the zone in which the oscillations in the water table take place have time to fully reach hydraulic equilibrium in case of high-frequency oscillations. Using the theory described in Chapter 3, we show that there is a power-law relationship between the absolute value of complex drainable porosity and the frequency, of which the slope is determined by the parameter β.

In **Chapter 5** a coupling is presented between a one-dimensional RE model to describe unsaturated zone dynamics, and the original HSB model. The capillary fringe in included as an integral part of the Boussinesq aquifer. The coupled model is formulated as two partial differential equations which are solved simultaneously, and the results are compared to those of a three-dimensional RE model and of the original HSB model.

The role of the unsaturated zone in transmitting the soil moisture pulses as a result of rainfall is investigated, and the relationships between rainfall, recharge, drainable porosity and unsaturated storage are analyzed. Besides the expected delaying effect of the unsaturated zone on recharge rates, the simulations also show that the unsaturated zone does not always dampen the rainfall signal, but can also amplify it, causing recharge rates to exceed rainfall rates under certain conditions. This effect is caused by water tables including water from the unsaturated zone into the saturated zone as they rise.

Comparison of the model results shows a very good match between the outflow rates of the HSB-coupled model and the RE model, whereas the original HSB model shows systematically underestimated outflow rates. Also the water table dynamics are modeled more accurately with the HSB-coupled model when compared to the original HSB model.

In **Chapter 6**, the HSB-coupled model is applied to a 36x18m hillslope plot near Troy (ID), USA. The model is slightly modified to allow handling of decreasing hydraulic conductivities with depth. The model is parameterized beforehand using data of soil water retention characteristics, and using the relationship between conductivity and depth. No further calibration was conducted. The model behavior is evaluated and compared to outflow and piezometric measurements from the hillslope plot obtained over a period of 130 days.

We conclude that the models hydrograph response is reasonable, showing slight underestimations of most peak flows, and slight overestimations during most recession periods. The timing of the peaks in the hydrographs and the water tables is generally good. Also the water table response is well captured, but also here the peaks are generally underestimated. This phenomenon may be caused by the low drainable porosity values during nearly saturated conditions, which causes a very quick response of the water tables under these conditions. The overestimation of water tables and fluxes during recession periods may be caused by using a single van Genuchten parameterization for the entire soil profile, whereas several soil horizons with slightly different retention characteristics are present. Recent experimental results indicate that porosity decreases with depth, which may explain the quick water table responses and decreased outflow rates.

7.2 Perspectives

The work presented in this thesis is aimed at an increased understanding of hillslope hydrological processes through (low-dimensional) modeling. Naturally, the research in this field is far from being finished. In this section, topics will be put forward that have not been mentioned before and that I believe are relevant to this field of research, and suggestions for future research are given.

Hillslope hydrological research is conducted to eventually better understand the catchments response as a whole. In order to fully test the value of the developed models, an effort should be made to scale from hillslope to catchment. A crucial step in this process is breaking down the catchment into a collection of hillslopes, such that the assumptions underlying the modeling work are not (or least) violated. To this end, one first has to determine how big the hillslopes are ([*Dietrich and Montgomery*, 1998]), and how to delineate the hillslopes based on topographic information, which is a topic of ongoing research. Also the effects of vegetation on the hillslope and catchment hydrological behavior, and the linkage of the hillslopes to the riparian zones in this type of modeling approach need to be investigated further. A subsequent approach in modeling catchment response could either be to numerically solve the model equations for the individual hillslopes, or to use similarity parameters for hillslope geometry such as presented in *Troch et al.* [2004] and *Berne et al.* [2005], thereby reducing computational demands and facilitating practical applicability.

In hillslope hydrology, macropore/pipe flow processes are often encountered (e.g., *Beven and Germann* [1982]; *Bronstert* [1999]). A coupling of the HSB model to a hillslope preferential flow model (e.g., *Tsutsumi et al.* [2005]) could be used for quantitative investigation of the effects of preferential flow processes on outflow rates and water table dynamics, and for model evaluation by comparison to measurements obtained from catchments where macropore flow processes are clearly noticeable, e.g., the Maimai catchment in New-Zealand ([*Woods et al.*, 1997]).

In studies of *Buttle* [1994] and *McDonnell* [1990], the predominance of pre-event water in storm hydrographs is shown, which underlines the importance of subsurface flow processes in generating storm hydrographs [*Genereux and Hooper*, 1998]. The dilemma of how this water can be stored for a long time and subsequently released in case of a storm, has become known as the first part of the double paradox in hydrology [*Kirchner*, 2003]. In *Bishop et al.* [2004] a solution to the double paradox of is presented but up to this time no quantitative testing of the presented hypotheses has been conducted. Therefore, a coupled subsurface flow/macropore flow model is expected to be of great value in an attempt to reproduce the phenomenon of rapid mobilization of "old" water in hillslopes during storms [*Kirchner*, 2003], and to investigate to what extent macropore flow plays a role in these processes.

With respect to the numerical aspects, it can be concluded that the discretization of the lateral and vertical coordinates is of crucial importance for the models calculation speed. Since the aim is to develop models that demand little computational power, the appropriate spatial discretization needs to be more carefully investigated. In the presented models the node spacing is equidistant. However, a significant increase in numerical performance of the models may be achieved when a finer resolution is used near the outlet and the soil surface, and a coarser resolution for the upslope areas and deeper soil sections [*Downer and Ogden*, 2004].

In Chapter 2 the conclusion is drawn that the validity of applying a kinematic wave assumption does not solely depend on the bedrock slope, but also on slope shape. Therefore, in addition to existing criteria for applying kinematic wave approaches for straight hillslopes, a generalized criterion needs to be derived in which slope shape and profile curvature are also accounted for.

In Chapters 3 and 5, two HSB models are described in which the water retention characteristics are parameterized with a van Genuchten function. In this thesis, the parameterization was conducted measurements obtained from soil cores, whereas the application of the model is on the hillslope scale. This discrepancy between the scales at which the model parameterization is conducted, and the scale at which the model is applied is not discussed in this thesis. However, the implications of using scaled parameters in this modeling framework is worth investigating. When moving from applications on the hillslope to the catchment scale, it is necessary to account for the heterogeneity of hydraulic properties and therefore stochastic upscaling is required ([*Bierkens et al.*, 2000; *Desbarats*, 1995]).

References

Abbott, M., J. Bathhurst, J. Cunge, P. O'Connell, and J. Rasmussen (1986), An introduction to the European Hydrological System – Systeme Hydrologique Europeen, "SHE", 1: History and philosophy of a physically-based, distributed modelling system, *J. Hydrol.*, *87*, 45–59.

Abdul, A., and R. Gillham (1989), Field studies on the effects of the capillary fringe on streamflow generation, *J. Hydrol.*, *112*, 1–18.

Anderson, M., and S. Brooks (Eds.) (1996), *Advances in Hillslope Processes*, vol. 2, 1306 pp., John Wiley, Hoboken.

Barry, D., S. Barry, and J.-Y. Parlange (1996), *Mixing process in estuaries and coastal seas*, vol. 50, chap. Capillary correction to periodic solution of the shallow flow approximation, pp. 496–510, AGU, Washington D.C.

Bear, J. (1972), *Dynamics of Fluids in Porous Media*, American Elsevier Publishing Company, New York.

Berkowitz, B., S. Silliman, and A. Dunn (2004), Impact of the capillary fringe on local flow, chemical migration, and microbiology, *Vadose Zone J.*, *3*, 534–548.

Berne, A., R. Uijlenhoet, and P. Troch (2005), Similraity analysis of subsurface flow response of hillslopes with complex geometries, *Water. Resour. Res.*, *41*, W09410, doi:10.1029/2004WR003629.

Betson, R. (1964), What is watershed runoff?, *J. Geophys. Res.*, *69*, 1541–1552.

Beven, K. (1981), Kinematic subsurface stormflow, *Water Resour. Res.*, *17*(5), 1419–1424.

Beven, K. (1982), On subsurface stormflow: prediction with simple kinematic theory for saturated and unsaturated flows, *Water Resour. Res.*, *18*(6), 1627–1633.

Beven, K. (2001), *Rainfall-Runoff Modelling: The Primer*, John Wiley, Hoboken, N.J.

Beven, K., and P. Germann (1982), Macropores and water flow in soils, *Water Resour. Res.*, *18*(5), 1311–1325.

Beven, K., and M. Kirkby (1979), A physically based variable contributing area model of basin hydrology, *Hydrol. Sci. Bull.*, *24*(1), 43–69.

Beven, K., and I. Moore (Eds.) (1992), *Terrain analysis and distributed modelling in hydrology*, Advances in hydrological processes, Wiley, Chichester.

Bierkens, M. (1998), Modeling water table fluctuations by means of a stochastic differential equation, *Water Resour. Res.*, *30*(10), 2485–2499.

Bierkens, M., P. Finke, and P. de Willigen (2000), *Upscaling and downscaling methods for environmental research*, 190 pp., Kluwer Academic Publishers, Dordrecht.

Bishop, K., J. Seibert, S. Köhler, and H. Laudon (2004), Resolving the double paradox of rapidly mobilized old water with highly variable responses in runoff chemistry, *Hydrol. Processes*, *18*, 185–189, doi:10.1002/hyp.5209.

Bixio, A., S. Orlandini, C. Paniconi, and M. Putti (2000), *Computational Methods in Water Resources*, vol. 2, chap. Physically-based distributed model for coupled surface runoff and subsurface flow simulation at the catchment scale, pp. 1115–1122, Balkema, Rotterdam, The Netherlands.

Boussinesq, J. (1877), Essai sur la thorie des eaux courantes, *Mm. Acad. Sci. Inst. France*, *23*, 1–680.

Bras, R. (1990), *Hydrology; An introduction to Hydrologic Science*, Addison-Wesley, Reading, Mass.

Bronstert, A. (1999), Capabilities and limitations of detailed hillslope hydrological modelling, *Hydrol. Processes*, *13*(1), 21–48.

Brooks, E. (2003), Distributed hydrologic modeling of the eastern palouse, Phd thesis, University of Idaho.

Brooks, E., J. Boll, and P. McDaniel (2004), A hillslope-scale experiment to measure lateral saturated hydraulic conductivity, *Water. Resour. Res.*, *40*, W04208, doi:10.1029/2003WR002858.

Brooks, E., J. Boll, and P. McDaniel (2006), Distributed and integrated response of a GIS-based distributed hydrologic model, *Hydrol. Processes*, in press.

Brooks, R. H., and A. T. Corey (1964), Hydraulic properties of porous media, *Hydrology Paper 3*, Colorado State University, Fort Collins, CO.

Brutsaert, W. (1994), The unit response of groundwater outflow from a hillslope, *Water Resour. Res.*, *30*(10), 2759–2763.

Buttle, J. (1994), Isotope hydrograph separations and rapid delivery of pre-event water from drainage basins, *Prog. Phys. Geogr.*, *18*, 16–41.

Cartwright, N., P. Nielsen, and P. Perrochet (2005), Influence of capillarity on a simple harmonic oscillating water table: Sand column experiments and modelling, *Water. Resour. Res.*, *41*, W08416, doi:10.1029/2005WR004023.

Chapman, T. (2005), Recharge-induced groundwater flow over a plane sloping bed: Solutions for steady and transient flow using physical and numerical models, *Water. Resour. Res.*, *41*, W07027, doi:10.1029/2004WR003606.

Childs, E. (1971), Drainage of groundwater resting on a sloping bed, *Water Resour. Res.*, *7*(5), 1256–1263.

Cho, H., and G. d. Rooij (1999), Fingered flow: the role of the induction zone below the soil surface and the capillary fringe, in *Proceedings of the international workshop on characterization and measurements of the hydraulic properties of unsaturated porous media*, edited by M. T. v. Genuchten, F. Leij, and L. Wu, pp. 423–432, University of California, Riverside, CA.

Desbarats, A. (1995), Upscaling capillary pressure-saturation curves in heterogeneous porous media, *Water Resour. Res.*, *31*(2), 281–288.

Dietrich, W., and D. Montgomery (1998), *Scale dependence and scale invariance in hydrology*, chap. Hillslopes, Channels, and Landscape Scale, pp. 30–60, Cambridge University Press, Cambridge.

Dingman, S. (2002), *Physical Hydrology*, Prentice Hall, Upper Saddle River, New Jersey.

Downer, C., and F. Ogden (2004), Appropriate vertical descretization of richards' equation for two-dimensional watershed-scale modelling, *Hydrol. Processes*, *18*, 1–22, doi:10.1002/hyp.1306.

Duffy, C. (1996), A two-state integral-balance model for soil moisture and groundwater dynamics in complex terrain, *Water Resour. Res.*, *32*(8), 2421–2434.

Dunne, T., and R. Black (1970), An experimental investigation of runoff production in permeable soils, *Water Resour. Res.*, *6*(2), 478–489.

Fan, Y., and R. Bras (1998), Analytical solutions to hillslope subsurface storm flow and saturated overland flow, *Water Resour. Res.*, *34*(4), 921–927.

Fink, J., J.-Y. Parlange, and A. El-Kadi (2001), One last visit to the capillarity correction for free surface flow, *Water Resour. Res.*, *37*(3), 827–829.

Fipps, G., and R. Skaggs (1989), Influence of slope on subsurface drainage of hillsides, *Water Resour. Res.*, *25*(7),), 1717–1726.

Frankenberger, J., E. Brooks, M. Walter, M. Walter, and T. Steenhuis (1999), A gis-based variable source area hydrology model, *Hydrol. Processes*, *13*(6), 805–822.

Freeze, R. (1972a), Role of subsurface flow in generating surface runoff 1. Base flow contributions to channel flow, *Water Resour. Res.*, *8*(3), 609–623.

Freeze, R. (1972b), Role of subsurface flow in generating surface runoff 2. Upstream source areas, *Water Resour. Res.*, *8*(5), 1272–1283.

Freeze, R., and J. Cherry (1979), *Groundwater*, Prentice-Hall, Englewood Cliffs, New Jersey.

Genereux, D., and R. Hooper (1998), *Isotope Tracers in Catchment Hydrology*, chap. Oxygen and hydrogen isotopes in rainfall-runoff studies, pp. 319–346, Elsevier Science B.V., Amsterdam, The Netherlands.

Gillham, R. (1984), The capillary fringe and its effect on water-table response, *J. Hydrol.*, *67*, 307–324.

Harr, M. (1962), *Groundwater and Seepage*, McGraw-Hill Book Company, New York.

Heidari, M., and A. Moench (1997), Evaluation of unconfined-aquifer parameters from pumping test data by nonlinear least squares, *J. Hydrol.*, *192*, 300–313.

Henderson, F., and R. Wooding (1964), Overland flow and groundwater flow from a steady rainfall of finite duration, *J. Geophys. Res.*, *69*(8), 1531–1540.

Hewlett, J., and A. Hibbert (1967), Factors affecting the response of small watersheds to precipitation in humid areas, in *Forest Hydrology*, edited by W. Sopper and H. Lull, pp. 275–290, The Pennsylvania State University, Pergamon Press, University Park, PA.

Hilberts, A., E. van Loon, P. Troch, and C. Paniconi (2004), The hillslope-storage Boussinesq model for spatially variable bedrock slope, *J. Hydrol.*, *291*, 160–173.

Hilberts, A., P. Troch, and C. Paniconi (2005), Storage-dependent drainable porosity for complex hillslopes, *Water. Resour. Res.*, *41*, W06001, doi:10.1029/2004WR003725.

Hilberts, A., P. Troch, C. Paniconi, and J. Boll (2006), Low-dimensional modeling of hillslope subsurface flow: the relationship between rainfall, recharge, and unsaturated storage, *Water. Resour. Res.*, *42*, doi:10.1029/2006WR006496, in review.

Hillel, D. (1980), *Applications of Soil Physics*, Academic Press, New York.

Hogarth, W. L., J.-Y. Parlange, M. B. Parlange, and D. Lockington (1999), Approximate analytical solution of the Boussinesq equation with numerical validation, *Water Resour. Res.*, *35*(10), 3193–3197.

Hooghoudt, S. (1947), Waarnemingen van grondwaterstanden voor de landbouw, *Versl. Tech. Bijeenk. 1-6*, Tech. Natuurw. Onderz. (T.N.O.), The Netherlands.

Hornberger, G., and E. Boyer (1995), Recent advances in watershed modelling, *U.S. Natl. Rep. Int. Union Geod. Geophys., 1991-1994*, *Rev. Geophys.*, *33*, 949–957.

Horton, R. (1933), The role of infiltration in the hydrologic cycle, *Eos Trans. AGU*, *14*, 446–460.

Ivanov, V., E. Vivoni, R. Bras, and D. Entekhabi (2004), Catchment hydrological response with a fully distributed triangulated irregular network model, *Water. Resour. Res.*, *40*, W11102, doi:10.1029/2004WR003218.

Jayatilaka, C., and R. Gillham (1996), A deterministic-empirical model of the effect of the capillary fringe on near-stream area runoff 1. Description of the model, *J. Hydrol.*, *184*, 299–315.

Johnson, A. (1967), Specific yield - compilation of specific yields for various materials, *U.S. Geol. Survey Water-Supply Paper 1662-D.*

Kim, C., and M. Bierkens (1995), A formula for computation of time-varying recharge of ground water – Comment, *J. Hydrol.*, *171*, 191–193.

Kim, C., G. Salvucci, and D. Enthekhabi (1999), Groundwater-surface water interaction and the climatic spatial patterns of hillslope hydrological response, *Hydrol. Earth Syst. Sci.*, *3*(3), 375–384.

Kirchner, J. (2003), A double paradox in catchment hydrology and geochemistry, *Hydrol. Processes*, *17*, 871–874, doi:10.1002/hyp.5108.

Kirkby, M. (Ed.) (1978), *Hillslope Hydrology*, John Wiley, New York.

Kirkby, M. (1988), Hillslope runoff processes and models, *J. Hydrol.*, *100*, 315–339.

Koster, R., M. Suarez, A. Ducharne, M. Stieglitz, and P. Kumar (2000), A catchment-based approach to modeling land surface processes in a general circulation model, *J. Geophys. Res.*, *105*(D20), 24,809–24,822.

Koster, R., M. Suarez, R. Higgins, and H. van den Dool (2003), Observational evidence that soil moisture variations affect precipitation, *Geophys. Res. Lett.*, *30*(5), doi:10.1029/2002GL016571.

Liang, X., Z. Xie, and M. Huang (2003), A new parameterization for surface and groundwater interactions and its impact on water budgets with the variable infiltration capacity (VIC) land surface model, *J. Geophys. Res.*, *108*(D16), doi:10.1029/2002JD003090.

Luthin, J. (1966), *Drainage Engineering*, Wiley, New York.

Luthin, J., and P. Day (1955), Lateral flow above a sloping water table, *Soil Sci. Soc. Am. Proc.*, *19*, 406–410.

Luthin, J., and R. Miller (1953), Pressure distribution in soil columns draining into the atmosphere, *Soil Sci. Soc. Am. Proc.*, *17*, 329–333.

McDonnell, J. (1990), A rationale for old water discharge through macropores in a steep, humid catchment, *Water Resour. Res.*, *26*(11), 2821–2832.

McGlynn, B., J. McDonnell, J. Seibert, and C. Kendall (2004), Scale effects on headwater catchment runoff timing, flow sources, and groundwater-streamflow relations, *Water Resour. Res.*, *40*, 1795–1804, doi:10.1029/2003WR002494.

Moench, A. (1994), Specific yield as determined by type-curve analysis of aquifer-test data, *Ground Water*, *32*(6), 949–957.

Moench, A. (2003), Estimation of hectare-scale soil-moisture characteristics from aquifer-test data, *J. Hydrol.*, *281*, 82–95.

Nachabe, M. (2002), Analytical expressions for transient specific yield and shallow water table drainage, *Water Resour. Res.*, *38(10)*, doi:10.1029/2001WR001071.

Neuman, S. (1987), On methods of determining specific yield, *Ground Water*, *25*(6), 679–684.

Nieber, J. (1982), Hillslope soil moisture flow: approximations by a one-dimensional formulation, *Pap. Am. Soc. Agric. Engng*, *82-2026*, 1–26.

Nieber, J., and M. Walter (1981), Two-dimensional soil moisture flow in a sloping rectangular region: experimental and numerical studies, *Water Resour. Res.*, *17*(6), 1722–1730.

Niedzialek, J., and F. Ogden (2004), Numerical investigation of saturated source area behavior at the small catchment scale, *Adv. Water Resour.*, *27*, 925–936.

Nielsen, P., and P. Perrochet (2000), Watertable dynamics under capillary fringes: Experiments and modelling, *Adv. Water Resour.*, *23*, 503–515.

Nwankwor, G., R. Gillham, G. van der Kamp, and F. Akindunni (1992), Unsaturated and saturated flow in response to pumping of an unconfined aquifer: field evidence of delayed drainage, *Ground Water*, *30*(5), 690–700.

Ogden, F., and B. Watts (2000), Saturated area formation on nonconvergent hillslope topography with shallow soils: A numerical investigation, *Water Resour. Res.*, *36*(7), 1795–1804.

O'Loughlin, E. (1981), Saturation regions in catchments and their relations to soil and topographic properties, *J. Hydrol.*, *53*, 229–246.

Paniconi, C., and M. Putti (1994), A comparison of Picard and Newton iteration in the numerical solution of multidimensional variably saturated flow problems, *Water Resour. Res.*, *30*(12), 3357–3374.

Paniconi, C., and E. Wood (1993), A detailed model for simulation of catchment scale subsurface hydrological processes, *Water Resour. Res.*, *29*(6), 1601–1620.

Paniconi, C., P. Troch, E. van Loon, and A. Hilberts (2003), The hillslope-storage Boussinesq model for subsurface flow and variable source areas along complex hillslopes: 2. Intercomparison with a three-dimensional Richards equation model, *Water. Resour. Res.*, *39*(11), 1317, doi:10.1029/2002WR001730.

Parlange, J. Y., and W. Brutsaert (1987), A capillarity correction for free surface of groundwater, *Water Resour. Res.*, *23*(5), 805–808.

Parlange, J. Y., W. Brutsaert, J. Fink, and A. El-Kadi (1990), A capillarity correction for free surface flow revisited, *Water Resour. Res.*, *26*(7), 1691–1692.

Parlange, J. Y., F. Stagnitti, A. Heilig, J. Szilagyi, M. B. Parlange, T. S. Steenhuis, W. L. Hogarth, D. A. Barry, and L. Li (2001), Sudden drawdown and drainage of a horizontal aquifer, *Water Resour. Res.*, *37*(8), 2097–2101.

Pikul, M., R. Street, and I. Remson (1974), A numerical model based on coupled one-dimensional Richards and Boussinesq equations, *Water. Resour. Res.*, *10*(2), 295–302.

Putti, M., and C. Paniconi (2004), Time step and stability control for a coupled model of surface and subsurface flow, in *Computational Methods in Water Resources*, vol. 2, edited by C. Miller, M. Farthing, W. Gray, and W. Pinder, pp. 1391–1402, Elsevier, Amsterdam, The Netherlands.

Ragan, R. (1968), An experimental investigation of partial area contributions, in *Proc. Berne Symp., Int. Assoc. Sci. Hydrol.*, vol. 76, pp. 241–249.

Reggiani, P., M. Sivapalan, and S. Hassanizadeh (1998), A unifying framework for watershed thermodynamics: balance equations for mass, momentum, energy and entropy, and the second law of thermodynamics, *Adv. Water Res.*, *22*(3), 367–398.

Richards, L. (1931), Capillary conduction of liquids through porous mediums, *Physics*, *1*, 318–333.

Rockhold, M., C. Simmons, and M. Fayer (1997), An analytical solution technique for one-dimensional, steady vertical water flow in layered soils, *Water Resour. Res.*, *33*(4), 897–902.

Seibert, J., and J. McDonnell (2002), On the dialog between experimentalist and modeler in catchment hydrology: Use of soft data for multicriteria model calibration, *Water Resour. Res.*, *38*(11), 1241, doi:10.1029/2001WR000978.

Sloan, P., and I. Moore (1984), Modeling subsurface stormflow on steeply sloping forested watersheds, *Water Resour. Res.*, *20*(12), 1815–1822.

Sloan, W. (2000), A physics-based function for modeling transient groundwater discharge at the watershed scale, *Water Resour. Res.*, *36*(1), 225–241.

Smith, R., and R. Hebbert (1983), Mathematical simulation of interdependent surface and subsurface hydrologic processes, *Water Resour. Res.*, *19*(4), 987–1001.

Stagnitti, F., M. B. Parlange, T. S. Steenhuis, and J.-Y. Parlange (1986), Drainage from a uniform soil layer on a hillslope, *Water Resour. Res.*, *22*(5), 631–634.

Su, N. (1994), A formula for computation of time-varying recharge of groundwater, *J. Hydrol.*, *160*, 123–135.

Szilagyi, J. (2004), Vadose zone influences on aquifer parameter estimates of saturated-zone hydraulic theory, *J. Hydrol.*, *286*, 78–86.

Szilagyi, J., M. Parlange, and J. Albertson (1998), Recession anaylsis for aquifer parameter determination, *Water Resour. Res.*, *30*(7), 1851–1857.

Thornthwaite, C., and J. Mather (1955), *The water balance*, The Laboratory of Climatology, publ. No. 8, Centerton NJ.

Torres, R., W. Dietrich, D. Montgomery, S. Anderson, and K. Loague (1998), Unsaturated zone processes and the hydrologic response of a steep, unchanneled catchment, *Water Resour. Res.*, *34*(8), 1865–1879.

Tritscher, P., W. Read, and P. Broadbridge (2000), Specific yield for a two-dimensional flow, *Water Resour. Res.*, *36*(6), 1393–1402.

Troch, P. (1992), Conceptual basin-scale runoff process models for humid catchments: analysis, synthesis and applications, Ph.D. thesis, Ghent University.

Troch, P., E. van Loon, and A. Hilberts (2002), Analytical solutions to a hillslope-storage kinematic wave equation for subsurface flow, *Adv. Water Resour.*, *25*, 637–649.

Troch, P., C. Paniconi, and E. van Loon (2003), The hillslope-storage Boussinesq model for subsurface flow and variable source areas along complex hillslopes: 1. Formulation and characteristic response, *Water Resour. Res.*, *39*(11), 1316, doi: 10.1029/2002WR001728.

Troch, P., A. van Loon, and A. Hilberts (2004), Analytical solution of the linearized hillslope-storage Boussinesq equation for exponential hillslope width functions, *Water Resour. Res.*, *40*, W08601, doi:10.1029/2003WR002850.

Tsutsumi, D., R. Sidle, and K. Kosugi (2005), Development op a simple lateral preferential flow model with steady state application in hillslope soils, *Water Resour. Res.*, *41*, W12420, doi:10.1029/2004WR003877.

Vachaud, G., and M. Vauclin (1975), Comment on "A numerical model based on coupled one-dimensional Richards and Boussinesq equations" by Mary F. Pikul, Robert L. Street, and Irwin Remson, *Water Resour. Res.*, *11*, 506–509.

van Genuchten, M. (1980), A closed-form equation for predicting the hydraulic conductivity of unsaturated soils, *Soil Sci. Am. J.*, *44*, 892–898.

Verhoest, N., and P. Troch (2000), Some analytical solutions of the linearized Boussinesq equation with recharge for a sloping aquifer, *Water Resour. Res.*, *36*(3), 793–800.

Walter, M., J.-S. Kim, T. Steenhuis, J.-Y. Parlange, A. Heilig, R. Braddock, J. Selker, and J. Boll (2000), Funneled flow mechanisms in a sloping layered soil: Laboratory investigation, *Water Resour. Res.*, *37*(4), 841–849.

Weiler, M., and J. McDonnell (2004), Virtual experiments: a new approach for improving process conceptualization in hillslope hydrology, *J. Hydrol.*, *285*, 3–18.

Werner, A., and D. Lockington (2003), Influence of hysteresis on tidal capillary fringe dynamics in a well-sorted sand, *Adv. Water Resour.*, *26*, 1199–1204.

Whipkey, R. (1965), Subsurface stormflow from forested slopes, *Bull. Int. Assoc. Sci. Hydrol.*, *2*, 74–85.

Wigmosta, M., L. Vail, and D. Lettenmaier (1994), A distributed hydrology-vegetation model for complex terrain, *Water Resour. Res.*, *30*(6), 1665–1679.

Wood, E., D. Lettenmaier, and V. Zartarian (1992), A land-surface hydrology parameterization with subgrid variability for general circulation models, *J. Geophys. Res.*, *97*(D3), 2717–2728.

Woods, R., M. Sivapalan, and J. Robinson (1997), Modeling the spatial variability of subsurface runoff using topographic index, *Water Resour. Res.*, *33*, 1061–1073.

Woolhiser, D., and J. Liggett (1967), Unsteady one-dimensional flow over a plane: the rising hydrograph, *Water Resour. Res.*, *3*, 753–771.

Zecharias, Y., and W. Brutsaert (1988), Recession characteristics of groundwater outflow and base flow from mountainous watersheds, *Water Resour. Res.*, *24*(10), 1651–1658.

Samenvatting

In dit proefschrift staat de vraag centraal of men laagdimensionale dynamische modellen ter beschrijving van bergings- en stromingsprocessen op hellingen kan ontwikkelen, zodanig dat het relevante fysische gedrag van het natuurlijke systeem goed beschreven wordt.

In **Hoofdstuk 1** geef ik een korte inleiding op het gebied van stroomgebieds- en hellingshydrologie, waarin ik het belang van het ontwikkelen van laagdimensionale modellen aangeef. De modellen die het meest relevant zijn voor dit proefschrift worden hier beschreven.

In **Hoofdstuk 2** wordt een veralgemeniseerd HSB model gepresenteerd, waarmee het hydrologische gedrag op hellingen met een kromming in de ondoorlatende laag onderzocht kan worden. De modelresultaten worden vergeleken met een driedimensionaal RE-model en een bergingsgebaseerd KW-model op negen karakteristieke hellingen en voor twee verschillende hellingshoeken (5% en 30%). Met betrekking tot de nauwkeurigheid van het KW model kunnen we stellen dat de toepassing van deze modellen beperkt is tot omstandigheden waarin de effecten van hydraulische diffusie beperkt zijn, hetgeen bepaald wordt door de hellingshoek van de ondoorlatende laag en de gradiënten in de grondwaterspiegel. De gradiënten worden bepaald door de hellingshoek van de ondoorlatende laag, de hellingsvorm en de kromming van het hellingsprofiel. Wanneer de gradiënt van de grondwaterspiegel groot is en de hellingshoek klein, dan zijn de effecten van diffusie het duidelijkst merkbaar. Onder deze omstandigheden is de overeenkomst tussen de resultaten van het KW-model en het RE model het kleinst. Voor toenemende divergentie van hellingvorm neemt de gradiënt van de grondwaterspiegel af. Ook voor toenemende hellingshoek worden de effecten van diffusie minder merkbaar, doordat de drainage dusdanig snel verloopt dat de relatief trage diffusieprocessen niet voldoende tijd krijgen om zich te ontwikkelen. Om deze reden zijn de resultaten van het KW- en het RE-model het meest gelijkend voor grote hellingshoeken en divergente hellingsvorm. Het is vermeldenswaardig te noemen dat een convergente hellingsvorm of een concaaf hellingsprofiel kan zorgen voor een slechte prestatie van het KW-model, zelfs wanneer de hellingshoeken groot zijn.

Met betrekking tot de vergelijking van de resultaten van het HSB- en het RE-model concluderen we dat de grondwaterspiegels (of de bergingsprofielen) van beide modellen erg sterk overeenkomen voor alle hellingshoeken en hellingsvormen. Ook de hydrogrammen van beide modellen vertonen een grote overeenkomst,

hoewel het hydrogram van het RE-model een lichte vertraging heeft ten opzichte van dat van het HSB-model. Dit wordt veroorzaakt door de vertraagde nalevering vanuit de onverzadigde zone, hetgeen niet gemodelleerd is in het HSB model.

In **Hoofdstuk 3** worden de effecten van de onverzadigde berging op grondwaterberging en oppervlakkige stroming deels verrekend door de invoering van een analytische uitdrukking voor de parameter draineerbare porositeit. Dit wordt gedaan voor bodems op zowel horizontale als hellende ondoorlatende lagen. De uitdrukking wordt afgeleid voor drainage-experimenten en koppelt draineerbare porositeit direct aan de diepte van de onverzadigde zone. De uitdrukking verschaft een fysische basis voor de interpretatie van de bewuste parameter. De uitdrukking wordt geïmplementeerd in het HSB-model en de resultaten met gebruikmaking van dit model worden vergeleken met a) meetresultaten van een schaalmodel van een helling in een laboratoriumopstelling en b) de resultaten van een gecalibreerde en een ongecalibreerde versie van het originele HSB-model. Wat betreft de hydrogrammen presteert het originele HSB-model met twee calibratieparameters beter dan het gereviseerde HSB-model, behalve voor de piekafvoer gedurende de eerste minuten van de simulaties. Voor de ongecalibreerde hydrogrammen geldt dat het best presterende model afhangt van de hellingshoek van de ondoorlatende laag; het originele HSB-model vertoonde de grootste overeenkomst voor de 10% en 15% hellingen, terwijl het geriviseerde HSB-model beter presteert voor de 5% hellingen. Voor alle hellingshoeken en hellingvormen geldt dat de vorm van de grondwaterspiegel met het gerviseerde HSB-model veel accurater gesimuleerd wordt.

Er wordt geconcludeerd dat de grondwaterdynamiek beter wordt gesimuleerd wanneer de volcapillaire zone (ook wel funiculaire zone of *capillary fringe*) wordt gezien als een integraal onderdeel van de Boussinesq aquifer. Aangezien de dynamische effecten van de onverzadigde zone de hydrogrammen gedurende de eerste minuten van het experiment lijken te beïnvloeden, wordt de conclusie getrokken dat een dynamische weergave van de onverzadigde zone de nauwkeurigheid van het model zal vergroten.

In **Hoofdstuk 4** wordt een toepassing beschreven van de theorie uit Hoofdstuk 3. De theorie wordt toegepast op een grondwatersysteem dat onder invloed staat van getijdenwerking en beschreven wordt in *Cartwright et al.* [2005]. In *Cartwright et al.* [2005] worden de effecten van een oscillerende grondwaterstand op de waarde van de draineerbare porositeit getoond. De draineerbare porositeit in het werk van *Cartwright et al.* [2005] is een complex getal dat de vertraging en de demping van de grondwaterstand ten opzichte van het getijdesysteem weergeeft. Een merkwaardig fenomeen voor de oscillaties bij hoge frequenties wordt opgemerkt, namelijk de lineare afname op een dubbellogaritmische schaal van de absolute waarde van de complexe draineerbare porositeit voor toenemende frequenties. De richtingscoëfficient van de rechte blijkt bovendien bepaald te worden door de waarde van de retentieparameter β. In dit hoofdstuk tonen we aan dat voor oscillaties met lage frequentie de waarde van de draineerbare porositeit niet noodzakelijkwijs convergeert naar $(\theta_s - \theta_r)$ zoals wordt verondersteld in *Cartwright et al.* [2005], maar dat het onder invloed van de capillaire werking in de onverzadigde zone ook naar lagere waarden kan convergeren. Verder wordt een mogelijke verklaring voor het merkwaardige gedrag bij hoge frequenties gegeven, waarvan de afleiding is gebaseerd op de aanname dat voor deze hoge frequenties alleen het domein waarover grondwaterschommelingen plaatsvinden tot volledig hydraulisch evenwicht kan geraken. Gebruikmakend van de theorie beschreven in Hoofdstuk 3 kan worden aangetoond dat de relatie tussen de frequentie en de absolute waarde van de complexe draineerbare porositeit de vorm heeft van een machtsfunctie, van welke de richtingscoëfficient bepaald wordt door de parameter β.

In **Hoofdstuk 5** wordt een koppeling beschreven tussen een één-dimensionaal RE-model ter bechrijving van de onverzadigde zone dynamiek en het originele HSB-model. In dit hoofdstuk wordt de volcapillaire zone als een integraal onderdeel van de Boussinesq aquifer beschouwd. Het gekoppelde model wordt beschreven middels een stelsel van twee niet-lineaire partiële differentiaalvergelijkingen die simultaan opgelost worden. De resultaten van het model worden vergeleken met een drie-dimensionaal RE-model en met het originele HSB-model.

De rol van de onverzadigde zone in het doorgeven van bodemvochtpulsen als gevolg van neerslag wordt onderzocht en de relatie tussen neerslag, grondwater-aanvulling, draineerbare porositeit en onverzadigde berging wordt geanalyseerd. Behalve de verwachte vertragende werking van de onverzadigde zone op de relatie tussen neerslag en grondwateraanvulling, tonen de simulaties ook aan dat de onverzadigde zone niet onder alle omstandigheden de neerslagpulsen dempt maar ze ook kan versterken. Dit wordt veroorzaakt doordat water uit de onverzadigde zone wordt opgenomen in de verzadigde zone, hetgeen zorgt voor een een versterkte grondwateraanvulling ten tijde van stijgende grondwaterspiegels.

De vergelijking van de resultaten van het gekoppelde HSB model (HSB-coupled) met het RE-model en het originele HSB-model, toont een erg sterke overeenkomst tussen de hydrogrammen van HSB-coupled en het RE-model, terwijl het orginele HSB-model een systematische onderschatting geeft. Ook de grondwaterdynamiek wordt veel nauwkeuriger beschreven met het HSB-coupled model.

In **Hoofdstuk 6** wordt het HSB-coupled-model toegepast op een 36x18m helling nabij Troy (Idaho), USA. Het gekoppelde model is aangepast, zodanig dat de met de diepte afnemende verzadigde doorlatendheden verrekend kunnen worden. Het model is vooraf geparameteriseerd, gebruikmakend van de waterretentie karakteristiek en de relatie tussen doorlatendheid en diepte. Geen verdere calibratie is uitgevoerd. Het model gedrag is geëvalueerd en vergeleken met metingen van oppervlakkige afvoer en stijghoogtemetingen in piezometers over een periode van 130 dagen.

We concluderen dat de overeenkomst tussen de modelresultaten en de metingen van oppervlakkige afvoer redelijk is, met lichte onderschattingen voor de meeste piekafvoeren en lichte overschattingen gedurende de meeste recessies. De *timing* van de hydrogrammen is goed over het algemeen. Ook de grondwaterdynamiek wordt goed beschreven, hoewel ook de grondwaterstanden onderschat worden tijdens pieken. Dit fenomeen wordt mogelijk veroorzaakt door de beperkte vrije poriënruimte door de sterke effecten van capillariteit tijdens bijna verzadigde omstandigheden, waardoor de grondwaterstanden erg gevoelig reageren op kleine verschillen in oppervlakkige afvoer. Ook het gegeven dat slechts één parameterisatie voor de onverzadigde zone karakteristiek wordt gebruikt om het retentie gedrag van de verschillende horizonten (met licht verschillende eigenschappen) te beschrijven, vormt een mogelijke oorzaak voor de overschatting van oppervlakkige afvoer en grondwaterstanden tijdens recessies. Recent experimenteel onderzoek in het gebied toont ook aan dat de porositeit afneemt met de diepte.

Dankbetuiging / Acknowledgement

Het werk dat ik heb uitgevoerd tijdens mijn promotieonderzoek is tot stand gekomen met de hulp en steun van verschillende mensen. Ten eerste wil ik Peter Troch bedanken voor het mogelijk maken van dit onderzoek. Peter, behalve als promotor heb je ook gefungeerd als dagelijkse begeleider. Ik heb de manier waarop we samenwerkten als bijzonder prettig ervaren. De informele sfeer tijdens onze besprekingen maakte het mogelijk om op een open manier ideeën uit te wisselen en te bespreken. Ik wil je van harte bedanken voor de motivatie die je me gegeven hebt en voor je zeer bekwame hulp op het technische en analytische vlak.

Also Claudio Paniconi has been involved in developing the ideas that are presented in this thesis. Claudio, thanks a lot for the inspiration and all the rigorous checks of the text and the mathematical derivations in our work: you have been a great help, and I have learned a lot from Peters and your approach to science.

Jan Boll and Erin Brooks have been involved in collecting the data that are presented in Chapter 6. You have shown great support and hospitality during my visit to the University of Idaho, and you have helped me a lot with the interpretation and analysis of the data from the Troy-site. Your help is greatly appreciated. Het gezelschap van Roel Dijksma, die in hetzelfde huis woonde als ik gedurende enkele weken van mijn verblijf, was een welkome afwisseling op het dagelijks werk. De trips naar Mount St. Helens en Mount Rainier waren schitterend en zal ik niet snel vergeten.

I would also like to thank Reinder Feddes for coming up with the idea to organize a session on the hillslope scale as the link between the core and the catchment scale, at the European Geophysical Union meeting in Nice 2004, which was organized by Nunzio Romano and me. Nunzio and Reinder, thanks a lot for allowing me the experience of co-convening a session. I enjoyed it a lot.

Gedurende de eerste maanden van mijn promotieonderzoek was Emiel van Loon mijn kamergenoot. Na het vertrek van Emiel naar de Universiteit van Amsterdam werd zijn werkplek ingenomen door Patrick Bogaart. Beide wil ik graag bedanken voor de hulp die ze hebben verleend en de discussies die we gevoerd hebben omtrent het hillslope-storage Boussinesq model en aanverwante onderwerpen. Emiel, in het bijzonder bedankt voor de hulp met de Matlab code en de productie van mijn eerste papers en het helpen opzetten van de laboratoriumopstelling. Patrick, van harte bedankt voor alle hulp met Latex vraagstukken en voor het beschikbaar stellen van je foto's van de veldexcursie naar België en Luxemburg. De foto op de voorkant is een bewerking van één van je foto's.

Verder wil ik ook de AIO's (uit Wageningen, Utrecht en Delft), de overige postdocs en de vaste staf van de leerstoelgroep Hydrologie en Kwantitatief Waterbeheer bedanken voor de leuke tijd, interessante gesprekken en de hulp bij een heel scala van onderwerpen. In het bijzonder geldt dit voor Paul Torfs, die met zijn kritische opmerkingen bij heeft gedragen aan het verbeteren van het onderzoek dat hier gepresenteerd wordt. Ik ben ook dank verschuldigd aan de studenten (Frank, Eric en Suzanne) die me hebben geholpen met het werk in het laboratorium.

De sociale contacten buiten de werkplek zijn natuurlijk ook onmisbaar. Ik wilde mijn ouders bedanken voor alles en ik wil al mijn vrienden (in Tegelen en Wageningen) bedanken voor het zorgen voor de nodige afleiding tijdens mijn AIO-schap. Mede dankzij jullie heb ik de hele periode van mijn promotieonderzoek als een erg leuke tijd ervaren. In het bijzonder wil ik in deze context Roel Stappers bedanken voor de vele interessante discussies over elkaars promotieonderzoek en de nodige tips op het gebied van wiskunde en programmering.

Ten slotte: Greetje, je hebt er een mooie omslag van gemaakt. Bedankt voor alles!

Arno Hilberts
Wageningen, juli 2006.

This research was partly financed by Delft Cluster (project DC-030604).

Curriculum vitae

Arno Gerardus Jeanne Hilberts was born on April 30th, 1977 in Tegelen, The Netherlands. After having finished his secondary school "Rijksscholengemeenschap Den Hulster" in Venlo in 1995, he started with the study "Bodem, Water en Atmosfeer" ("Soil, Water and Atmosphere") at Wageningen Agricultural University (now Wageningen University), where he graduated in 2001. His two masters theses were on the short term predictions of fresh water consumption using artificial neural networks, and on analytical and numerical modeling of subsurface flow processes using a kinematic wave model. His internship was conducted at "Centro di Ricerca, Sviluppo e Studi Superiori in Sardegna" ("Centre for Advanced Studies, Research and Development in Sardegna") near Cagliari, Italy, where he was involved in the research that would later result in the publication of *Paniconi et al.* [2003]. In November 2001 he started as a Ph.D. student at the Department of Water Resources at Wageningen University, which resulted in this thesis. Starting December 2006, he will be working at Risk Management Solutions Ltd.(http://www.rms.com) in London, U.K., as a flood risk modeler.

List of publications

Peer-reviewed papers, published

Hilberts, A.G.J., P.A. Troch, and C. Paniconi, Storage-dependent drainable porosity for complex hillslopes, *Water Resour. Res., 41*, W06001, doi:10.1029/2004WR003725, 2005.

Troch, P.A., A.H. van Loon, and A.G.J. Hilberts, Analytical solution of the linearized hillslope-storage Boussinesq equation for exponential hillslope width functions, *Water Resour. Res., 40*, W08601, doi:10.1029/2003WR002850, 2004.

Hilberts, A.G.J., E.E. van Loon, P.A. Troch, and C. Paniconi, The hillslope-storage Boussinesq model for non-constant bedrock slope, *J. Hydrol., 291*, 160–173, 2004.

Paniconi, C. P.A. Troch, E.E. van Loon, and A.G.J. Hilberts, Hillslope-storage Boussinesq model for subsurface flow and variable source areas along complex hillslopes: 2 Intercomparison with a three-dimensional Richards equation model, *Water Resour. Res., 39*(11), 1317, doi:10.1029/2002WR001730, 2003.

Troch, P., E. van Loon, and A. Hilberts, Analytical solutions to a hillslope-storage kinematic wave equation for subsurface flow, *Adv. Water Resour., 25*, 637–649, 2002.

Peer-reviewed papers, in press

Hilberts, A.G.J., P.A. Troch, Comment on "Influence of capillarity on a simple harmonic oscillating water table: Sand column experiments and modeling" by N. Cartwright et al., *Water Resour. Res., 42*, doi:10.1029/2006WR005042, 2006.

Peer-reviewed papers, in review

Hilberts, A.G.J., P.A. Troch, C. Paniconi, and J. Boll, Low-dimensional modeling of hillslope subsurface flow: the relationship between rainfall, recharge, and unsaturated storage dynamics, *Water Resour. Res., 42*, doi:10.1029/2006WR004964, 2006.